71-15,084

ASKELAND, Donald Raymond, 1942-
LIQUID METAL-DROSS REACTIONS IN THE MAGNESIUM-SILICON-OXYGEN SYSTEM.

The University of Michigan, Ph.D., 1970
Engineering, metallurgy

University Microfilms, A XEROX Company, Ann Arbor, Michigan

THIS DISSERTATION HAS BEEN MICROFILMED EXACTLY AS RECEIVED

LIQUID METAL-DROSS REACTIONS

IN THE

MAGNESIUM-SILICON-OXYGEN SYSTEM

by
Donald Raymond Askeland

A dissertation submitted in partial fulfillment
of the requirements for the degree of
Doctor of Philosophy
(Metallurgical Engineering)
in The University of Michigan
1970

Doctoral Committee:

Professor Richard A. Flinn, Co-Chairman
Professor Paul K. Trojan, Co-Chairman
Professor Lawrence H. Van Vlack, Co-Chairman
Professor Wilbur C. Bigelow
Associate Professor Paul L. Cloke
Associate Professor Orville F. Kimball

ABSTRACT

LIQUID METAL-DROSS REACTIONS IN THE
MAGNESIUM-SILICON-OXYGEN SYSTEM

by

Donald Raymond Askeland

Co-Chairman: Richard A. Flinn
Co-Chairman: Paul K. Trojan
Co-Chairman: Lawrence H. Van Vlack

In the production of nodular iron, a magnesium silicon alloy is added to liquid cast iron containing 3.4% carbon and 2.5% silicon at a temperature of 2700 to 2750°F. This results in the solution of about 0.05%Mg in the melt and leads to the production of spheroids of graphite in the castings. An important and undesirable side effect is the formation of considerable quantities of inclusions or "dross" in the castings poured from this metal. The objectives of the investigation were to determine the nature of the dross, the reactions leading to its formation, and the methods for alleviating the problem.

By x-ray diffraction and microprobe analysis, the important phases in the dross were found to be

Magnesium oxide

Silica

Forsterite (Mg_2SiO_4)

Oxide glass containing Mg, Si, Fe, Al, Ca, O

Since magnesia, silica, and magnesium silicate were major constituents, it appeared that the major problem was to investigate the possible paths by which these could form. First, the formation of the simple oxides SiO_2 and MgO was studied, then the more complex silicates.

1. The Formation of Silica

The data showed that silica was formed by oxidation of the melt

$$Si \text{ (in melt)} + O_2 = SiO_2$$

and by the oxidation of high silicon nodularizer and post-inoculant alloys. Silica appears rapidly on the melt surface below an inversion temperature which varied from 2400 to 2600°F depending on the atmosphere, ladle refractory, and other characteristics of the melting. Above the inversion temperature, carbon reduces the film and it disappears.

2. Formation of MgO

The magnesium dissolved in the melt oxidizes and vaporizes at the surface of the melt as a function of time and the rate varies with atmosphere, refractory, temperature, and the type of nodularizing alloy. Another source of MgO is the oxidation of Mg_2Si, added during the ladle treatment, in an air atmosphere

$$Mg_2Si + O_2 = 2MgO + Si$$

3. Formation of Magnesium Silicate (Forsterite)

The absence of direct reaction between MgO and silicon and also between SiO_2 and magnesium to form forsterite points out the necessity for both MgO and SiO_2 to be present before forsterite can be produced. Isothermal reaction rate curves were determined starting with MgO and SiO_2 powders, and the maximum rate was found at 2550°F and higher, depending on composition.

With this information as to the morphology and rate of generation of dross, critical experiments were conducted to indicate methods of dross reduction. The quantity, type, and rate of dross formation were determined under controlled treatment conditions.

The total quantity of dross increased with the amount of magnesium added, the amount of silicon added to the ladle, the time of holding, the temperature of holding, and the chemistry of the melt, nodularizer, and post-inoculant.

The character of the dross changed from a filmy type to one high in lumpy crystalline silicates as the silicon added to the ladle increased. The filmy type is less objectionable because it tends to stay on the outer surface of the casting rather than leading to subsurface inclusions.

The roles of other elements in the ladle addition, such as cerium as well as the sulfur level in the melt, are also important and were evaluated.

PREFACE

I wish to express my sincere appreciation to all those who have aided me in this investigation and particularly to the following:

Professors Paul K. Trojan, Richard A. Flinn, and Lawrence H. Van Vlack, Co-Chairmen of the Doctoral Committee, for their guidance and constructive criticism during this investigation.

Professors W. C. Bigelow, O. F. Kimball, and P. L. Cloke, members of the Doctoral Committee, for their interest and advice.

Mr. D. Flynn, Chevrolet Iron Foundries, Saginaw, Michigan, for invaluable services rendered.

The National Aeronautics and Space Agency for fellowship support.

The American Foundrymen's Society for partial support of the work, and in particular the Ductile Iron Research Committee 12K for their interest and advice.

Paul Nesbitt and Liz Allen for their help in the preparation of the thesis, and my fellow students who have brightened my days.

Especially Mary and Per.

TABLE OF CONTENTS

	Page
PREFACE	ii
LIST OF TABLES	vi
LIST OF FIGURES	vii
ABSTRACT	xi
INTRODUCTION AND OBJECTIVES	1
REVIEW OF THE LITERATURE	2
I. Dross in Nodular Iron	3
A. Effect of Processing Variables on Dross Formation	3
B. Previous Analyses of Dross Chemistry	4
C. Classification of Dross Defects in Castings	5
II. The Magnesium-Silicon-Oxygen System	5
A. Formation of MgO	6
B. Formation of SiO_2	7
C. Reactions between Magnesium and SiO_2	9
D. Reactions between Silicon and MgO	9
E. Reactions between MgO and SiO_2	9
EXPERIMENTAL METHOD	11
I. Experimental Design	11
II. Experimental Procedure and Analysis	16
A. Pressure Vessel Procedure	18
1. Description of the Equipment	18
2. The Conduct of a Typical Heat	21
B. Analysis of the Mg-SiO_2 Reaction	23
C. Powder Compact Procedure	27
1. Preparation of the Powder Compacts	27
2. The Experimental Resistance Furnace	27
3. The Sample Receptacles	30
4. The Typical Conduct of a Heat	30
D. Analyzing the Composition of the Powder Compacts	33
RESULTS AND DISCUSSION	40
I. Formation of SiO_2	41
A. Oxidation of Silicon from Iron-Carbon-Silicon Melts.	41
B. Oxidation of Silicon from Iron Silicides	46
II. Formation of MgO	47
A. Oxidation of Magnesium Silicide	47
B. Magnesium Loss Rates from Nodular Iron	48
1. One-Pound Melts--The Effect of Atmosphere and Refractory	48

Page

2. Five-Pound Melts--The Effect of Nodularizer. . . 50
3. One Hundred-Pound Melts--The Effect of Temperature 50
4. Discussion of the Magnesium Loss Rates 51

C. Oxidation Versus Vaporization 57

III. Reactions between Dissolved Magnesium and SiO_2 60
A. The Nature of the Reaction in Magnesium-Saturated Melts 60
B. The Kinetics of the Reaction in Magnesium-Saturated Melts 66
C. The Effect of Metal Chemistry 67

IV. Reactions between Dissolved Silicon and MgO 69
A. Microstructure of Powder Compacts after Firing . . . 69
B. The Kinetics of the Reaction 71
C. The Effect of Iron-Silicon Solutions 77

V. Reactions between MgO and SiO_2 78
A. The Reaction between MgO and SiO_2 in Argon 79
1. The Mechanism of Formation of Forsterite and Enstatite 79
2. The Effect of Temperature and Composition . . . 83
3. The Effect of Vitreous Silica 93
4. The Rate Constants for the Reaction 94
5. The Activation Energy for the Reaction 97

B. Reaction in an Air Atmosphere 99
C. The Effect of Other Oxides on the Reaction 101
D. Summary 111

ENGINEERING ASPECTS 113

I. Experimental Procedure 114
A. Experimental Equipment 114
1. The Transfer Method--One Hundred-Pound Heats . . 114
2. The Plunging Method--Five-Pound Heats 115

B. Analysis of the Dross 117

II. Discussion of the Results for the Formation of Ladle Dross in Nodular Iron 119
A. The Effect of Time 120
B. The Effect of Holding and Nodularization Temperature 127
1. Holding Temperature 127
2. Nodularizing Temperature 128

C. The Effect of Atmosphere 130
D. The Effect of Chemistry of Melt, Nodularizer, and Post-inoculant 131
1. Sulfur in the Metal 131
2. Magnesium in the Metal 132
3. Cerium in the Nodularizer 135
4. Silicon in the Metal, Nodularizer, and Post-inoculant 136

Page

III. Discussion of Dross Formation and Dross Defects in Nodular Iron Castings 138
A. A Model for the Formation of Dross Defects in Nodular Iron 141
B. The Effect of Processing Variables on Dross Defects in the Casting 142
1. The Effect of Metal Chemistry 142
a. Magnesium 143
b. Sulfur 143
c. Silicon 144
d. Aluminum and Calcium 144
e. Cerium 144
2. The Effect of Nodularizer and Post-inoculant Alloys 147
3. The Effect of Holding and Pouring Times 147
4. The Effect of Nodularization and Holding Temperatures 148
5. The Effect of Mold Design and Turbulence 148
6. Fluxes 148

CONCLUSIONS 150

APPENDIX I: Chemical Analysis of Raw Materials 153

APPENDIX II: Calculation of Average Penetration 155

APPENDIX III: Rate Constants for $MgO-SiO_2$ Powder Reactions . . . 156

APPENDIX IV: Summary of Ladle Dross Heats 158

BIBLIOGRAPHY 161

LIST OF TABLES

Table		Page
I	X-ray Diffraction Data	34
II	Experimental CO/SiO_2 Inversion Temperatures	42
III	Magnesium Balance for Iron Melt and Dross	58
IV	Effect of Metal Chemistry on the Reactions between Dissolved Magnesium and Silicon	67
V	Activation Energies for the Reactions between Dissolved Silicon and MgO	77
VI	Effect of Composition on the Time Required to Reach the Maximum in the Forsterite Curve at 2650°F	85
VII	Calculated Maximum and Equilibrium Forsterite for High SiO_2 Powder Compositions	92
VIII	The Effect of the Type of Silica on the Rate Constant for the Formation of Forsterite at 2650°F in Argon	94
IX	Activation Energies for the Formation of Forsterite and Enstatite	97
X	Effect of Atmosphere on the Rate Constant	100
XI	Summary of Trends in the Ternary Powder Compacts	103
XII	Effect of Holding Temperature on Quantity and Chemistry of Dross	127
XIII	Effect of Nodularizing Temperature on the Quantity and Chemistry of Dross in 100-Pound Melts	128
XIV	Effect of Nodularizing Temperature on the Quantity and Chemistry of Dross in Five-Pound Melts	128
XV	Effect of Atmosphere on Quantity and Chemistry of Dross	130
XVI	Effect of Sulfur on Quantity and Chemistry of Dross	131
XVII	Effect of Cerium on Quantity and Chemistry of Dross	135
XVIII	Effect of Melt Silicon on Quantity and Chemistry of Dross	137
XIX	Effect of Post-inoculant on Quantity and Chemistry of Dross	137
XX	Summary of the Effect of Processing Variables on the Quantity and Chemistry of Dross	138

LIST OF FIGURES

Figure		Page
1	The Equilibrium Phase Diagram for $MgO-SiO_2$	13
2	Possible Sequences for the Reactions between Dissolved Magnesium plus Silica and for Dissolved Silicon plus MgO	15
3	The Sequence of the Reactions in the Mg-Si-O System.	17
4	Sectional View of the Pressure Vessel Showing Internal Details	19
5	Internal Arrangement of the Crucible, Silica Tube, and Thermocouples in the Induction Coil	20
6	Calibration of the Thermocouples in the Pressure Vessel	22
7	Time-temperature Relations during the Operation of the Pressure Vessel	24
8	Typical Section Showing the Reaction Zone in a Silica Tube	26
9	The Effect of Initial Compaction Pressure on the Solid State Reaction between 57.3 wt%MgO and 42.7 wt%SiO_2	28
10	Cross-sectional View of the Silicon Carbide Resistance Furnace	29
11	The Heat-up Rate for the Powder Compacts Measured with Optical Pyrometer and with Thermocouple Embedded in Center of Specimen	32
12	X-ray Diffraction Calibration Curves for MgO, Quartz, and Forsterite	35
13	The Effect of the Accompanying Material on the Calibration Curves for MgO and Quartz	36
14	A Typical Curve for the Reactants and Reaction Products during Firing of a 57.3 wt%MgO - 42.7 wt%SiO_2 Powder Compact	38
15	The Composition Parameter $D(\alpha)$ Versus Time for the Formation of Forsterite from a 57.3 wt%MgO - 42.7 wt% SiO_2 Powder Compact	39

Figure		Page
16	Schematic Diagram Showing Thermodynamic Equilibrium and the Critical Temperature Ranges for the CO/SiO_2 Inversion Temperature in Air and Argon Atmospheres	45
17	Schematic Diagram Showing the Plunging Apparatus in the Silicon Carbide Resistance Furnace	49
18	Magnesium Loss Rates in One-Pound Melts as Affected by Atmosphere and Refractory	52
19	Magnesium Loss Rates in Five-Pound Melts as Affected by Nodularizer	53
20	Magnesium Loss Rates in One Hundred-Pound Melts as Affected by Holding Temperature	54
21	Maximum Solubility of Carbon and Magnesium in Iron as a Function of Temperature	61
22	Silica Tube Fired at 2800°F for 20 Minutes, Showing Severe Attack of the Surface as well as Penetration of the Reaction Zone	62
23	Silica Tube Fired at 2585°F for 10 Minutes	62
24	Typical Microstructure of the Reaction Zone	64
25	Electron Micrograph of the Interface between the Reaction Zone and the Silica Tube	64
26	Micrograph of the Interface between the Iron Melt and the Reaction Zone Showing Attack of the Surface . .	65
27	Micrograph of the Interface between the Iron Melt and the Reaction Zone with No Surface Attack	65
28	Typical Microstructure in the Reaction between Silicon and MgO	70
29	Typical Rates of Formation of Forsterite for the Reaction between Silicon and MgO	72
30	Rate Constants Versus Reciprocal Temperature for the Reaction between Silicon and MgO in Air and Argon Atmospheres	73
31	Microstructure of the MgO-Si Powder Compacts, Showing Angular Silicon Particles	74

Figure		Page
32	Microstructure of the MgO-Si Powder Compacts, with Round Silicon Particles	74
33	Electron Microprobe Trace through the Interface between $Si/Mg_2SiO_4/MgO$ in an MgO-Silicon Compact	76
34	Typical Development of Forsterite and Enstatite as a Function of Composition in $MgO-SiO_2$ Powder Compacts at 2450°F	80
35	Electron Microprobe Trace through the Interface between $SiO_2/MgSiO_3/Mg_2SiO_4$ in $MgO-SiO_2$ Powder Compacts . . .	82
36	Effect of Temperature on the Development of Forsterite in Stoichiometric Enstatite Compositions	84
37	Isothermal Transformation Curves for the Development of Forsterite in 80 wt%MgO - 20 wt%SiO_2 Powder Compacts .	87
38	Isothermal Transformation Curves for the Development of Forsterite in 57.3 wt%MgO - 42.7 wt%SiO_2 Powder Compacts	88
39	Isothermal Transformation Curves for the Development of Forsterite and Enstatite in 50 wt%MgO - 50 wt%SiO_2 Powder Compacts	89
40	Isothermal Transformation Curves for the Development of Forsterite and Enstatite in 40 wt%MgO - 60 wt%SiO_2 Powder Compacts	90
41	Isothermal Transformation Curves for the Development of Forsterite and Enstatite in 20 wt%MgO - 80 wt%SiO_2 Powder Compacts	91
42	Micrograph of a Silica Grain Showing the Presence of a Boundary Phase	95
43	Rate Constants Versus Reciprocal Temperature for the Formation of Forsterite and Enstatite	96
44	Activation Energies for Forsterite and Enstatite as a Function of Percent SiO_2 in the Powder Compacts . . .	98
45	The Effect of $\%Fe_2O_3$ on the Development of Forsterite in Ternary $MgO-SiO_2-Fe_2O_3$ Powder Compacts with a 2:1 Molar Ratio of MgO to SiO_2	104
46	The Effect of $\%Fe_2O_3$ on the Development of Forsterite and Enstatite in Ternary $MgO-SiO_2-Fe_2O_3$ Powder Compacts with a 1:1 Molar Ratio of MgO to SiO_2	105

Figure		Page
47	The Effect of $\%Fe_2O_3$ on the Interplanar Spacing d_{021} of Forsterite in Ternary $MgO-SiO_2-Fe_2O_3$ Powder Compacts with 2:1 Molar Ratio of MgO to SiO_2	107
48	The Effect of Time on the Interplanar Spacing d_{031} of Forsterite in a Ternary $MgO-SiO_2-Fe_2O_3$ Powder Compact with a 2:1 Molar Ratio of MgO to SiO_2	108
49	Micrograph Showing the Presence of $MgO \cdot Fe_2O_3$ in a $MgO-SiO_2-Fe_2O_3$ Powder Compact	110
50	Experimental Apparatus for the Production of Nodular Iron in the Five-Pound Induction Furnace	116
51	Schematic Diagram of the Graphite Bell Assembly for Plunging in the Five-Pound Induction Furnace	118
52	The Effect of Holding Time on the Quantity and Chemistry of Dross	121
53	The Effect of Holding Time on the Quantity and Chemistry of Dross	122
54	The Effect of Holding Time on the Chemistry of Dross .	124
55	The Effect of Holding Time on the Ratio of Fine Dross to Total Dross for the Experiment in Fig. 54	126
56	The Effect of the Magnesium Added to the Melt on the Quantity and Chemistry of Dross	133
57	The Effect of the Silicon Present in the Nodularizer on the Fine Dross and Forsterite	134
58	The Effect of the Silicon Present in the Nodularizer and Post-inoculant on the Fine Dross	139
59	The Effect of the Silicon Present in the Nodularizer and Post-inoculant on the Forsterite	140
60	(a) Electron microprobe Sample Current Micrograph Showing a Piece of 75%FeSi Post-inoculant alloy and Forsterite	145
	(b) Electron Microprobe Trace from the Remains of a 75%FeSi Post-inoculant Alloy through a Glass Phase and into Forsterite	146

ABSTRACT

In the production of nodular iron, a magnesium silicon alloy is added to liquid cast iron containing 3.4% carbon and 2.5% silicon at a temperature of 2700 to 2750°F. This results in the solution of about 0.05%Mg in the melt and leads to the production of spheroids of graphite in the castings. An important and undesirable side effect is the formation of considerable quantities of inclusions or "dross" in the castings poured from this metal. The objectives of the investigation were to determine the nature of the dross, the reactions leading to its formation, and the methods for alleviating the problem.

By x-ray diffraction and microprobe analysis, the important phases in the dross were found to be

Magnesium oxide

Silica

Forsterite (Mg_2SiO_4)

Oxide glass containing Mg, Si, Fe, Al, Ca, O

Since magnesia, silica, and magnesium silicate were major constituents, it appeared that the major problem was to investigate the possible paths by which these could form. First, the formation of the simple oxides SiO_2 and MgO was studied, then the more complex silicates.

1. The Formation of Silica

The data showed that silica was formed by oxidation of the melt

$$Si \text{ (in melt)} + O_2 = SiO_2$$

and by the oxidation of high silicon nodularizer and post-inoculant alloys. Silica appears rapidly on the melt surface below an inversion temperature which varied from 2400 to 2600°F depending on the atmosphere, ladle refractory, and other characteristics of the melting. Above the inversion temperature, carbon reduces the film and it disappears.

2. Formation of MgO

The magnesium dissolved in the melt vaporizes and oxidizes at the surface of the melt as a function of time and the rate varies with atmosphere, refractory, temperature, and the type of nodularizing alloy. Another source of MgO is the oxidation of Mg_2Si, added during the ladle treatment, in an air atmosphere

$$Mg_2Si + O_2 = 2MgO + Si$$

3. Formation of Magnesium Silicate (Forsterite)

The absence of direct reaction between MgO and silicon and also between SiO_2 and magnesium to form forsterite points out the necessity for both MgO and SiO_2 to be present before forsterite can be produced. Isothermal reaction rate curves were determined starting with MgO and SiO_2 powders, and the maximum rate was found at 2550°F and higher, depending on composition.

With this information as to the morphology and rate of generation of dross, critical experiments were conducted to indicate methods of dross reduction. The quantity, type, and rate of dross formation were determined under controlled treatment conditions.

The total quantity of dross increased with the amount of magnesium added, the amount of silicon added to the ladle, the time of holding, the temperature of holding, and the chemistry of the melt, nodularizer, and post-inoculant.

The character of the dross changed from a filmy type to one high in lumpy crystalline silicates as the silicon added to the ladle increased. The filmy type is less objectionable because it tends to stay on the outer surface of the casting rather than leading to subsurface inclusions.

The roles of other elements in the ladle addition, such as cerium as well as the sulfur level in the melt, are also important and were evaluated.

INTRODUCTION AND OBJECTIVES

The development of nodular cast iron about twenty years ago provided an excellent new engineering material for the foundry industry. However, the production of nodular iron requires the addition of magnesium to molten cast iron, thus introducing several new production problems. The magnesium alloys, or nodularizers, are expensive and exhibit extensive loss of magnesium through vaporization during the nodularizing treatment. In addition, the magnesium plays an important role in the formation of dross, a slag composed principally of oxide, sulfide, and undissolved metallic phases on the surface of nodular iron melts. Frequently some of the dross finds its way into the casting itself, resulting in expensive cleaning procedures or scrapping of the casting.

Extensive effort has been expended in developing nodularizing alloys which reduce the magnesium loss rate. However, efforts to reduce or eliminate the occurrence of dross defects in nodular iron castings have been generally primitive. More important, little effort has been made to understand the fundamental mechanisms by which the dross forms. Previous investigators have shown that magnesium oxide and silica constitute a large percentage of dross as it is found both on the molten metal during treatment and in the casting as defects.

The objectives of this research were (1) to determine the mechanisms by which MgO, SiO_2, and the magnesium-silicate compounds might form, (2) to determine the effect of environmental conditions such as temperature, atmosphere, and metal and refractory chemistry on these basic mechanisms, and (3) to suggest methods of avoiding dross based on the fundamental mechanisms by which dross is formed.

REVIEW OF THE LITERATURE

Only the addition of magnesium during nodularization and of silicon during post-inoculation differentiates the production of nodular iron (also known as ductile iron, spherulitic iron, spherulitic graphite iron, and SG iron) from gray iron. The magnesium, necessary for the graphite to form as spheres rather than flakes, is generally added by one of two techniques--plunging, in which the magnesium alloy, or nodularizer, is placed within a bell and held beneath the surface of the melt, or the sandwich method, in which the magnesium alloy is placed in a pocket in the bottom of an empty ladle, covered with a layer of steel scrap or ferrosilicon, and then the molten metal to be treated is added. The nodularizing alloys used commercially include magnesium-ferrosilicon (5 to 10 percent magnesium), nickel-magnesium (15 to 20 percent magnesium), magnesium-impregnated coke, and nickel-magnesium-ferrosilicon.

Next an addition of ferrosilicon or other alloy is added to increase the nucleation rate and refine the shape of the graphite spheroids. The more common post-inoculant alloys include ferrosilicon (75 or 85 percent silicon) and calcium-silicon (as CaSi compound). The post-inoculant may be added during reladling of the metal after nodularizing, by stirring the silicon alloy into the ladle, or by inoculation in the mold. In some instances, no post-inoculant is used at all.

During the nodularization and post-inoculation treatments, oxidation of the magnesium and silicon, as well as calcium and aluminum which are also found in these alloys, occurs. The result is the formation of an oxide slag, or dross, on the surface of the ladle. There is a question as to whether dross will continue to form if the initial dross is removed.

The literature will be reviewed in the following order:

I. Previous Investigations on Dross in Nodular Iron

A. Effect of Processing Variables on Dross Formation

B. Previous Analyses of Dross Chemistry

C. Classification of Dross Defects in Castings

II. Previous Investigations in the Mg-Si-O System

A. Formation of SiO_2

B. Formation of MgO

C. Reactions between Magnesium and SiO_2

D. Reactions between Silicon and MgO

E. Reactions between MgO and SiO_2

I. DROSS IN NODULAR IRON

Previous investigations on dross in nodular iron have included the effect of processing variables on dross formation and the composition and classification of dross and dross defects in castings.

A. Effect of Processing Variables on Dross Formation

Dross formation and the incidence of dross defects in castings were found to be dependent on the temperature and on the availability of oxygen to the molten metal. Heine and Loper[1] observed that the nature of dross on the surface of inoculated nodular iron as well as the nature and location of dross defects in nodular iron castings were related to the temperature of the bath and the pouring temperature of the castings. As the bath temperature decreased, the nature of the surface changed from dross-free to a liquid dross film and finally to a solid, chunky dross layer. The amount of dross increased when a

blast of air was directed at the surface of the melt. Castings poured above 2600°F possessed a filmy dross on the casting surface while those poured below 2600°F exhibited large chunky dross particles within the body of the casting.

A number of other phenomena have been related to the temperature and oxidation effects. Thus long holding times in the ladle prior to pouring[1] (allowing a large temperature drop) and long pouring times[1,2] (increasing the time of contact between the metal and air) were found to increase the extent of dross defects in the castings. Ladle and mold design also played a role in dross formation: ladles with a large surface area to volume ratio[2] and molds which allowed the metal to enter the mold cavity in a turbulent fashion[1,2,3] were found to increase the dross defect problems. Excessive moisture in the molding sands was also detrimental.[3,4]

The chemistry of the metal and of the inoculants also affected the incidence of dross. Melts containing large amounts of residual magnesium,[1,4] sulfur,[2,3] aluminum,[2,3] carbon,[2] and silicon[4] were found to have a higher incidence of dross defects, while those containing cerium[2,3,4] and tellurium[2,3] appeared to be relatively free of defects. A melt containing zero silicon was observed to show no defects at all.[4] Nodularizing and post-inoculant alloys low in silicon, calcium, and aluminum appeared to minimize dross defects.[2,3,4]

B. Previous Analyses of Dross Chemistry

A few analyses of ladle dross and of large dross defects have been reported in the literature. While the bulk of the dross was oxide material, numerous metallic particles in a wide variety of sizes were also observed. The oxides in the ladle dross included from 20 to 50

weight percent SiO_2, 10 to 35 weight percent MgO, 20 to 25 weight percent FeO, and less than 10 weight percent each of Al_2O_3, CaO, and MnO.[1,3] Large dross defects appeared to contain higher percentages of $SiO_2$and lower percentages of MgO than ladle dross.[1] X-ray diffraction results have shown that MgO, SiO_2, and Mg_2SiO_4 (forsterite) exist as crystalline phases in ladle dross and in large dross defects.[4,5]

C. Classification of Dross Defects in Castings

Dross defects in the castings have been analyzed and typed according to their size and shape.[5] Three types--gross, due to trapped ladle dross, stringers, slag films trapped in the casting, and fine dross, small inclusions in the casting--have been analyzed and found to contain forsterite, MgO, MgS, iron particles, and Mg_2Si inclusions. Enstatite ($MgSiO_3$) inclusions have been identified in nodular iron by Kiessling and Lange.[6] Numerous other types of inclusions have also been reported in nodular iron by Arsent'ev and Orlova.[7] Glasses rich in calcium, aluminum, and silicon oxides also appear in the gross dross defects.

Although nodular iron dross appears very complex, MgO, SiO_2, and Mg_2SiO_4 (forsterite) have frequently been reported in large quantities. MgO and SiO_2 can account for over fifty percent of the dross. Because the addition of the magnesium and silicon alloys makes the nodular iron unique from other casting alloys, it is quite logical to begin the investigation by focusing on an isolated system--that of magnesium-silicon-oxygen.

II. THE MAGNESIUM-SILICON-OXYGEN SYSTEM

Magnesium, silicon, and oxygen can react in a number of ways, including the formation of magnesium and silicon oxides, reactions between

an oxide and a metal phase, and reactions between the oxide phases. Some information on each of these reactions can be found in the literature and is summarized below.

A. Formation of MgO

During the nodularization of iron magnesium is added, generally in the form of a magnesium ferrosilicon alloy, to the molten iron at 2650° to 2800°F. However, pure magnesium boils at 2030°F; even when alloyed in ferrosilicon the vapor pressure is high enough so that boiling occurs during nodularization. The result is a significant loss of magnesium during the nodularizing treatment, with recoveries in commercial processes on the level of 20 to 50 percent of the initial magnesium added. This recovery can be improved when the nodularizing alloys contain lower amounts of magnesium--the efficiency of magnesium solution improves but more alloy is required.[8] Recoveries of 70 percent or more are obtained when the magnesium content of the alloy is two percent.[9] The addition of cerium or mischmetal to the alloy further increases the recovery.[10]

Some of the magnesium is lost due to deoxidation and desulfurization, as the compounds MgO and MgS have very large negative free energies of formation. Oxygen dissolved in the iron combines with magnesium to form MgO, which floats out of the metal. The oxygen content of the iron can be reduced by a factor of ten or more during nodularization.[11] However, much more magnesium is lost from the melt as a vapor which eventually oxidizes and frequently deposits on the sides of the ladle.

Following the flare-up in the first minute after addition, the magnesium continues to vaporize at a constant rate determined by a first

order rate equation. The loss rate during this period depends on the temperature and the type of nodularizer and post-inoculant alloy used. Levchenko[12] found that the loss rate, or fading, of magnesium occurs most rapidly at 2462°F. He speculated that at low temperatures the magnesium separates from the iron and forms a separate phase. As the temperature increases the magnesium returns to solution, thus effectively lowering the loss rate. Simultaneously the mass transport of magnesium to the surface of the melt increases, thus increasing the loss rate. The peak in loss rate with temperature supposedly reflects an optimum temperature where the sum of the two competing mechanisms results in a very high loss rate. The present work casts doubt on this explanation, however.

The fading effect has also been observed by Trojan, Bargeron, and Flinn[10] during an evaluation of strontium-bearing post-inoculants. Rate constants calculated from their data indicate that loss rates are higher with magnesium ferrosilicon than with cerium-bearing magnesium ferrosilicon. In addition, a strontium-bearing ferrosilicon used as a post-inoculant reduces the loss rate as compared to a standard 75 percent ferrosilicon alloy.

Therefore, the amount of magnesium available for oxidation can be affected during the initial treatment and also during holding by controlling the temperature and the chemistry of the nodularizing and post-inoculant alloys.

B. Formation of SiO_2

In gray cast iron an oxide film characteristically appears on the surface of the melt and remains until the temperature is raised above

2500 to 2650°F. The temperature at which the film disappears, the CO/SiO_2 inversion temperature, is determined under equilibrium conditions by the following reaction[13]

$$SiO_2 + 2\underline{C} = \underline{Si} + 2CO \qquad (1)$$

If a constant partial pressure of one atmosphere of CO is assumed, the inversion temperature can be calculated from the following equation:

$$\log \frac{[\%Si]}{[\%C]^2} = \frac{-27,486}{T} + 15.47 \qquad (2)$$

Above this temperature silica is reduced by carbon in the melt and CO is released to the atmosphere. At lower temperatures SiO_2 can form, covering the surface of the melt. Thus, at low temperatures a supply of SiO_2 is readily available at the melt surface.

However, de Sy[13] determined that in addition to the oxygen dissolved in the melt a non-equilibrium amount is present in the form of silica particles suspended in the melt. Very long superheat times are required to dissolve the silica and approach an equilibrium oxygen content.

Silicon can also be oxidized from the iron-silicon phases, frequently found as major constituents in the nodularizing and post-inoculant alloys. Baker[14] followed the oxidation of molten iron-silicon drops as they fell through a column of hot air. Low silicon drops (less than six percent silicon) oxidize rapidly, forming a thick brittle scale composed mainly of iron oxide. As the silicon content increases, the scale becomes increasingly enriched in silica until above seven percent silicon the oxide scale remains thin and passive. Drops containing carbon as well as silicon were also oxidized with similar results, although the amount of desiliconization is lower than in the pure iron-silicon drops. In all cases, the oxidation is accelerated as the temperature is increased.

C. Reactions between Magnesium and SiO_2

Large inclusions are frequently encountered in very large magnesium-base castings. The inclusions, visible to the naked eye, are observed to be circular in shape and are the remains of silica sand grains entrained in the metal from the mold walls during pouring. Lagowski and Pollard[15] observed that at the silica/melt interface a lamellar eutectic type of structure was observed to be growing into the melt; the phases were identified as MgO and Mg_2Si and were assumed to have formed according to the reaction

$$4Mg + SiO_2 = Mg_2Si + 2MgO \qquad (3)$$

Farther from the silica particle, massive Mg_2Si crystals form while the MgO lamellae break away from the interface as islands, with each lamella being separated by the magnesium solution. Similar inclusions have been described by Bergstrom and Bassett[16] and Emley[17]; none of the investigators observed metallic silicon in the inclusions. It is apparent, however, that silica particles can readily be reduced, forming silicon and MgO, when in contact with a high magnesium bath.

D. Reactions between Silicon and MgO

Even less information is available on the reverse reaction, the reduction of MgO by silicon metal. Economos and Kingery[18] placed a drop of pure silicon on a MgO plate and exposed the diffusion couple in a helium atmosphere at 1800°C for an extended period of time. The interface exhibited a very thin reaction layer of forsterite (Mg_2SiO_4). Unfortunately, no work was done using a more oxidizing atmosphere.

E. Reactions between MgO and SiO_2

The solid state reaction between MgO and SiO_2 powders has been studied thoroughly at low temperatures (less than 2370°F), showing that

the reaction is a diffusion controlled process.[19,20,21] The initial product formed, regardless of the mole ratio of the starting components, is always a thin layer of enstatite ($MgSiO_3$), which readily combines with additional magnesium ions to form forsterite (Mg_2SiO_4). The reaction continues in this manner until all of the magnesium is incorporated in forsterite. The reaction is controlled by the diffusion of magnesium ions through the enstatite layer; this enstatite layer continues to move into the silica grains as the reaction proceeds without a change in thickness. Consequently, the amount of enstatite continuously decreases, since the volume of the spherical silica grains is also decreasing.

The formation of forsterite follows a theoretical equation developed by Ginstling and Brounshtein.[22] Rate constants were calculated and the activation energy for the formation of forsterite was determined to be about 78 kcal/g·mole. Hayami and Ogura[23] performed similar experiments using MgO and enstatite as the starting materials and found that the activation energy for the formation of forsterite was 100 to 110 kcal/g·mole, supporting the contention that the rate limiting step is the diffusion through the enstatite layer.

The information obtained from the literature review indicates that a substantial portion of dross consists of MgO, SiO_2, and forsterite. Only limited investigation of the mechanisms by which these phases can form and interact appears in the literature. Thus a detailed, systematic evaluation of the Mg-Si-O system at this time appears to be warranted. With a more thorough understanding of the controlling mechanisms, the effect of numerous processing variables on dross formation in nodular iron may be interpreted on a more rational basis.

EXPERIMENTAL METHOD

There are a number of possible ways in which the complex silicate-oxide mixtures of the dross could be formed. It was decided to investigate each of these in an isolated situation. Often this meant using procedures far removed from actual nodular iron production. Following these experiments, nodular iron was produced under widely varying environmental conditions and the variations in the dross were interpreted in terms of the simple mechanisms studied earlier. The procedure for the second approach with its specialized experimental techniques will be discussed later under "Engineering Aspects." The experimental methods for the first approach are discussed here under the following headings:

I. Experimental Design

II. Experimental Procedure and Analysis of Data
   - A. Pressure Vessel Procedure
   - B. Analysis of Mg-SiO_2 Reaction
   - C. Powder Compact Procedure
   - D. Analysis of Powder Compacts

I. EXPERIMENTAL DESIGN

As described earlier, an understanding of the reactions in the Mg-Si-O system is an important step towards the eventual control of dross defects. The logical starting point is therefore the determination of the origin of the crystalline magnesium-silicate compounds, forsterite (Mg_2SiO_4) and enstatite ($MgSiO_3$). To this end, a number of reactions have been proposed which could contribute to the formation of

either compound. These are listed below for the formation of forsterite:

$$2Mg + Si + 2O_2 = Mg_2SiO_4 \quad (4)$$

$$2MgO + SiO_2 = Mg_2SiO_4 \quad (5)$$

$$2Mg + SiO_2 + O_2 = Mg_2SiO_4 \quad (6)$$

$$2MgO + Si + O_2 = Mg_2SiO_4 \quad (7)$$

The possibility of the first reaction is considered to be remote, since the magnesium or silicon would oxidize initially and the system would revert to one of the other reactions considered.

The second reaction is a solid state reaction at temperatures below 2750°F, the usual ladle treatment temperature of nodular iron. This is illustrated by the $MgO-SiO_2$ phase diagram, Fig. 1, where under equilibrium conditions no liquid is present below 2810°F.

The last two reactions, as originally envisaged, would entail a simultaneous combination of oxygen, a metallic phase, and an oxide phase to form the magnesium silicate compounds. However, there is a possibility that the reactions actually occur in several steps, with the oxidation of the metallic phase occurring before the reaction to form the magnesium-silicate compounds. The feasibility of these reactions can be evaluated by calculating the free energies associated with the reactions.

For the reaction between magnesium and SiO_2 (Eq. 6), calculations are based on an iron-carbon-magnesium melt saturated in both carbon and magnesium. The activity coefficients γ°_{Mg} required for determining the free energies associated with the reaction

$$Mg = \underline{Mg} \quad (8)$$

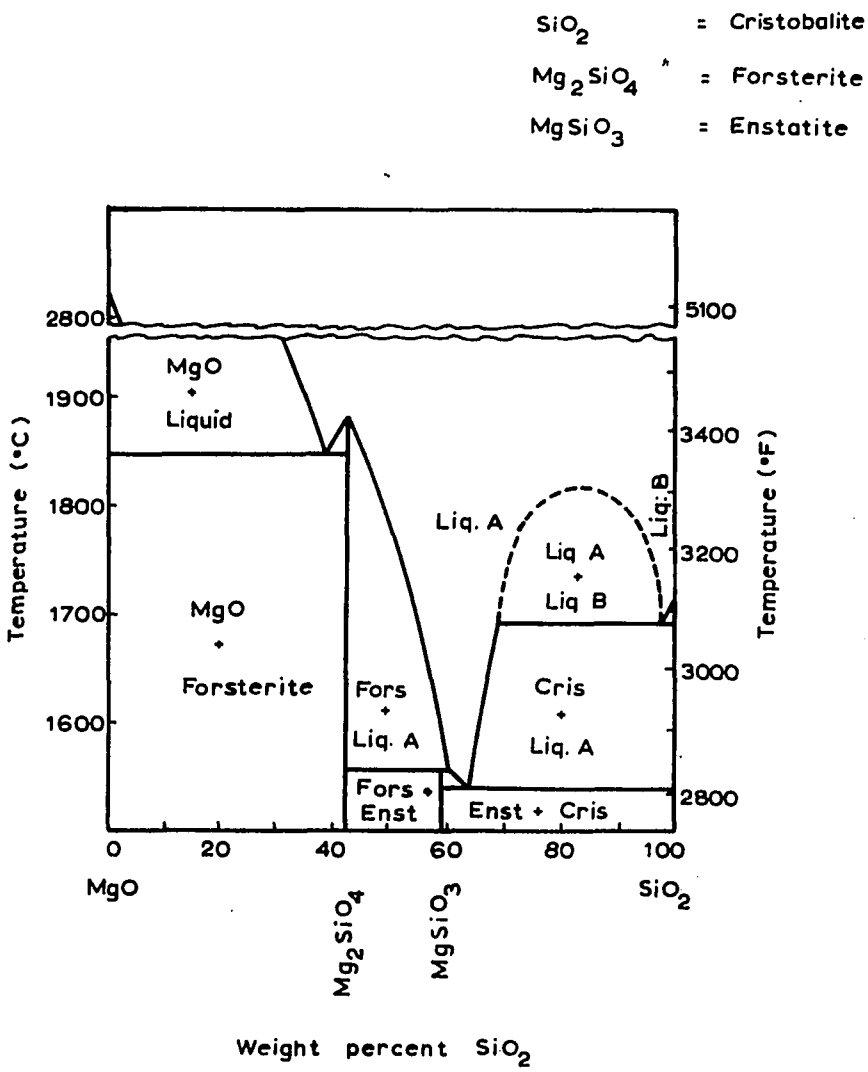


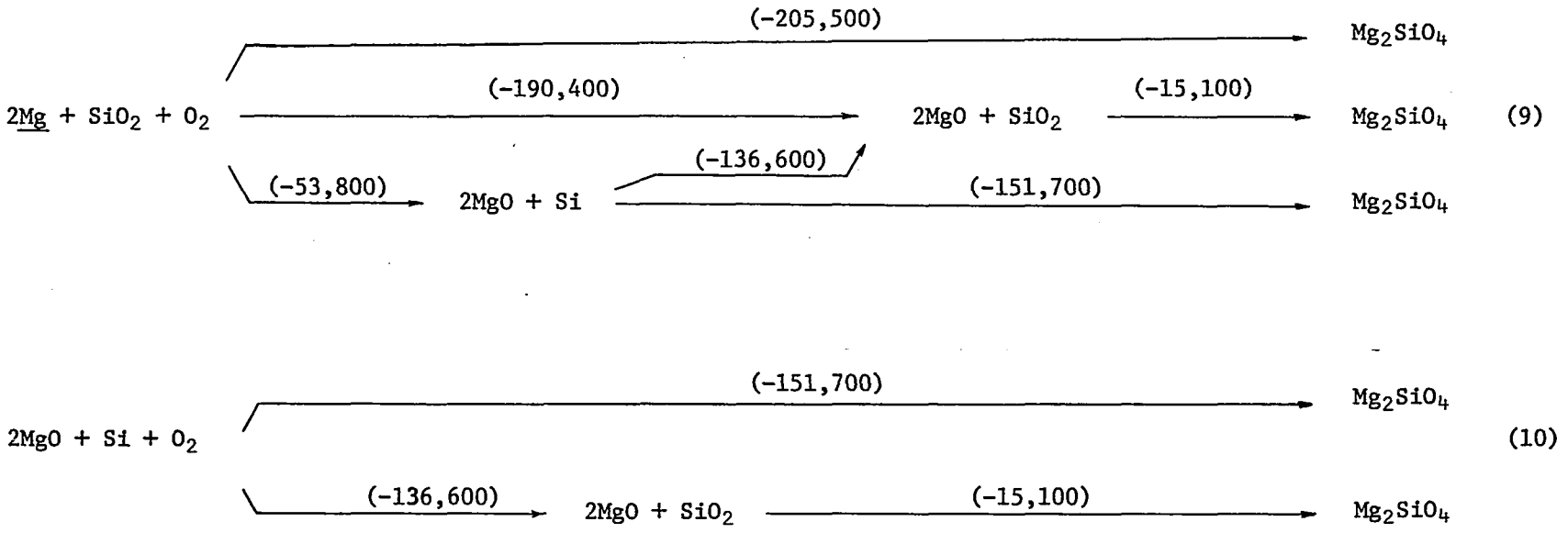
Figure 1: The equilibrium phase diagram for MgO - SiO_2.

were obtained from the data of Trojan.[24] The remaining thermodynamic data were obtained from references 25-28. Thus, the reaction between magnesium dissolved in an iron-carbon melt and SiO_2 can be rewritten in Eq. 9, (Fig. 2), as a number of possible paths by which forsterite may be formed. The free energies (in cal/g·mole) associated with each step in the reaction are shown in the parentheses for 2650°F.

The reaction between silicon and MgO can also be written with intermediate steps, Eq. 10, (Fig. 2), for pure metallic silicon at 2650°F.

Because the free energy changes associated with the single step reactions are very large, there is a strong driving force for reaction directly to forsterite. However, the single step reactions require very extensive diffusion. In order to increase the kinetics of the reaction, the reaction should instead occur in several steps, each step lowering the over-all free energy of the system (Ostwald's Rule or the rule of successive reactions).[29] Thus, in Eq. 9, the reaction between dissolved magnesium and SiO_2, silica would be reduced to MgO and silicon, the silicon would then oxidize, and finally forsterite would form. Similarly in Eq. 10, silicon would initially oxidize (since the reduction of MgO would require an increase in free energy) and subsequently react with MgO to form forsterite.

Similar diagrams of sequential reactions could be written for the formation of enstatite. The determining factors as to whether forsterite or enstatite is actually found are the local Mg/Si ratios and the kinetics of the reactions.



*An error of 2500 - 8000 cal/g·mole·is associated with each of the free energy values[25-28]

Figure 2: Possible sequences for the reactions between dissolved magnesium plus silica and for dissolved silicon plus MgO.

The steps that would be followed according to Ostwald's Rule are shown in a sequential manner in Fig. 3, where the phases present are increasingly stable going from left to right on the diagram. Regardless of the original make-up of the system, the final step would be the reaction between MgO and SiO_2 to form forsterite or enstatite. The path followed in arriving at position E in Fig. 3 depends on the original sub-system, which includes the composition of the starting materials, atmosphere, and other environmental conditions.

The main effort in this research therefore is to investigate the reactions required to go from position A (Mg, Si, O) through each of the intermediate positions and finally to position F (forsterite or enstatite) and to determine the effect of various environmental conditions on the nature and extent of each of these reactions.

II. EXPERIMENTAL PROCEDURE AND ANALYSIS

Because each of the steps in the sequence is quite different, and particularly since magnesium metal has a very high vapor pressure (greater than ten atmospheres) at the temperatures of interest, a number of different experimental techniques were required. Two primary methods and sets of equipment were used and will be described in detail here. First, the experimental procedure and the method of analysis for the reaction between magnesium and silica will be discussed. The experimental equipment for this included a pressure vessel to avoid excessive loss of magnesium due to vaporization.

Secondly, the experimental procedure and analysis for the reactions between silicon and MgO and between MgO and silica will be discussed. This work was done in a silicon carbide resistance furnace.

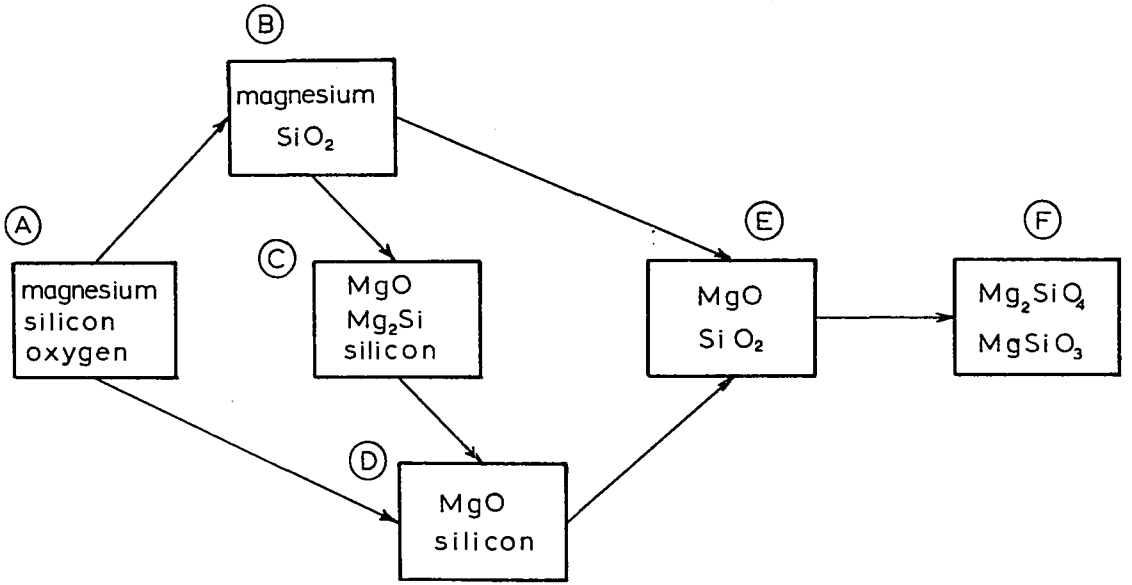


Figure 3: The sequence of the reactions in the Mg-Si-O system. The products are increasingly stable from left to right.

Variations on these techniques will be described in the text as required. The chemistry of the materials used is summarized in Appendix I.

A. Pressure Vessel Procedure

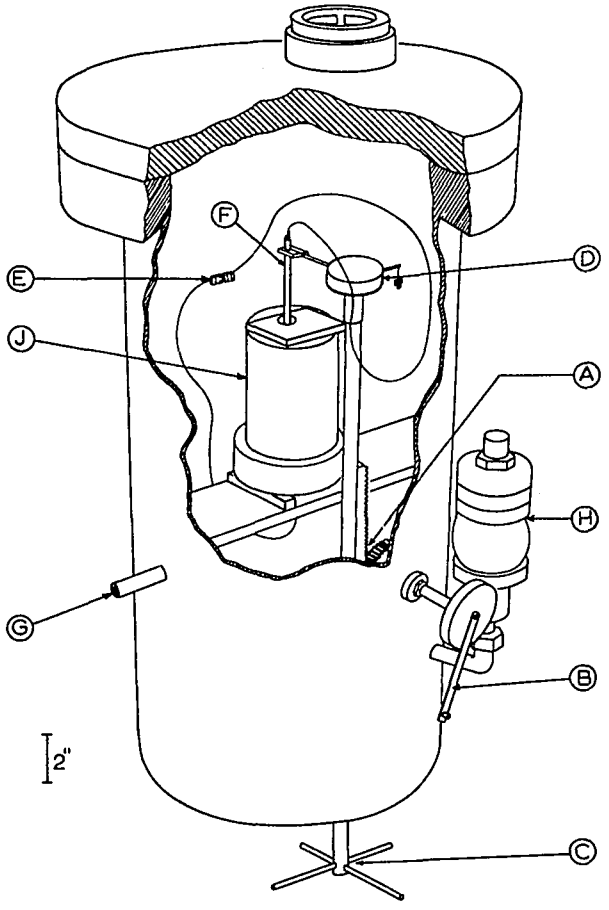
The purpose of this procedure was to investigate the reaction between dissolved magnesium and silica.

1. Description of the Equipment

To avoid the loss of magnesium through vaporization while studying the reactions involving metallic or dissolved magnesium (B → E and B → C in Fig. 3), a stainless steel pressure vessel originally built by Trojan[24] and later modified by Sponseller[30] and Guichelaar[31] was employed. The components and their arrangement in the vessel are shown in Fig. 4. The control head can be raised or lowered over a range of four inches and can be rotated through 360° by means of the rack and pinion mechanism.

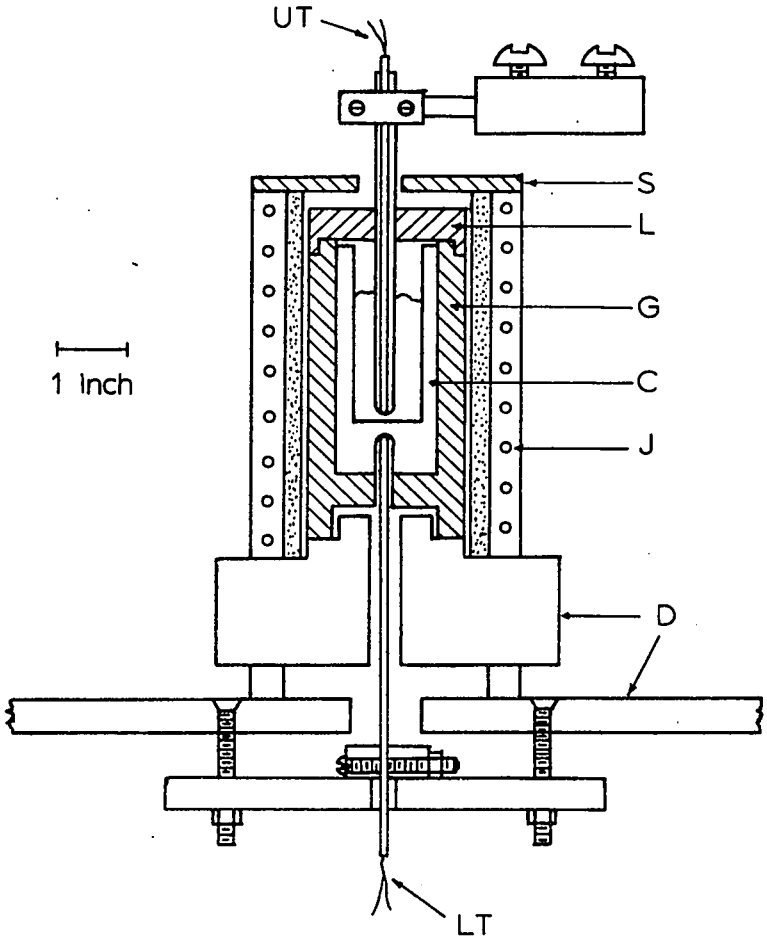
A cross-section of the critical portion of the equipment is shown in Fig. 5. The melt is contained in a graphite crucible, which is then placed in a graphite susceptor, and finally within the induction coil. An 8 mm O.D., 5 mm I.D. fused silica tube is supported by the control head and can be lowered into the melt.

Two Pt-Pt10%Rh thermocouples encased in alumina protection tubes are used to monitor the temperature. The bottom thermocouple is in the base of the crucible 1/4 inch below the melt; the upper thermocouple is located inside the silica tube, which is later lowered into the position shown. During melting, the lower thermocouple is used while attaining the desired temperature. Later the silica tube is plunged



A. Elevating Rack and Pinion Mechanism
B. Elevating Lever
C. Rotating Levers
D. Control Head
E. Thermocouple Port
F. Silica Tube
G. Argon Port
H. Safety Relief Valve
J. Induction Coil Assembly

Figure 4: Sectional view of the pressure vessel showing internal details.



S. Ceramic heat shield
UT. Upper thermocouple
LT. Lower thermocouple
J. Induction coil
C. Graphite crucible
L. Susceptor lid
G. Graphite susceptor
D. Support devices

Figure 5: Internal arrangement of the crucible, silica tube, and thermocouples in the induction coil.

into the melt and the temperature is monitored by the upper thermocouple. Because of a temperature gradient between the melt and the lower thermocouple location, the lower couple does not reflect the true melt temperature; consequently, the lower couple was calibrated versus the upper thermocouple to facilitate the attainment of the desired temperature, Fig. 6. It is important to emphasize that the measured temperature is taken to be that indicated by the upper thermocouple which is actually within the melt. The indicated temperature is estimated to be within 10°F of the true temperature.

2. The Conduct of a Typical Heat

In a typical heat, the graphite susceptor and crucible are placed within the induction coil and the lower thermocouple is put in place. The silica tube is mounted on the control head and adjusted so that after lowering the control head the bottom of the tube is 1/4 inch from the bottom of the crucible. The charge is then weighed and put in place. In general, iron-carbon-magnesium melts were prepared. The solubility of the magnesium was determined from Trojan's data[24] and the amount of magnesium added to the iron-carbon alloy was based on double the amount to be dissolved. Next the susceptor lid (L) with a 1/2 inch diameter hole in the center was put in place. Finally a ceramic heat shield (S) with a one-inch diameter hole in the center was cemented with fireclay to the top of the induction coil and the upper thermocouple was placed inside the silica tube. A graphite plug, suspended by a tungsten wire from the control head, fitted loosely into the hole on the susceptor lid to minimize vaporization and heat losses during melting. The pressure vessel was then closed.

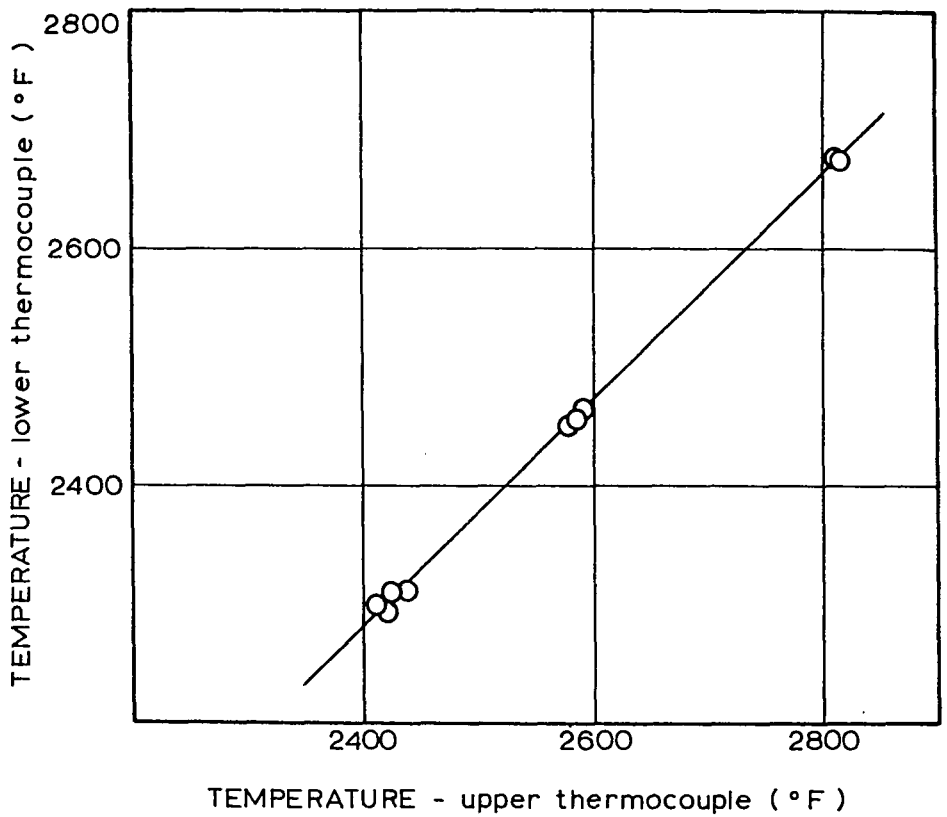


Figure 6: Calibration of the thermocouples in the pressure vessel.

The pressure chamber was evacuated to 500 microns pressure for one hour, flushed with argon gas, then evacuated again for thirty minutes. Argon was readmitted to the vessel to a pressure of 100 psig. The power was turned on and the charge heated; during the heating the argon pressure was continuously increased to the working pressure, about fifty psig above the vapor pressure of pure magnesium. The time required to attain the desired temperature was generally about ten minutes; the time to stabilize the temperature required an additional ten minutes, Fig. 7.

Once the temperature was stabilized, the graphite plug was withdrawn and the silica tube positioned and lowered into the melt. Simultaneously, a stop watch was started. The actual temperature was then measured using the upper thermocouple. The temperature was maintained for the desired time, at which point the power was turned off. About three minutes were required for the melt to solidify. After cooling to room temperature the argon pressure was exhausted, the vessel opened, and the crucible removed.

B. Analysis of the Mg-SiO_2 Reaction

The final product of a heat in the pressure vessel was a silica tube embedded in a solidified iron-carbon-magnesium melt. Before removing the sample from the graphite crucible, polyester resin was poured into the silica tube and on top of the metal to keep the silica tube from breaking during further treatment. After the resin set, the entire assembly, including melt, silica tube, and graphite crucible, was sectioned horizontally at 1/2 inch intervals to give a series of cross-sectional views of the silica tube and its interface with the melt. Without the polyester resin, the tube disintegrated during the cutting procedure.

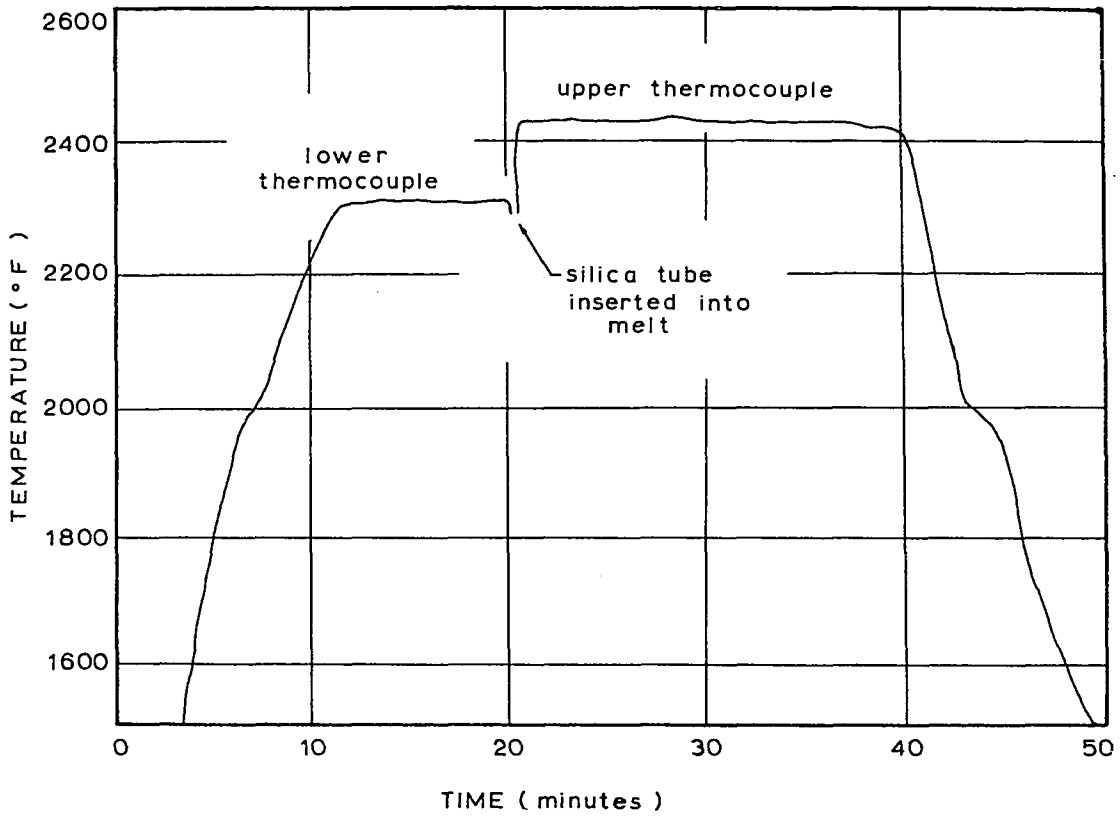


Figure 7: Time-temperature relations during the operation of the pressure vessel.

The sections were polished and macrographs were taken to record the appearance of the metal-silica tube interface. Fig. 8 shows a typical reaction zone in the silica tube.

The extent of the reaction was determined by the average penetration of the reaction zone into the silica tube. The area within the annulus of the original silica tube and the area within the rough annulus of the unreacted tube were measured with a planimeter and the reacted area determined by difference. On the basis of the original diameter of the silica tube, the average penetration (in millimeters) of the reaction zone into the tube can then be calculated from the following equation

$$P_{avg} = r_o - \sqrt{r_o^2 - (r_o^2 - r_i^2)A_r/A_o} \qquad (11)$$

where P_{avg} is the average penetration of the reaction zone into the tube, r_i and r_o the inner and outer radii of the silica tube, and A_o and A_r the initial and reacted areas of the tube. Generally r_o was 4 mm, r_i was 2.5 mm, and A_o was 30.6 mm^2. The derivation of this equation appears in Appendix II.

This procedure was repeated for each of the experiments encompassing a range of exposure times and temperatures. The penetration could be determined as a function of the depth below the surface of the melt as well as above the melt showing the effect of the vapor on the reaction.

Finally, the nature of the reaction zone was determined by removing portions of the reaction products from the tube and obtaining Debye-Scherrer x-ray diffraction patterns from the phases present. In addition, the microstructures of the polished specimens were observed using standard metallographic procedures.

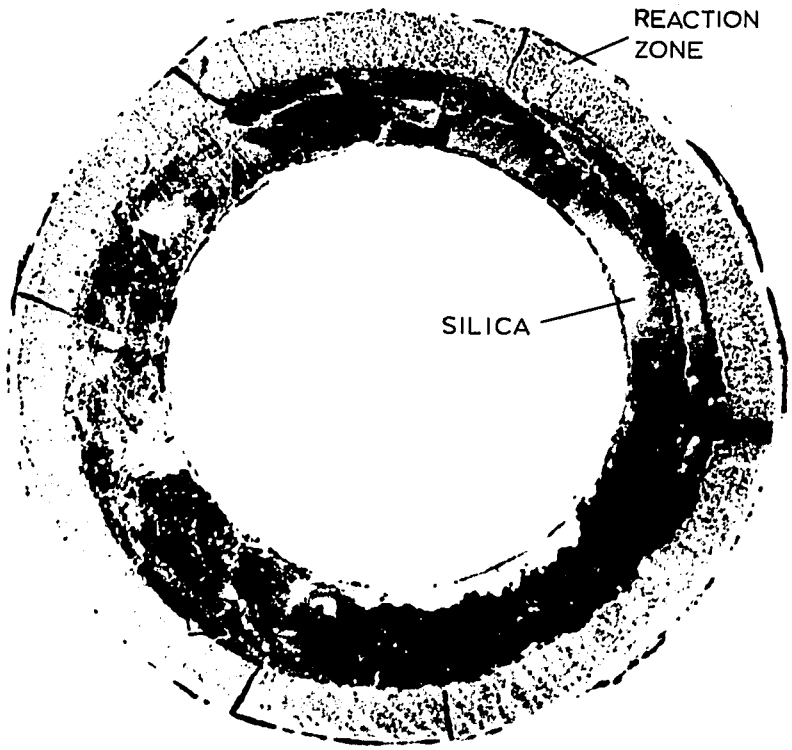


Figure 8: Typical section showing the reaction zone in a silica tube immersed in carbon and magnesium-saturated iron after 10 minutes at 2800°F. Initial tube diameter - 8mm.

C. Powder Compact Procedure

The reactions between MgO and silicon and between MgO and SiO_2 were investigated by mixing fine powders (-270 mesh) of the constituents in the desired composition, compacting them under pressure, and firing the compacts isothermally at high temperatures.

1. Preparation of the Powder Compacts

The powders were weighed on a balance scale and mixed in a roll mill for one to two hours. Then acetone was added and mixing continued by hand until the acetone had almost entirely evaporated. The mixture was placed in a Buehler metallurgical mounting press and compacted to 10,000 psi to produce disks 1 1/4 inches in diameter by 1/4 inch thick. These disks were cut into 1/4 inch cubes and were allowed to dry thoroughly.

The extent of the reaction was found to be relatively insensitive to the degree of compaction. As an example, MgO - SiO_2 powder compacts produced with different compaction pressures were fired and the forsterite formation followed as a function of time, Fig. 9. Very little change in reaction rate with compaction pressure was observed.

2. The Experimental Resistance Furnace

All powder compacts were fired in a vertical silicon carbide resistance furnace, shown in Fig. 10. The furnace had a 36" x 36" x 20" steel shell lined with insulating and refractory brick and was heated by four silicon carbide resistance elements. A double mullite tube arrangement was used to contain the desired atmosphere. The outer mullite tube (3 1/2 inches I.D., 4 inches O.D.) was sealed at the bottom with Glyptal cement to a brass plate; this plate also separated the inner mullite

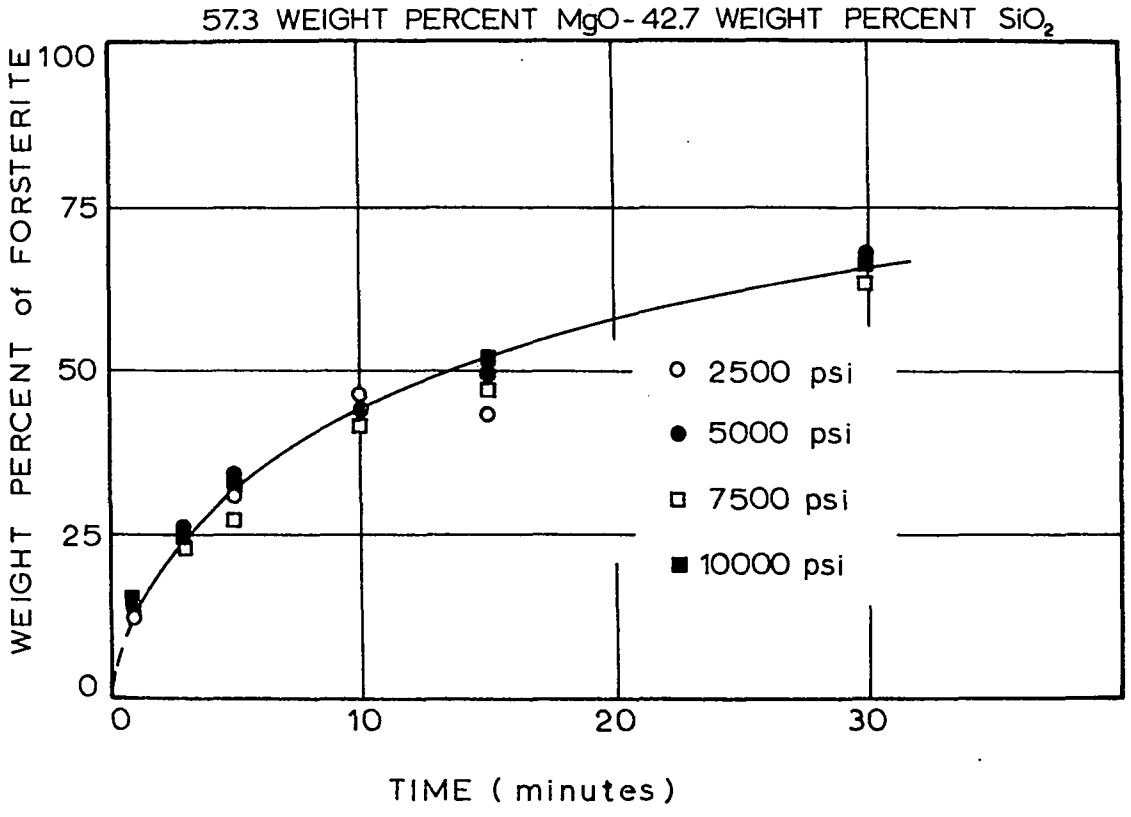


Figure 9: The effect of initial compaction pressure on the solid state reaction between 57.3 wt% MgO and 42.7 wt% SiO_2. Exposure temperature - 2400°F.

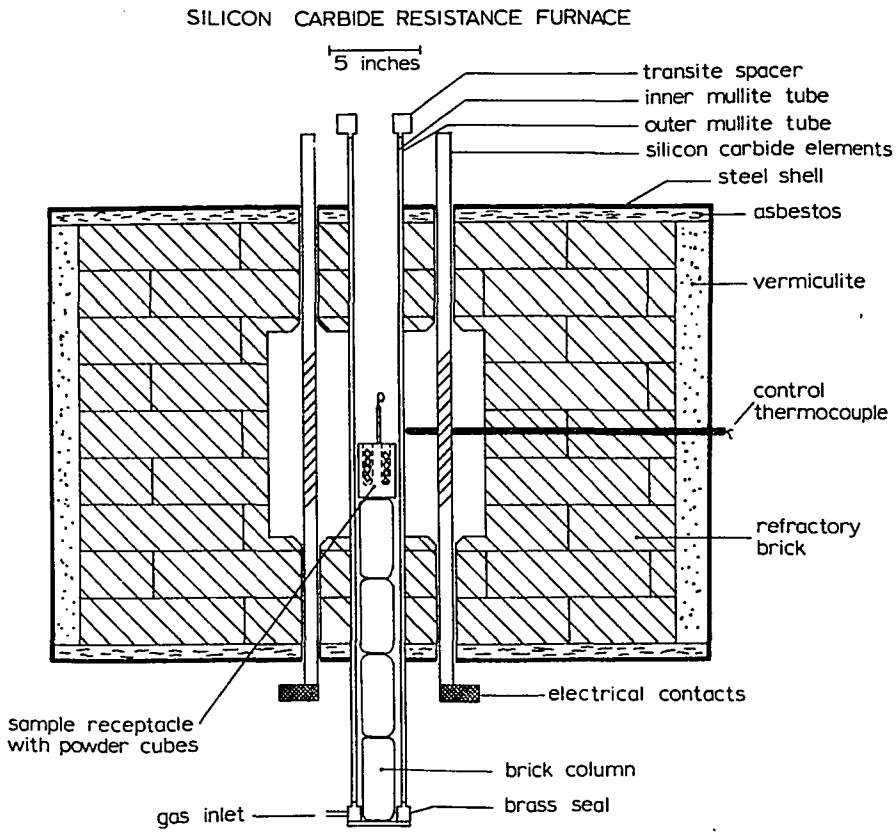


Figure 10: Cross-sectional view of the silicon carbide resistance furnace.

tube (2 7/8 inches I.D., 3 inches O.D.) from the outer tube. Both inner and outer tubes were impervious to the atmosphere.

The power input (20 amps maximum at 240 VAC) was regulated by a variable transformer and controlled by a proportional temperature controller activated by a Pt-Pt10%Rh control thermocouple. The hot zone of the silicon carbide elements was eleven inches; however, only the central portion of this zone was used because of temperature gradients at the ends.

3. The Sample Receptacles

The receptacles for the powder compact cubes were made from either graphite or castable alumina, depending on the atmosphere used. In an argon atmosphere, a graphite cylinder with six or seven 1/2 inch diameter by 1 1/2 inches deep holes was used. A tungsten hook encased in an alumina protection tube was used to raise and lower the assembly into the working area of the furnace. In air atmospheres a castable alumina receptacle was constructed by pouring the wet slurry into a two-inch diameter mold and placing solid paper cylinders 1/2 inch in diameter by 1 1/2 inches deep into the top. After setting, the receptacle was fired at 500°F and the paper cylinders burned, leaving holes in the alumina receptacle. Additional holes were drilled in the side of the receptacle to facilitate insertion and removal from the furnace.

4. The Typical Conduct of a Heat

In the usual heat the furnace was stabilized at the desired temperature, the atmosphere was established, and the appropriate receptacle was lowered into the furnace to rest on a column of bricks

supported by the brass seal at the bottom of the mullite tube. The height of the bricks was pre-adjusted so that the receptacle was centered in the hot zone.

After the receptacle was inserted, the temperature of the furnace was re-established and stabilized. Powder cubes were then dropped into one of the holes in the receptacle by means of a long vycor tube held over the proper hole. Simultaneously, a mechanical clock was started. The temperature of the cubes was followed by an optical pyrometer and checked occasionally by lowering a Pt-Pt10%Rh thermocouple encased in a powder cube into one of the holes. The two temperature measurements agreed to within 10°F on all occasions. At pre-determined time intervals, cubes were inserted into the other holes in the receptacle until all holes were filled. Generally, these were spaced over a period of one hour. Finally the entire receptacle was removed from the furnace and the receptacle quenched in water to cool the powder compacts quickly. Care was taken to insure that water only contacted the receptacle and did not touch the compacts.

Fig. 11 shows the composite curve for the rate at which the powder compacts heat immediately after insertion into the receptacle (held at 2400°F). From 60 to 100 seconds are required for the mass to heat within 5°F of the final temperature. In an effort to heat the cubes more quickly, a single cube with a thermocouple embedded in its center was lowered into the furnace (Fig. 11). Again 60 seconds or more were required to reach within 5°F of the final temperature, so that there is little difference between the two methods. This was subsequently confirmed by determining the extent of the reaction by each method.

The cooling rates were found to be from 70 to 90°F/second, depending on the starting temperature.

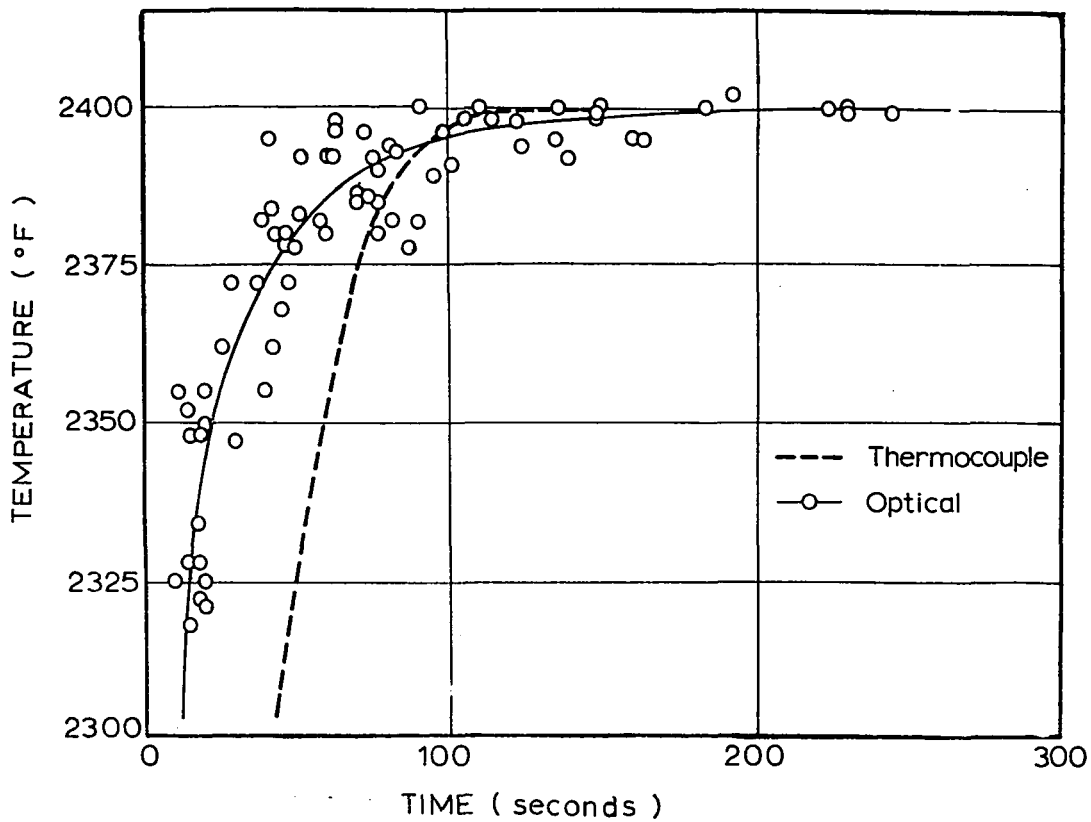


Figure 11: The heat-up rate for the powder compacts, measured with optical pyrometer and with a thermocouple embedded in the center of the specimen. Ambient temperature - 2400°F.

D. Analyzing the Composition of the Powder Compacts

The results of a single experiment using the powder compacts yield a series of compositions as a function of time at a given temperature and composition. One cube for each time interval was removed, impregnated with resin to reduce the friability of the sample and mounted and polished to retain a record of the microstructure. The remainder of the sample was analyzed quantitatively by x-ray diffraction[32] to determine the amounts of the crystalline phases present after each exposure time in a single experiment. Thus, for each experiment up to seven samples were prepared for x-ray analysis.

Each sample was crushed and ground to -270 mesh and then carefully weighed. Next 10% by weight of sodium chloride was added and the mixture was blended by hand. A small amount of Duco cement and acetone was added as a binder and thoroughly blended with the mixture until the mixture was nearly dry. Finally, the mixture was spread onto a one-inch diameter aluminum sample holder and allowed to dry. Excess sample was removed by scraping the surface with a razor blade.

A Norelco vertical goniometer x-ray diffraction unit was used for the quantitative analysis. Nickel-filtered copper radiation was used throughout. The goniometer was rotated at 1° (2θ) per minute and the x-ray trace recorded by a strip chart recorder running at two inches per minute. Strong diffraction peaks for each phase were used, since it was desired to detect small amounts of each phase whenever they were present.

The peaks traversed for each phase are listed in Table I.[33]

TABLE I

X-RAY DIFFRACTION DATA

Phase	Miller Indices	2θ	d-value
α-cristobalite (SiO_2)	(101)	21.94	4.05
α-quartz (SiO_2)	(101)	26.66	3.343
forsterite (Mg_2SiO_4)	(021)	22.92	3.88
enstatite ($MgSiO_3$)	(240),(221)	28.17	3.167
periclase (MgO)	(200)	42.86	2.11
sodium chloride (NaCl)	(200)	31.72	2.821

The integrated intensity, or the area under each diffraction peak, was determined by a planimeter and the ratio of the intensity of the oxide phase to that of the sodium chloride was calculated.

Calibration curves were determined for each phase by mixing various combinations of pure oxide materials with 10 weight percent sodium chloride, measuring the integrated intensity of each peak and forming the intensity ratio for each oxide phase with sodium chloride. The calibration curves were then plotted as intensity ratios versus weight percent oxide phase in the mixture. Consequently, the calculated ratios obtained from each of the fired samples could be used to determine directly the amount of each phase in weight percent. The calibration curves are shown in Fig. 12.

The intensity ratio yields the same percentage of a given phase regardless of the type of accompanying material,[32] as demonstrated in Fig. 13 where mixtures were prepared containing iron, iron oxide, CaO, and glass. The same calibration curves for MgO and quartz were found regardless of the other phases present.

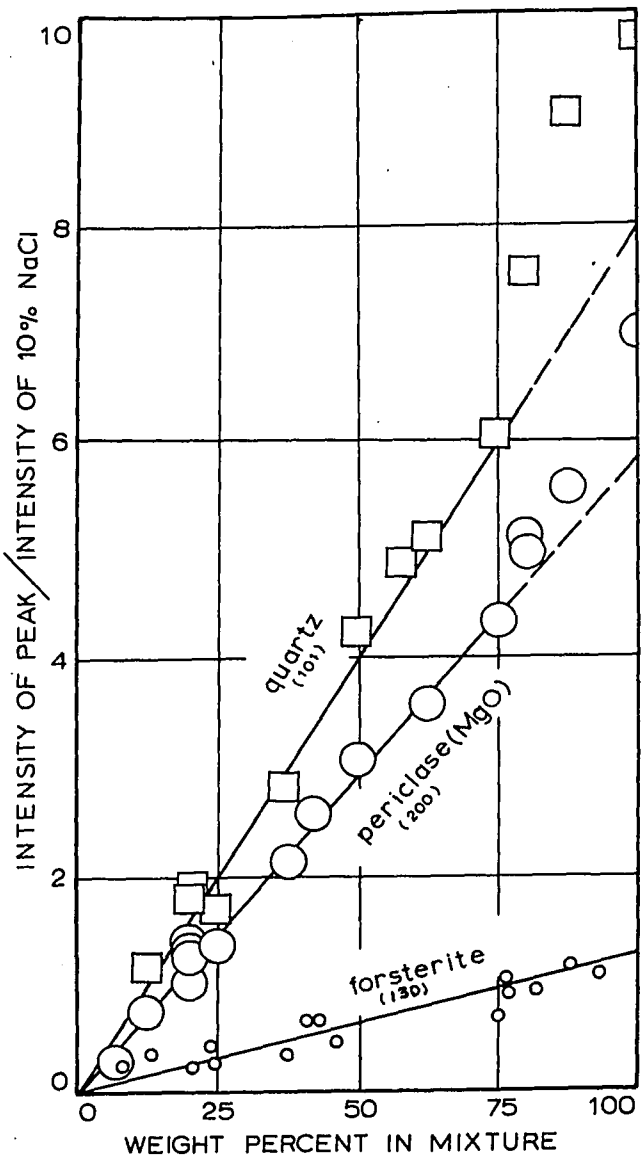


Figure 12: X-ray diffraction calibration curves for MgO, quartz, and forsterite.

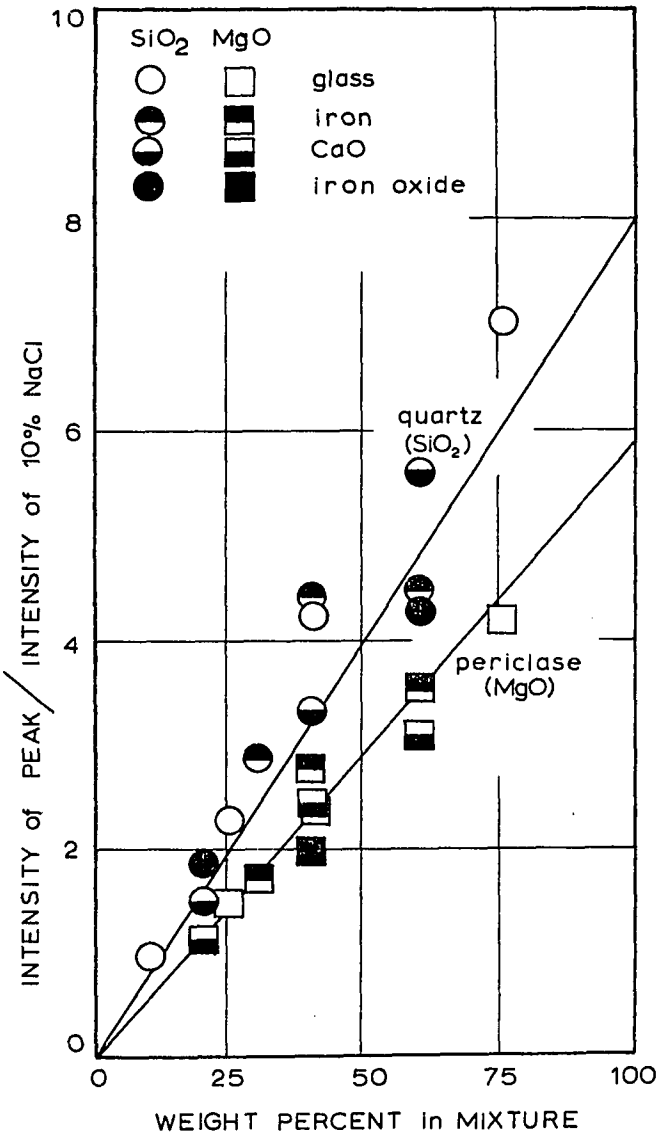


Figure 13: The effect of the accompanying material on the calibration curves for MgO and quartz.

Thus, for each experiment, a plot similar to Fig. 14 was produced, showing the increasing amount of reaction products and the decreasing amounts of reactants at 2450°F for a composition of MgO and SiO_2 powders such that the equilibrium phase is stoichiometric forsterite. Similar curves could be drawn for each temperature and composition studied in this investigation.

Brindley and Hayami[21] found that these data could be represented by a straight line (particularly when the reaction was less than 80 percent complete) when the data were plotted as $D(\alpha)$ versus time. Here α is the weight fraction of the reaction product divided by the equilibrium weight fraction of the reaction product and the function $D(\alpha)$, determined theoretically by Ginstling and Brounshtein,[22] is given by

$$D(\alpha) = (1 - \tfrac{2}{3}\alpha) - (1 - \alpha)^{2/3} \qquad (12)$$

Fig. 15 demonstrates the validity of this approach for the data in Fig. 14. Furthermore, a rate constant K can be calculated from the slope of this straight line by the use of the following equation

$$D(\alpha) = \frac{K}{R^2}t \qquad (13)$$

where R is the particle radius (60 microns) and t is the time. Therefore, by measuring the slope of the straight line in Fig. 15 and multiplying the slope by the value of R^2, the rate constant K can be calculated for each temperature and composition.

Finally, for a single composition the plot of the logarithms of the rate constants versus reciprocal temperature gives a straight line whose slope is related to the activation energy for the reaction.

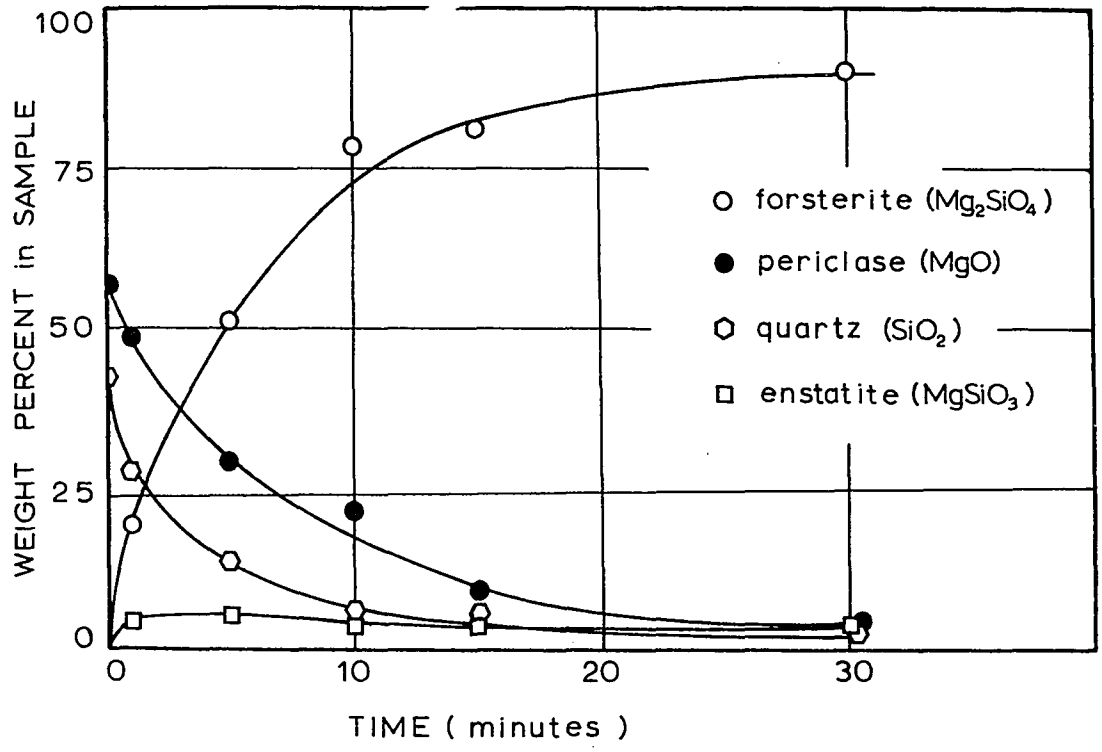


Figure 14: A typical curve for the reactants and reaction products during firing of a 57.3 wt% MgO - 42.7 wt% SiO_2 powder compact at 2450°F.

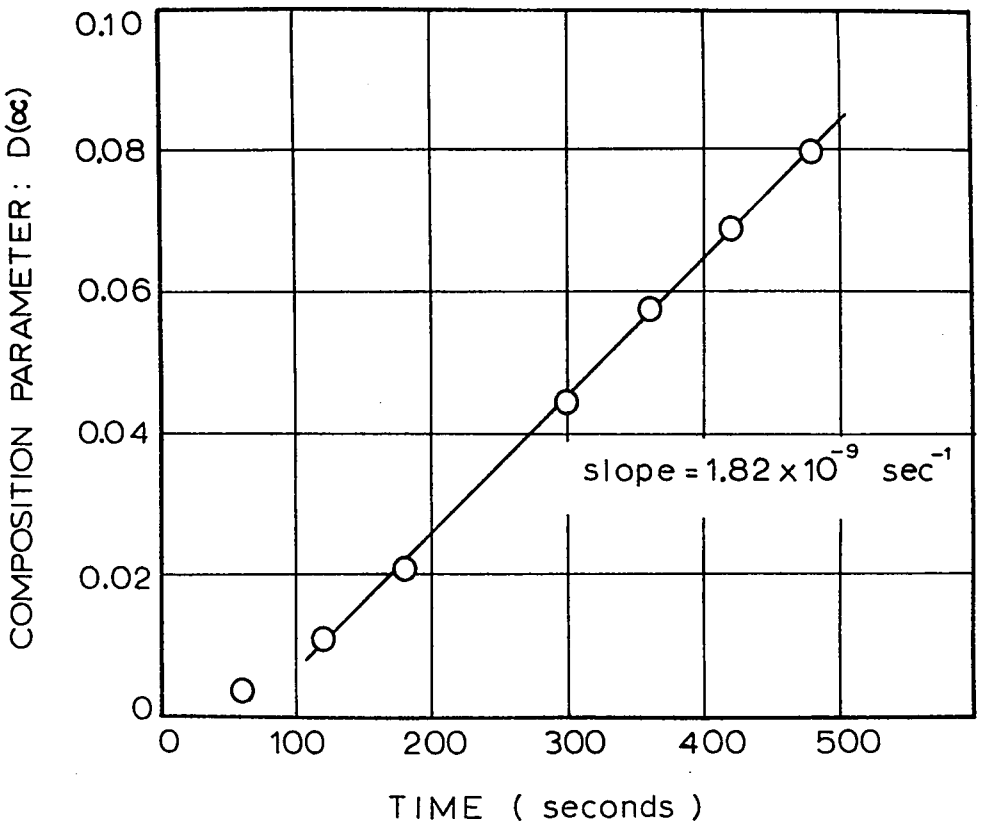


Figure 15: The composition parameter D(α) versus time for the formation of forsterite from a 57.3 wt% MgO - 42.7 wt% SiO_2 powder compact at 2450°F.

RESULTS AND DISCUSSION

The importance of the reactions in the magnesium-silicon-oxygen system has been pointed out in the discussion in the literature review. A number of reactions were proposed by which magnesium, silicon, and oxygen might combine to form the constituents commonly found in dross. The results of the experiments in which these reactions were investigated will be discussed in the following sections. The order in which they will be presented is given below:

I. The Formation of SiO_2

II. The Formation of MgO

III. The Reactions between Magnesium and SiO_2

IV. The Reactions between Silicon and MgO

V. The Reactions between MgO and SiO_2

The discussion will focus on the products of each reaction, the rate at which the reactions occur, and the effect of environmental conditions on the nature of the reactions. Finally, it will be demonstrated that the sequence of reactions presented in Fig. 3 as a result of the application of Ostwald's Rule is the actual sequence which occurs in the Mg-Si-O system.

The initial step in the sequential reactions must be the oxidation of magnesium or silicon. This oxidation will then provide MgO and SiO_2 by which further reactions between the oxides and between the oxides and metal can occur.

The oxygen will be present dissolved in the melt, combined in oxides (usually silica) in the refractories and suspended particles in the melt,

and as a gas in the atmosphere or trapped in the refractories and molding materials. This oxygen is available to oxidize the magnesium or silicon as they are introduced into the melt.

I. FORMATION OF SiO_2

Silicon can be oxidized from the melt, which contains from one to two percent silicon, and from the nodularizer and post-inoculant alloys, where silicon is found as magnesium silicide, iron silicides, and pure silicon. The ease with which the silicon is oxidized depends on the environmental conditions to which it is exposed. The most important factor is the CO/SiO_2 inversion temperature, which can be affected by metal chemistry, atmosphere, refractory, and the nature of the melting unit. Factors which lower the inversion temperature minimize the formation of silica in nodular iron.

A. Oxidation of Silicon from Iron-Carbon-Silicon Melts

It was stated in the literature review that under equilibrium conditions there exists a CO/SiO_2 inversion temperature below which silica is stable but above which the silica is reduced by the carbon in the melt. However, Orths[34] has observed that up to 120°F supercooling below the inversion temperature is required before the oxide film appears. Other investigators[35-38] have observed that the inversion temperature during cooling depends on the composition of the melt, notably manganese and sulfur. The inversion temperature increases with increasing sulfur and silicon contents and decreases with increasing carbon and manganese. The chemistry changes affect the activity of the carbon and silicon in the melt, thereby influencing the equilibrium constant, which finally determines the equilibrium inversion temperature.

The composition of the resulting oxide film is iron oxide plus silica (50 to 60 percent FeO and 40 to 50 percent SiO_2), although when the manganese level is high and the temperature is below 2370°F manganese cations can begin substituting for the iron cations.

Two types of slags associated with the presence of silica have been described.[39-41] A fluid slag nucleates first and remains near the center of the melt surface while the second, which nucleates at lower temperatures, forms at the ladle walls and is more viscous and perhaps solid. It appears that the second type is high in sulfur while the first is primarily a silicate slag.

Several experiments were made during the course of this research to determine the temperature at which the oxide film occurs under the conditions prevailing in this laboratory. One series of observations was obtained in a monolithic alumina-lined sixty-pound capacity induction furnace, while other observations were made on melts in a ten-pound capacity induction furnace lined with a pure magnesia crucible. The cast iron was cyclically heated and cooled through the temperature range 2300 to 2700°F with the temperature continuously monitored by a Pt-Pt10%Rh thermocouple. The temperature at which the film first appeared on cooling and began to disappear on heating was noted. The results appear in Table II.

TABLE II

EXPERIMENTAL CO/SiO_2 INVERSION TEMPERATURES

Melting Conditions	Melt Chemistry*	Apparent Inversion Temperature	
		Cooling	Heating
Air atmosphere (alumina lining)	3.6%C 1.6%Si	2510-2590°F	2590°F
Air atmosphere (MgO crucible)	3.4%C 1.7%Si	2455-2515°F	2485-2535°F
Argon atmosphere (MgO crucible)	3.4%C 1.7%Si	2350-2450°F	2315-2365°F

*The melts also contain 0.40%Mn, 0.017%P, and 0.016%S.

Two types of slags are observed in the experiments using the air atmosphere, in agreement with Dahlmann and Loeberg.[42] Whereas the average temperature at which the fluid slag film initiates on cooling is 2490°F, that for the more crusty film initiates at an average temperature of 2425°F. The first type contains hematite (Fe_2O_3), magnetite (Fe_3O_4), silica, and a solid solution $(Fe,Mn)_2SiO_4$ phase; only magnetite and the $(Fe,Mn)_2SiO_4$ are observed in the second type.

The second type of slag film, the crusty type, is not observed during cooling under the argon atmosphere, although the first type of fluid slag is obtained and is identical to that observed in air.

The inversion temperature is defined thermodynamically by the intersection of the free energy versus temperature curves for the following two equations:

$$\underline{Si} + 2\underline{O} = SiO_2 \qquad (14)$$

$$\underline{C} + \underline{O} = CO \qquad (15)$$

The free energies associated with these reactions are plotted in Fig. 16, with the data obtained from references 43 and 44. An alternate method of determining the equilibrium inversion temperature is by the equation[45]

$$SiO_2 + 2\underline{C} = \underline{Si} + 2CO \qquad \log K = \frac{-27,486}{T} + 15.47 \qquad (16)$$

where

$$K = \frac{(a_{Si})(P_{CO})^2}{(a_{SiO_2})(a_C)^2} = \frac{[\%Si]}{[\%C]^2} \quad P_{CO} = 1 \text{ , } a_{SiO_2} = 1 \qquad (17)$$

The inversion temperature predicted by thermodynamic equilibrium is therefore 2565°F. When melting in air in the alumina-lined induction furnace, the apparent inversion temperature, ranging from 2510 to 2590°F, agrees quite well with the equilibrium temperature.

However, as can be observed in Fig. 16, the inversion temperature obtained in the magnesia crucible-lined induction furnace is less defined. A wide temperature range is observed during which the silica film starts to form during cooling and begins to disappear during heating. The temperature at which the surface is completely covered (during cooling) or completely clear (during heating) is even more variable. The temperatures are generally considerably below the equilibrium inversion temperature, particularly in the argon atmosphere.

There appears to be a difference in the inversion temperature for alumina and magnesia linings. In fact, a difference is expected because of the well-known effect of refractory on the oxygen solubility in iron alloys.[46] A number of other factors, including the porosity of the lining, reaction between the silica film and the lining, the surface area to volume ratio of the furnace, the intensity of the inductive stirring of the melt, and the heating and cooling rate of the melt, will all exert an influence on the apparent inversion temperature, even though thermodynamically the equilibrium inversion temperature is not greatly affected. These factors are so inter-related that the effect of each on the apparent inversion temperature cannot be separated without a prolonged series of investigations.

Most important, however, is that an inversion temperature does exist and silica is available on the surface of the melt in the temperature range 2350 to 2600°F. Because this temperature range is included in the processing history of nodular iron and the pouring temperature of nodular iron is frequently between 2500 to 2600°F, the inversion phenomenon can contribute to dross formation by providing necessary silica.

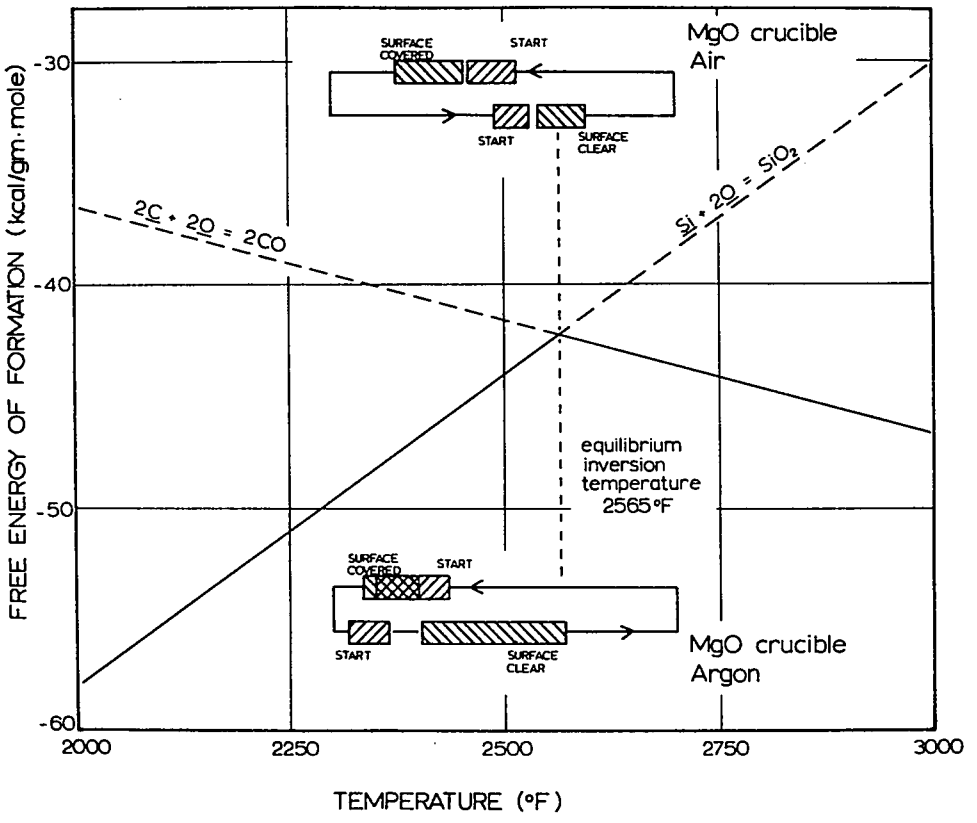


Figure 16: Schematic diagram showing thermodynamic equilibrium and the critical temperature ranges for the CO/SiO_2 inversion temperature in air and argon atmospheres.

B. Oxidation of Silicon from Iron Silicides

Pieces of silicon and commercial 75% ferrosilicon alloy were exposed in air at elevated temperatures above and below the melting points and the surfaces examined. Very little oxidation of the silicon occurred because, as described by Baker,[14] a passive silica film forms in high silicon irons, preventing extensive oxidation. Large amounts of oxide can then only be found if the particles of silicon or silicon compounds are very small so that there is more surface area exposed to the atmosphere.

In summary, several sources of silica are available in nodular iron. Silica can first be introduced by the refractory and mold materials. Secondly, the high silicon inoculant alloys may oxidize as they are added. Most important, silica can form as a consequence of the CO/SiO_2 inversion phenomenon.

The temperature at which inversion occurs can be affected by the melt composition, atmosphere, type of melting unit, type of refractory, heating and cooling rate, and intensity of stirring. In general, the observed inversion will occur somewhere between 2350 and 2600°F, while 2565°F is predicted under equilibrium. The silica produced as a consequence of the inversion phenomenon will then be available to enter into the dross reactions.

II. FORMATION OF MgO

Magnesium is present in the environment of the melt as a compound in the nodularizer, as dissolved in the iron melt, or as a vapor phase in and just above the melt. The magnesium may either vaporize or oxidize, and the oxidation occurs more readily than the oxidation of silicon due to the larger negative free energy of formation of MgO.

In this section, the oxidation of the magnesium compounds in the nodularizer will be investigated. Next, the over-all loss of magnesium from the melt will be followed and found to depend on temperature, nodularizer, refractory, and atmosphere. Finally, an estimate of the amount of magnesium lost through oxidation as compared to vaporization will show that most of the magnesium is lost by vaporization.

A. Oxidation of Magnesium Silicide

The decomposition of the magnesium compounds in the nodularizer occurs very rapidly. As an index of this instability, small pieces of Mg_2Si (found in the magnesium ferrosilicon alloys) were placed in the silicon carbide resistance furnace at 2475°F and held in an air atmosphere. Combustion began almost immediately with blue flames appearing intermittently for about one minute. The specimens, removed after one minute, showed that the Mg_2Si had totally disappeared and only MgO and silicon metal remained. A large weight loss indicated that much of the magnesium had departed as a vapor. No forsterite was observed after such short times. Similar results were obtained with pieces of a commercial magnesium ferrosilicon nodularizing alloy.

Therefore, the first step during nodularization is the complete oxidation or vaporization of magnesium. No SiO_2 or Mg_2SiO_4 can form until all of the magnesium is reacted. When the experiments with the

Mg_2Si were continued for longer periods of time (up to one hour), the silicon metal began to oxidize. However, there was poor contact between the two oxides and no forsterite was observed.

The same type of behavior should occur in nodularization, although the silicon can begin to oxidize as the magnesium content becomes depleted in local regions, particularly at the surface when the melt is not vigorously stirred.

B. Magnesium Loss Rates from Nodular Iron

It is difficult to assess how much magnesium is lost through oxidation as compared to vaporization. However, the total loss of magnesium can be determined from the chemistry of the melt and this is found to be dependent on a number of environmental conditions. In the literature survey, the loss of magnesium during the nodularization treatment itself was cited as being dependent on the chemistry of the nodularizer and post-inoculant alloys. The subsequent rate of magnesium loss during holding depended not only on the nodularizer and post-inoculant but on the temperature as well.

These observations have been verified and other parameters investigated in the present work by a variety of techniques. These techniques include:

1. One-Pound Melts--The Effect of Atmosphere and Refractory

Small one-pound melts of cast iron containing 3.48 - 3.91% carbon, 2.23 - 2.9% silicon, 0.40 - 0.50% manganese, and 0.010 - 0.025% sulfur were nodularized by a plunging technique.

The experimental apparatus is shown in Fig. 17. A graphite bell was machined; the stem of the bell fit through a graphite splash plate

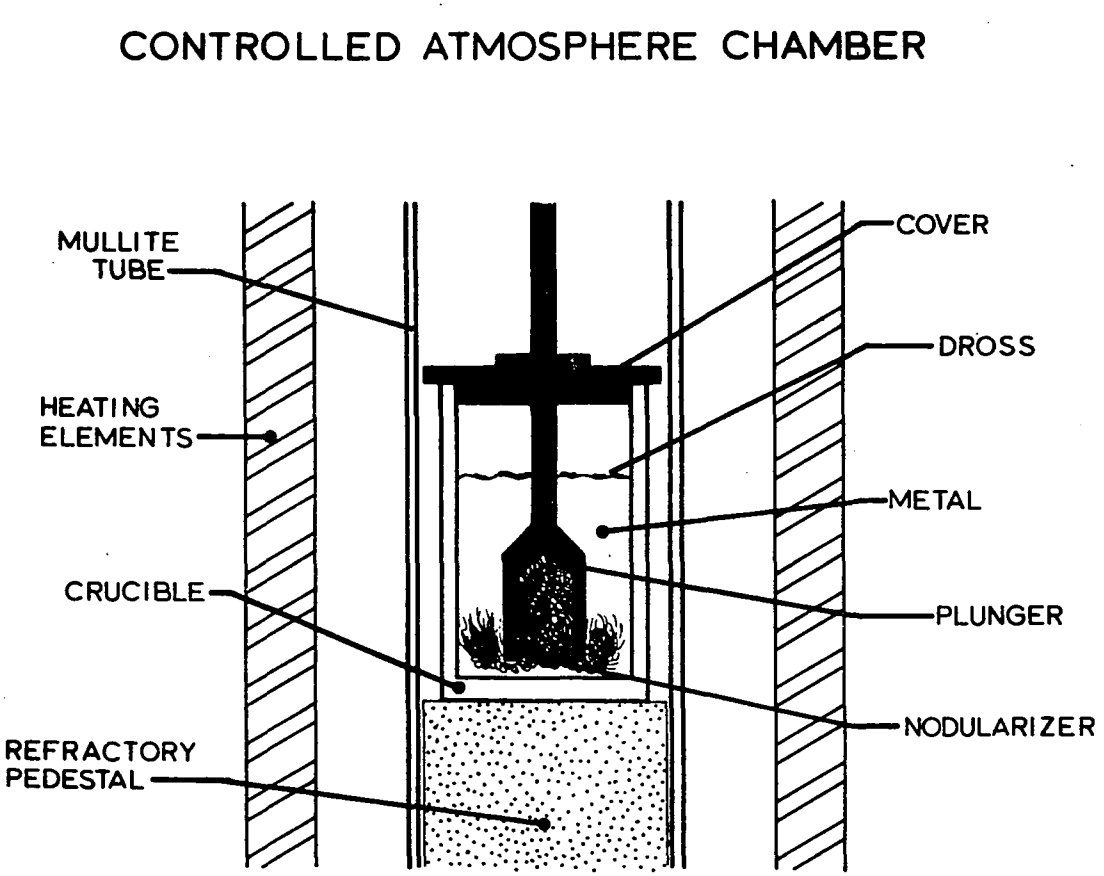


Figure 17: Schematic diagram showing the plunging apparatus in the silicon carbide resistance furnace.

which fit over the top of the crucible and provided a seal to prevent iron from splashing out during nodularization.

The nodularizing alloy (see Appendix I for analysis) was weighed so that 0.15% magnesium was added, wrapped in iron foil, and wedged into the bell. A pin in the stem was positioned so that pressure could be maintained to keep the splash plate in place, while the bottom of the bell was just above the bottom of the crucible. Finally, a steel rod attached to the end of the stem allowed the bell to be lowered into place, held during treatment, and removed. No post-inoculant was added.

Melting was achieved in the silicon carbide resistance furnace (Fig. 10); thus, either an air or argon atmosphere could be maintained. Crucibles rested on a column of bricks inside the mullite tube.

Metal samples were removed as a function of time with a vycor suction tube and a dross sample was occasionally removed by dipping a molybdenum mesh screen into the melt and picking up the dross.

2. Five-Pound Melts--The Effect of Nodularizer

A second series of heats in a ten-pound magnesia-lined induction furnace with an air atmosphere was run. Different nodularizing alloys were added to a cast iron of composition 3.6% carbon, 0.40% manganese, and 2.2% silicon. A plunging technique similar to that discussed in the previous section was used and will be described in more detail in "Engineering Aspects." No post-inoculant was added.

3. One Hundred-Pound Melts--The Effect of Holding Temperature

A final series of melts was produced in a 100-pound alumina-lined induction furnace using 9%MgFeSi for the nodularizer and one-half percent silicon as 75% ferrosilicon for the post-inoculant. The

nodularizer and post-inoculant were added by the transfer technique (see "Engineering Aspects"). The chemistry of the melt was 3.9%C, 2.5%Si, and 0.40%Mn. After treatment, the melts were held in the furnace at different temperatures.

The results are found to follow a first order rate equation given by

$$Mg_o = Mg\exp(Kt) \qquad (18)$$

where Mg_o is the original magnesium content at zero time and t is the time, which is taken to be zero when the first chemistry sample is obtained. The results for each series of heats are plotted in Figs. 18 to 20 in accordance with Eq. 18, and the rate constants are noted.

4. Discussion of the Magnesium Loss Rates

A number of conclusions can be drawn from these data concerning the loss of magnesium during holding after treatment.

a. Both Figs. 18 and 19 show that the cerium-bearing magnesium ferrosilicon results in a low magnesium loss rate under comparable conditions, probably because the cerium may partially substitute for magnesium during deoxidation and desulfurization of the melt. However, overall there is relatively little difference between the magnesium loss rates when different nodularizers are used. The effect is small compared to the effects of atmosphere, refractory, and temperature.

b. MgO and Al_2O_3 crucibles generally result in lower magnesium loss rates than silica crucibles because neither magnesium nor MgO will react appreciably with either crucible at the nodularizing and holding temperatures. The data from the silica crucibles suggest that a reaction

(1) SiO_2; MgFeSi; Argon; 2650°F; k=0.28 min.$^{-1}$

(2) MgO; MgFeSi; Air; 2665°F; k=0.11 min.$^{-1}$

(3) SiO_2; CeMgFeSi; Argon; 2600°F; k=0.087 min.$^{-1}$

(4) SiO_2; MgFeSi; Air; 2675°F; k=0.083 min.$^{-1}$

(5) Al_2O_3; MgFeSi; Argon; 2600°F; k=0.053 min.$^{-1}$

(6) MgO; MgFeSi; Argon; 2680°F; k=0.039 min.$^{-1}$

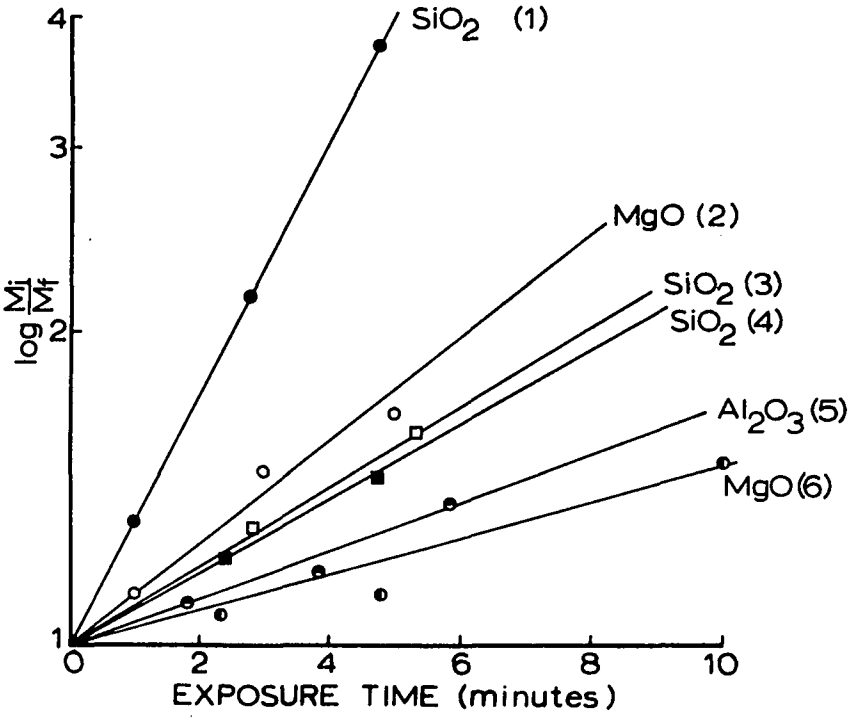


Figure 18: Magnesium loss rates in one-pound melts as affected by atmosphere and refractory. 0.15%Mg added at 2750°F, no post-inoculant. Mg_i = original Mg content.

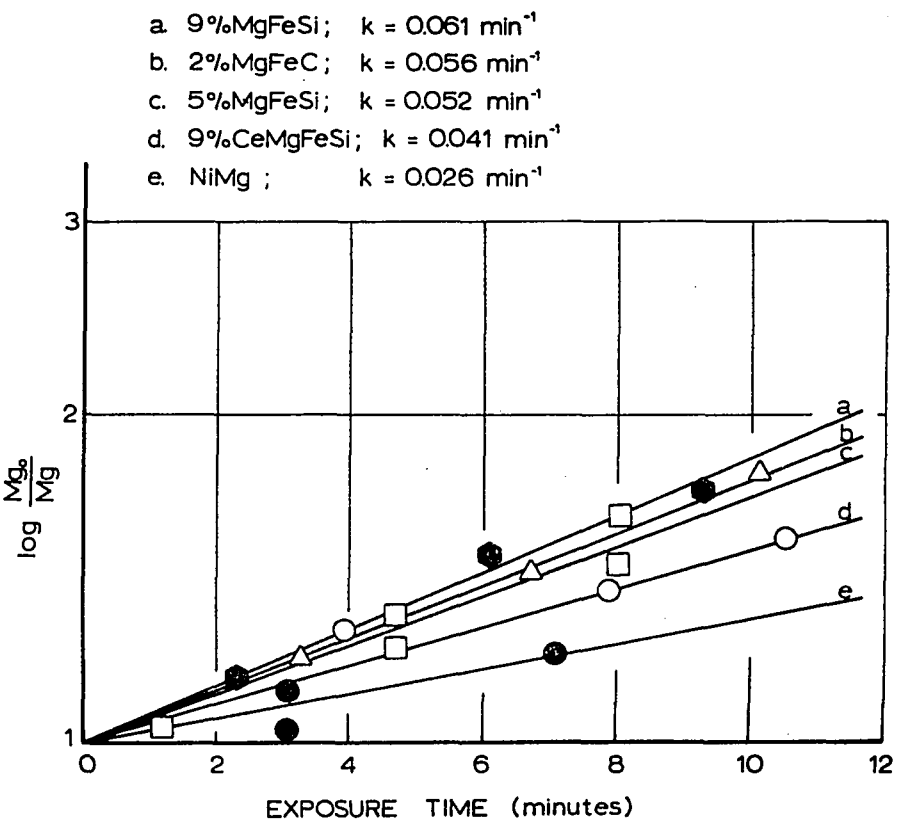


Figure 19: Magnesium loss rate in five-pound melts as affected by nodularizer. 0.15%Mg added at 2750°F; no post-inoculant; held at 2500°F in air atmosphere. A MgO crucible was used.

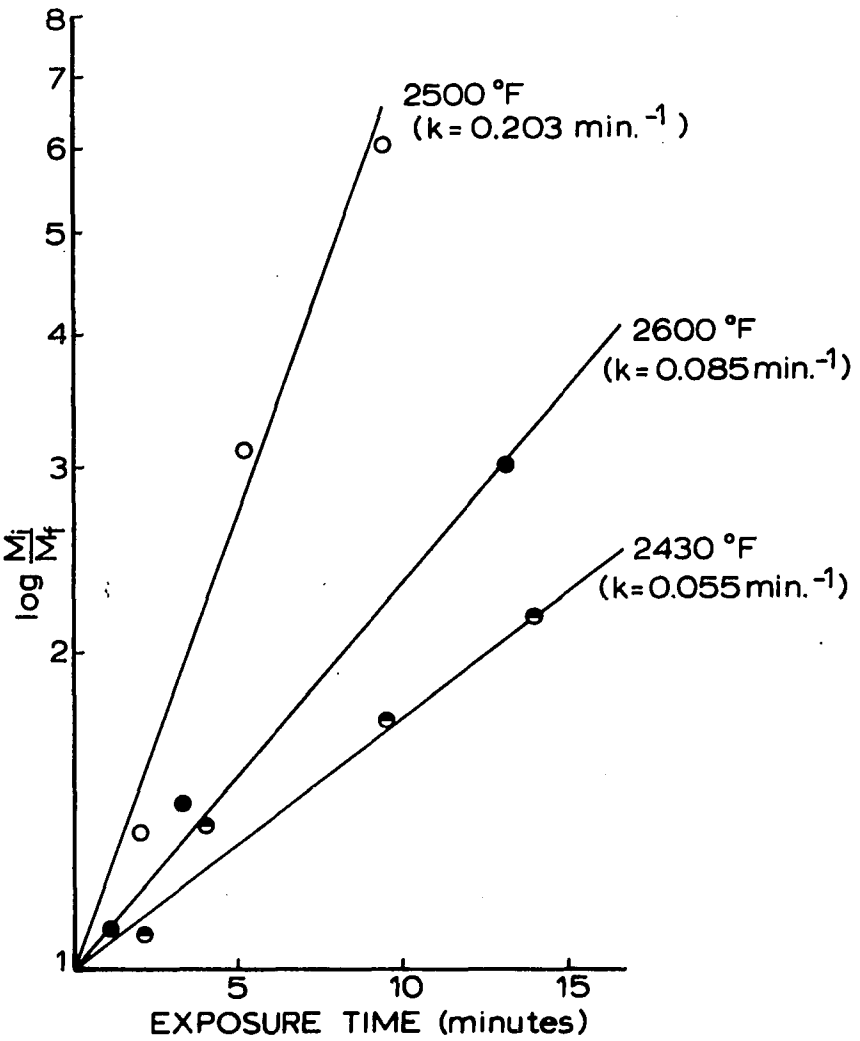


Figure 20: Magnesium loss rate in 100-pound melts as affected by holding temperature. 0.15%Mg added as 9%MgFeSi at 2750°F; 75%FeSi added as post-inoculant; held in air atmosphere. Mg_i = original Mg content. An alumina refractory was used.

occurs between the silica and the melt or dross which can affect the magnesium loss rate.

c. The atmosphere plays a role in the rate of magnesium loss. Therefore, in an MgO crucible more magnesium is lost when an air atmosphere is present than in an argon atmosphere. This increased loss rate must be due to increased oxidation.

Anomalous behavior is observed for the loss rates in silica crucibles, with the loss rates being lower in air than in argon. Section III will show that the magnesium in the melt does not react appreciably with the silica. However, the atmosphere may affect the manner in which the dross interacts with the silica crucible. The dross is high in MgO, and, as will be shown in "Engineering Aspects," is accentuated when the oxygen partial pressure is lowered over the melt. Because MgO can react readily with silica, the dross will react with the crucible. This may help to clear the surface of the melt of dross, with the silica crucible acting as a "sink" for MgO in the dross. Such behavior would not be expected for magnesia or alumina. Cleaning the melt surface could then accentuate the rate at which the magnesium is lost by vaporization. Furthermore, a good argon atmosphere is expected to lower the total amount of dross formed, again causing the surface of the melt to remain clean.

In air, by contrast, both the quantity and chemistry of the dross will be different, and such reactions with the crucible will be reduced. It will even be shown in Section V that the rate at which MgO and SiO_2 react to form the magnesium silicates is reduced in air atmospheres. Thus, a protective cover of dross may remain in an air atmosphere and lower the loss of the magnesium.

Other effects, such as the wettability of the crucible with the dross film, will also be affected by the atmosphere and the chemistry of the dross and will therefore affect the loss rates.

d. When other environmental factors are held constant, the magnesium loss rate is found to depend on the holding temperature. The loss rate was found to reach a maximum at about 2500°F, near that found by Levchenko.[12] Although the magnitude of the rate constant is considerably different from that reported by Levchenko (0.04 min^{-1}) the difference may be attributed to different experimental techniques and treatment processes.

The increasing magnesium loss rate with increasing temperature at the low temperatures is expected, as the rate of oxidation and vaporization increases. However, at higher temperatures the nature of the dross is expected to be different since the silica formed by the inversion temperature will be minimal at the higher holding temperatures and cannot act as a sink for MgO which oxidizes. Thus, once again the nature of the dross may affect the resultant loss rate. Furthermore, above the inversion temperature a CO blanket will be expected which could then help protect the magnesium from oxidizing.

The interactions between the different variables are very complex. It appears that the magnesium loss rate can be minimized by using cerium-bearing nodularizers (except in this case the loss of the cerium may merely substitute for the magnesium loss problem), by avoiding temperatures in the vicinity of 2500°F, and by using refractories which do not react appreciably with the dross film. However, it

must be appreciated that the refractories used in this investigation were relatively pure and that a rammed, impure refractory, even though nominally unreactive, may alter this behavior.

C. Oxidation Versus Vaporization

The amount of MgO that is formed can not be obtained from the magnesium loss rates because of the simultaneous loss by vaporization. However, as a guide, the more magnesium lost during the treatment and holding of the metal, the greater the opportunity to form MgO.

In one instance, a rough estimate was made of the partition of the magnesium between oxidation and vaporization. An experiment was run in which an iron melt was nodularized with 9%MgFeSi and all of the dross was removed. The melt was then held at 2500°F for 15 minutes. During this time, the chemistry of the melt and the amount and chemistry of the dross were checked intermittently (Fig. 52) by a method which will be described in "Engineering Aspects."

First, the total amount of magnesium lost during the initial magnesium flare and the magnesium in the initial dross formed during this period was calculated. It was found that of the total magnesium lost from the melt, only about six percent was present in the dross as MgO and Mg_2SiO_4. Very small amounts might also be found in glasses and other phases present in the dross. The remainder of the magnesium was lost from the surroundings of the nodular iron melt by vaporization (as much as 94 percent).

Secondly, the total magnesium lost during holding at 2500°F, beginning at the time that the initial dross was removed and ending at the time that the later formed dross was removed, was determined. This was

compared to the magnesium found in the later formed dross as MgO and Mg_2SiO_4. Table III shows the steps in the calculation of the magnesium balance between oxidation and vaporization during holding at 2500°F.

TABLE III

MAGNESIUM BALANCE FOR IRON MELT AND DROSS

Calculation of total magnesium lost during holding

after initial dross removed: %Mg = 0.043

after later formed dross removed: %Mg = 0.0275

total Mg lost: (0.043 - 0.0275)(4.73 lb metal)(454 gm/lb)/100 = 0.33 gm.

Calculation of magnesium in the dross collected during holding

	Sample 1	Sample 2	Sample 3
time of collection (seconds after nodularization)	274	518	950
weight of collected dross (grams)	0.2169	0.1090	0.0583
weight fraction of MgO in dross	0.13	0.123	0.105
weight fraction of Mg_2SiO_4 in dross	0.184	0.173	0.200
grams of Mg in MgO (fraction MgO x 0.60 x wt of dross)*	0.0169	0.0080	0.0037
grams of Mg in Mg_2SiO_4 (fraction Mg_2SiO_4 x 0.345 x wt of dross)**	0.0138	0.0065	0.0040
total Mg in each dross sample (grams)	0.0307	0.0145	0.0077

total Mg in dross collected during holding = 0.0529 grams

Magnesium lost by oxidation to dross = 0.0529/0.33 = 16% of total

Magnesium lost by vaporization = balance = 84% of total

---

*weight fraction of Mg in MgO is 0.60

**weight fraction of Mg in Mg_2SiO_4 is 0.345

The magnesium is still lost primarily by vaporization, although the fraction which is oxidized increases during holding as compared to the loss during the initial flare.

It should be noted that in nodular iron making, however, the magnesium lost by vaporization can condense onto the treatment and pouring ladles as MgO. During transfer of the metal from the treatment ladle to the pouring ladle and during pouring, the metal can trap part of this MgO, which then returns to the dross film. Furthermore, during pouring through air, fresh metal can be exposed to the atmosphere, and the magnesium loss rate during this period would be expected to be high.

In summary, the magnesium is found to oxidize and vaporize rapidly from magnesium-inoculated nodular iron. The loss rate is a complicated function of atmosphere, refractory, nodularizer, and holding temperature. The effects of each can be explained on the basis of kinetics of oxidation, on the formation of a silica film by the CO/SiO_2 inversion phenomenon, and on the nature of the dross film which is formed.

Therefore, during the initial stages of dross formation, both MgO and SiO_2 can be formed and may appear on the surface of the melt. At the same time, some magnesium and silicon remain dissolved in the melt. Referring to the sequential reactions in Fig. 3, the situation may have moved to that found in positions B, C, or E. Either MgO can react with dissolved silicon, SiO_2 with dissolved magnesium, or MgO and SiO_2 with each other. The next sections deal with each of these possibilities in detail.

III. REACTIONS BETWEEN DISSOLVED MAGNESIUM AND SiO_2

In this section, the reaction between magnesium dissolved in the iron and silica will be described as one of the paths of Eq. 9. First, the reaction of the dissolved magnesium with silica using an argon atmosphere over the melt will be discussed and then the effect of admission of air. It should be recognized also that there are abundant sources of silica such as from the oxidation of silicon-bearing nodularizers or post-inoculants on the surface of the melt, the refractories and the mold material, and the oxidation of the silicon in the melt.

The principal possible reactions are:

$$2\underline{Mg} + 2SiO_2 = Mg_2SiO_4 + Si \quad (19)$$

$$\underline{Mg} + SiO_2 = MgO + Si \quad (20)$$

The first series of experiments was performed on a simple iron melt saturated with both magnesium and carbon. When a pronounced attack was observed, subsequent experiments were run to determine the effects of lower magnesium and the presence of silicon. The attack was found to be lower when the magnesium was lower and to be virtually eliminated when two percent silicon was present.

The discussion will first focus on the reactions in the simple high magnesium system; then the effects of changing the magnesium and adding silicon will be considered.

A. The Nature of the Reaction in Magnesium-Saturated Melts

An alloy composition saturated with carbon and magnesium was selected from the work of Trojan.[24] The iron was melted in a graphite crucible with excess magnesium always present and the saturation values read from Fig. 21. The macrostructures observed when the silica tubes were removed prior to the solidification of the melt are shown in Figs. 22 and 23.

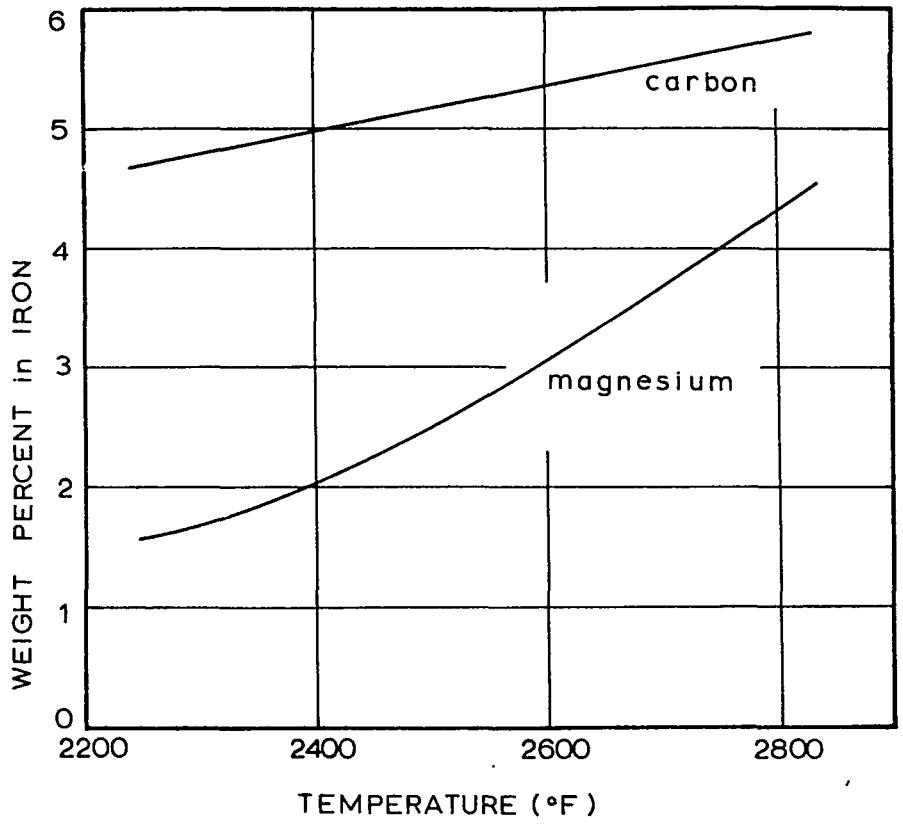


Figure 21: Maximum solubility of carbon and magnesium in iron as a function of temperature.[24]

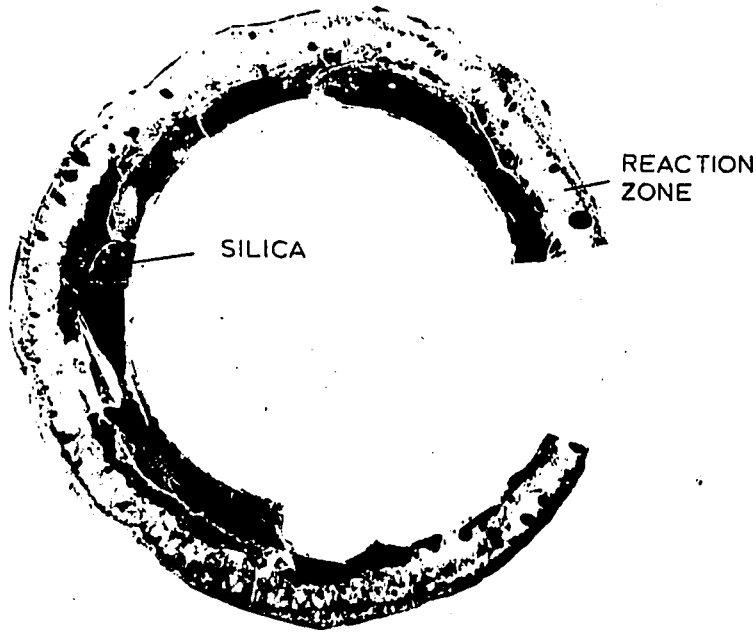


Figure 22: Silica tube fired at 2800°F for 20 minutes, showing severe attack of the surface as well as penetration of the reaction zone. Original diameter of tube - 8 mm.

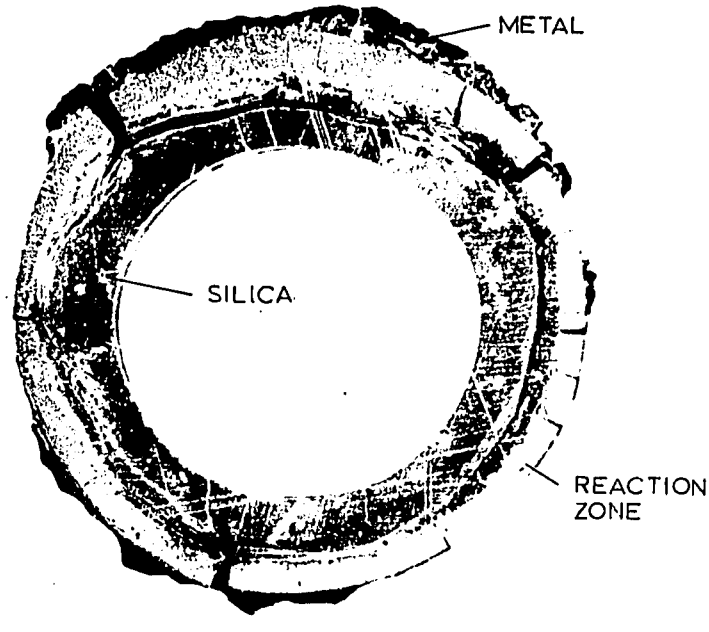


Figure 23: Silica tube fired at 2585°F for 10 minutes. A reaction zone is observed, but the surface is relatively undisturbed. Small metallic particles are fused on the tube. Original diameter of tube - 8 mm.

The reaction products in the silica were identified by x-ray diffraction and the electron microprobe as MgO, silicon, Mg_2Si and iron-silicon compounds. This suggests that the following side-reactions also occur:

$$2\underline{Mg} + Si = Mg_2Si \quad (21)$$

$$Si = \underline{Si} = \text{iron-silicon compounds} \quad (22)$$

Eq. 20, the reduction of silica by dissolved magnesium, is responsible for the penetration of the interface, producing the microstructure shown in Fig. 24. The structure appears to coarsen as the distance from the silica interface increases and the microstructure at this interface is too fine to be resolved with the optical microscope. This interface was examined with the electron microscope, and the structure is shown in Fig. 25; here it can be observed that the silicon is the continuous phase. The Mg_2Si generally occurs in veins or pockets of a silicon matrix and forms during cooling of the sample since the material is liquid (Mg_2Si formation temperature is 1985°F)[54] at the temperatures encountered in these experiments.

The possibility exists that the silicon metal produced during the reduction of silica can be dissolved in the iron melt. This occurs by the iron penetrating into the reaction layer through the silicon phase formed during the reduction reaction. At 2800°F, where the silicon phase is liquid, the iron penetrates into the reaction layer to produce iron-silicon solutions, Fig. 26. The MgO particles from the reaction float into the iron. Fig. 22 also shows that the interface is disturbed during the reaction.

In contrast, at lower temperatures where the silicon phase is solid, the iron does not penetrate the interface, Fig. 27. The interface is then

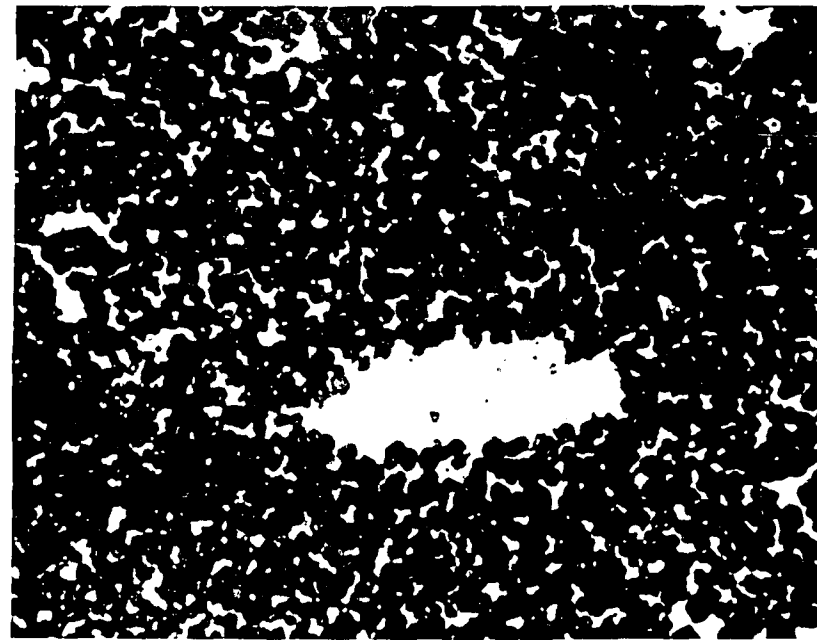


Figure 24: Typical microstructure of the reaction zone, with dark MgO particles surrounded by light silicon phase. Exposed at 2425°F for 20 minutes. 1000X.

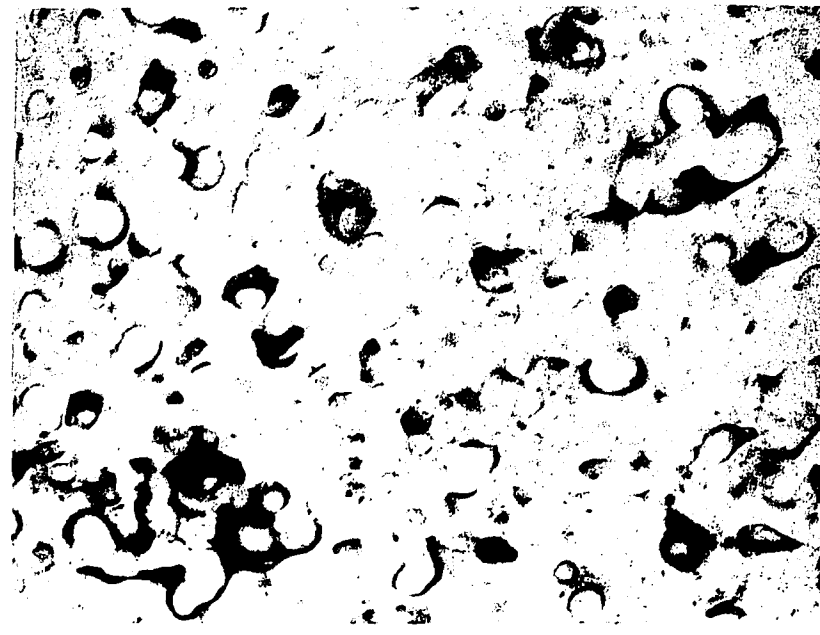


Figure 25: Electron micrograph of interface between reaction zone and silica tube. Round particles are MgO. Exposed at 2425°F for 20 minutes. 8000X.



Figure 26: Micrograph of interface between iron melt and reaction zone showing attack of surface. Exposed at 2810°F for 5 minutes. 400X.

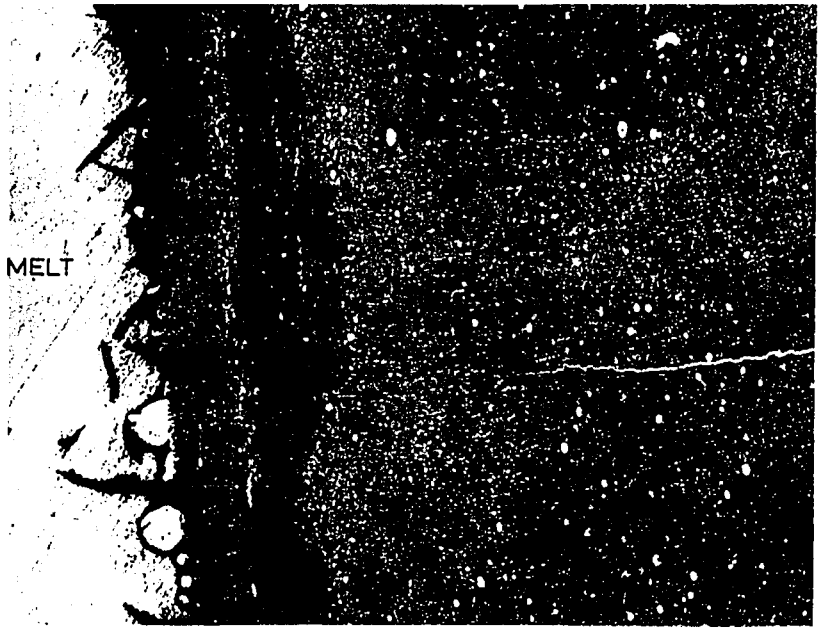


Figure 27: Micrograph of interface between iron melt and reaction zone with no surface attack. Particles at surface are $FeSi_2$. Exposed at 2425°F for 10 minutes. 150X.

relatively undisturbed, Fig. 23. Small iron-silicon inclusions are observed at the melt-reaction zone interface as a result of silicon diffusing to the iron.

Forsterite is never observed in the reaction layer; therefore, the reaction does not go to completion as shown in Fig. 3, the sequence of reactions. Even when oxygen is admitted to the pressure vessel, forsterite does not form. However, when the reaction layer is scraped away and then fired in the silicon carbide furnace in an air atmosphere, the Mg_2Si disappears and forsterite forms, probably by the oxidation of silicon and subsequent reaction between MgO and SiO_2.

This again points out the necessity for all of the magnesium available to be oxidized or otherwise combined before oxidation of silicon can occur. In the pressure vessel, even when some oxygen is present, no silicon oxidizes and no forsterite forms because all available oxygen is consumed by the magnesium. When firing in air, however, there is sufficient oxygen to first oxidize all magnesium present and then to start oxidizing the silicon.

B. The Kinetics of the Reaction in Magnesium-Saturated Melts

The kinetics of the reaction were followed by observing the penetration of the reaction layer into the silica tube, Eq. 11. A number of variables, including mechanical erosion of the tube by inductive stirring of the melt, melt chemistry changes as a result of solubility requirements, and the formation of free magnesium as a liquid and vapor, could not be completely controlled. As a result, the data cannot be treated quantitatively. However, several observations can be made.

1. In iron melts saturated in both carbon and magnesium, the attack was very severe. Particularly at lower temperature, the silica (1.5 mm thick initially) was totally consumed within 40 minutes after immersion.

2. The attack was more pronounced near the surface of the melt.

3. The attack was more pronounced when the silica was in contact with liquid magnesium and even more so with magnesium vapor.

4. Small amounts of air added to the pressure vessel in addition to the argon reduced the rate of attack slightly.

This unusual behavior, particularly the effects of temperature and location within the melt, may be caused by the inability to change only one variable at a time. Thus, the true effect of changing the temperature may be obscured by the concurrent changes in melt chemistry, presence of free magnesium, and intensity of inductive stirring.

C. The Effect of Metal Chemistry

The chemistry of the melt was also varied and the effect on the reaction investigated. Both magnesium and silicon were studied; the results are compared to data from zero silicon melts saturated in magnesium and carbon in Table IV.

TABLE IV

EFFECT OF METAL CHEMISTRY ON THE REACTION BETWEEN DISSOLVED MAGNESIUM AND SILICA

Variable	Chemistry			Penetration (mm)
	Carbon %	Magnesium %	Silicon %	
standard	5.0	2.1	0	0.46
magnesium decreased	4.9	1.0	0	0.05
silicon present	4.4	2.1	2.0	0.00

*Heats run at 2425°F for 20 minutes in graphite crucibles.

When the magnesium was decreased to 1%, the attack was greatly diminished. The most pronounced effect, however, was obtained when 2% silicon was added--the attack was eliminated even at 2.1%Mg. When the magnesium content was lowered, no excess magnesium was present and the possibility of free magnesium was diminished, therefore reducing the attack. The presence of silicon can affect the attack, first because it is one of the products of the principal reaction, and second because it can affect the activity of the magnesium.

The results from this section indicate that the reaction between magnesium and silica reduces the silica to form MgO and silicon metal. This occurs at a rapid rate when the magnesium is very concentrated; however, the data suggest that in nodular iron, where the magnesium is very low, the reaction will be negligible.

As a consequence, a reaction between the melt and the refractory or mold wall is not expected by this mechanism. For a reaction to occur at a silica mold wall, magnesium must first oxidize to MgO; this can then be followed by a reaction between the two oxides to form forsterite. Molding materials, such as green sand, which can potentially supply oxygen to the molten metal, might permit such a sequence of reactions to occur. However, a shell mold, which derives its strength from a polymerization process, will provide only a minimum of oxygen for the oxidation of the magnesium in the melt. In this case, little mold wall reaction would be expected. If the gating system to the casting is kept full of metal, preventing the inspiration of air into the mold by the metal stream, even less reaction would be observed.

Furthermore, for a reaction to occur on the surface of the melt with silica (perhaps formed by the CO/SiO_2 inversion phenomenon), the magnesium must first oxidize. MgO will not be formed by the reduction of the silica.

IV. REACTIONS BETWEEN DISSOLVED SILICON AND MgO

In the preceding sections, it was pointed out that MgO may be present both as a result of the oxidation of magnesium and as a consequence of the reduction of silica. The cast iron melt also contains ample silicon (2% Si) for a reaction between MgO and silicon.

Other cases where there may be a significant reaction between MgO and silicon include (1) from the reduction of silica in the ladle or mold walls, where silicon may be trapped, and (2) after nodularization or post-inoculation where the high silicon compounds have not completely dissolved (recall the experiments with Mg_2Si particles reacting with air to form MgO and silicon).

According to Ostwald's Rule, the first step in the reaction is the oxidation of silicon to SiO_2, followed by the reaction between MgO and SiO_2. The alternative possibility is the direct reaction between MgO, silicon, and oxygen. The following discussion will evaluate these two reaction sequences and quantify the rate of the reaction in both air and argon atmospheres. Finally, the effect of iron-silicon solutions on the rate of the reaction will be discussed.

A. Microstructure of Powder Compacts after Firing

The reaction was followed by mixing powders of silicon and MgO (both finer than 270 mesh), compacting them, and firing them in the silicon carbide resistance furnace. Both air and argon atmospheres were evaluated. The compacts were then examined with the optical microscope, the electron microprobe, and with quantitative x-ray diffraction. A typical microstructure appears in Fig. 28, where small angular particles of forsterite are observed growing into the silicon. The reaction appears to proceed

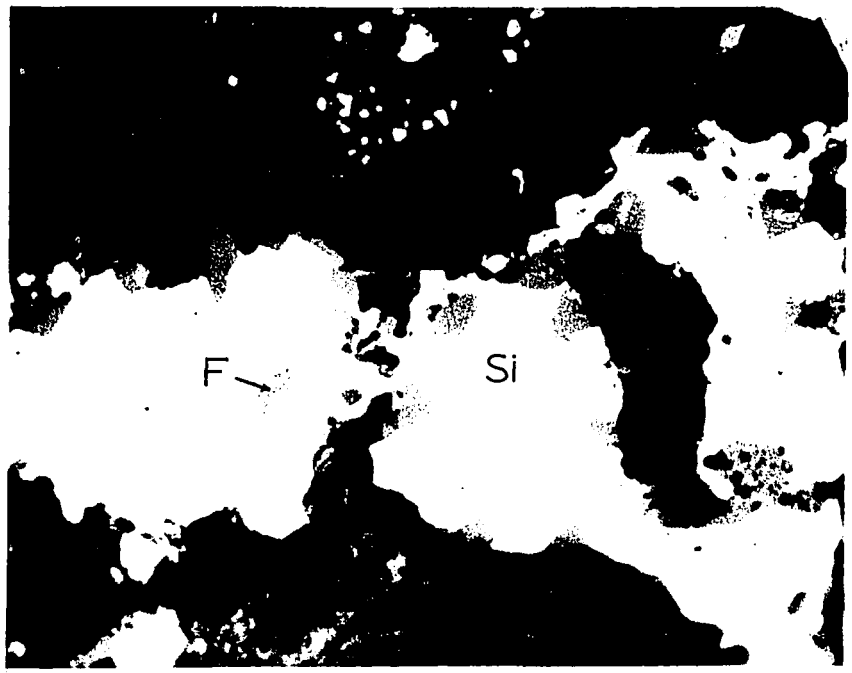


Figure 28: Typical microstructure in the reaction between silicon and MgO, with angular forsterite particles growing into the silicon. Exposed at 2530°F for 15 minutes in air.
1000X.

by the mechanism of magnesium diffusing from the MgO into the silicon and reacting there to form forsterite.

B. The Kinetics of the Reaction

The results of some typical experiments are given in Fig. 29 for air and argon atmospheres at temperatures above and below the melting point of the silicon phase (2608°F). The data were found to fit the Ginstling-Brounshtein[22] equation (Eq. 12). Rate constants were calculated for each temperature and are plotted in Fig. 30. The following conclusions may be drawn:

1. The rate of the reaction increases as the temperature increases up to the melting point of the silicon phase. At the melting point there is a discontinuity in the rate constant versus temperature curve. The rate of formation of forsterite is higher at a temperature just below the melting point than just above the melting point. Finally, when the temperature increases above the melting point, the rate constant again begins to increase.

The most plausible explanation for the discontinuity is that after melting the silicon particles may coalesce and become more spherical. The lowering of the surface area would reduce the contact area between silicon and MgO and the extent of forsterite formation would be decreased. For example, if the silicon particles were cubes below the melting point and spheres above the melting point, the surface area would be reduced by 25%. In Fig. 29, the forsterite is also reduced by about 25% just above the melting of silicon.

However, as the temperature is further increased, the reaction will increase because of the higher diffusion rates. This coalescence is confirmed by metallographic examination, Figs. 31 and 32.

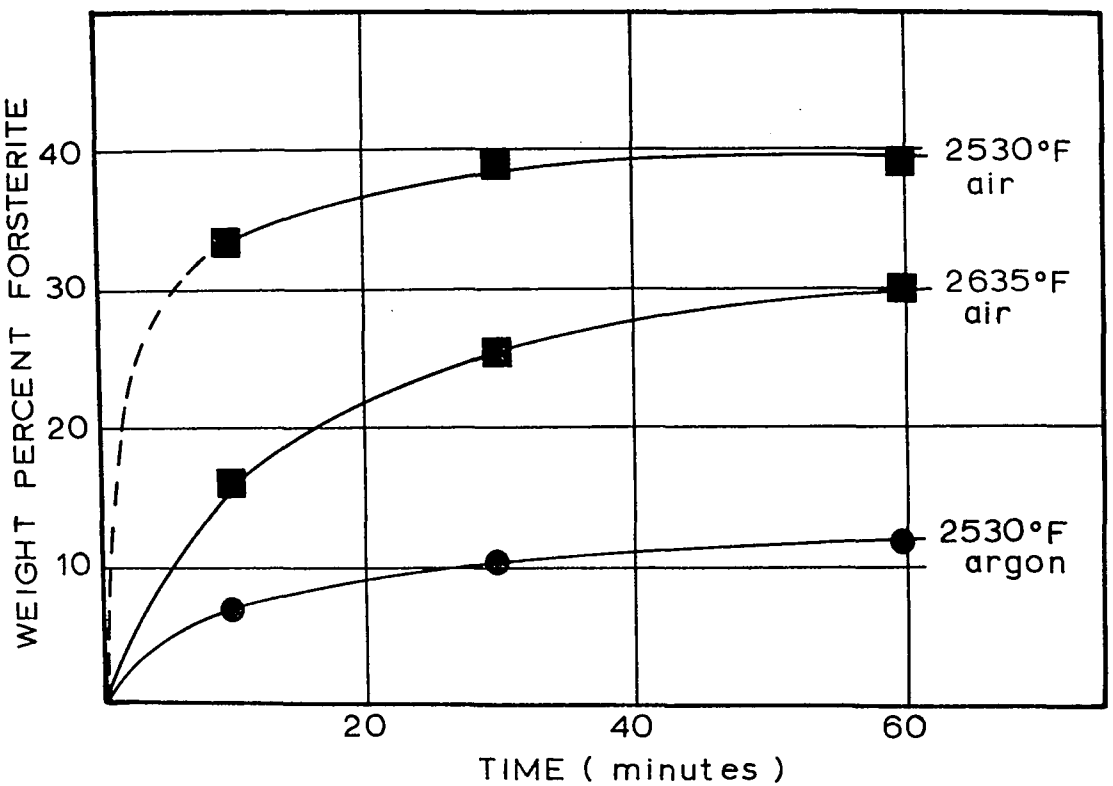


Figure 29: Typical rates of formation of forsterite for the reaction between silicon and MgO.

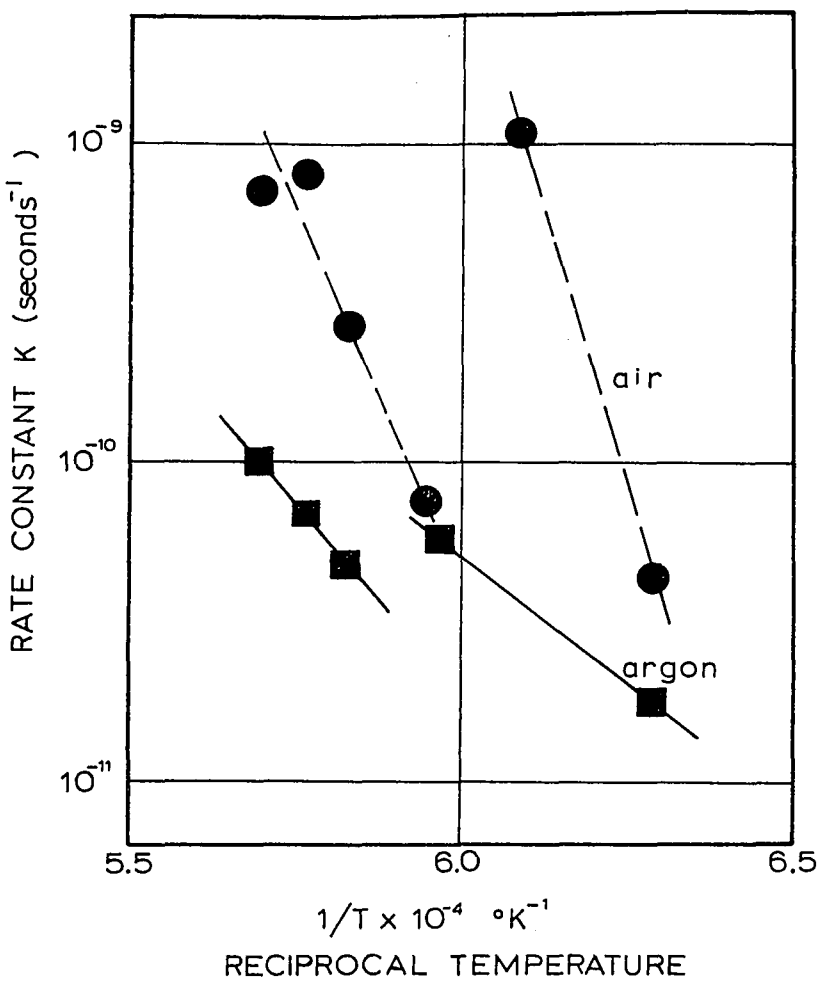


Figure 30: Rate constants versus reciprocal temperature for the reaction between silicon and MgO in air and argon atmospheres.

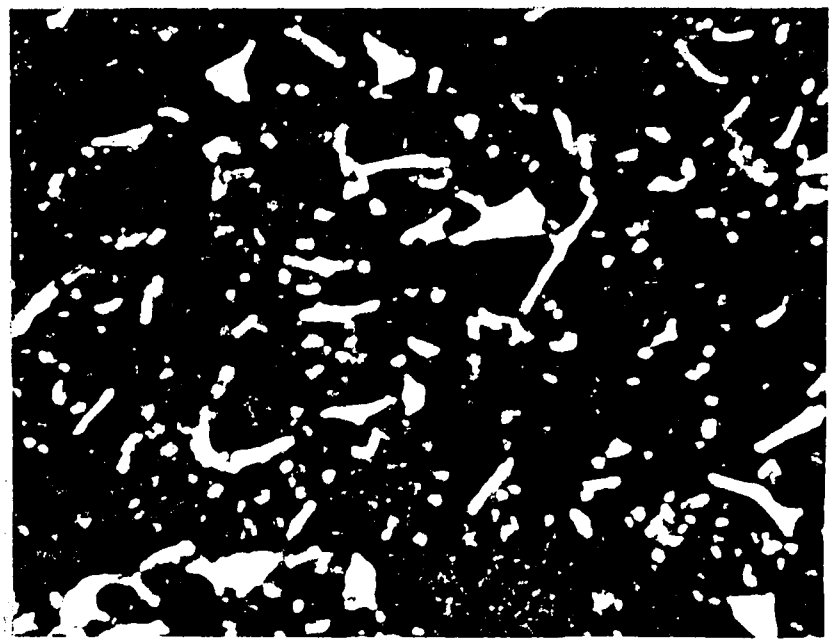


Figure 31: Microstructure of the MgO - Si powder compacts, showing angular silicon particles. Exposed at 2400°F for 15 minutes in air. 150X.

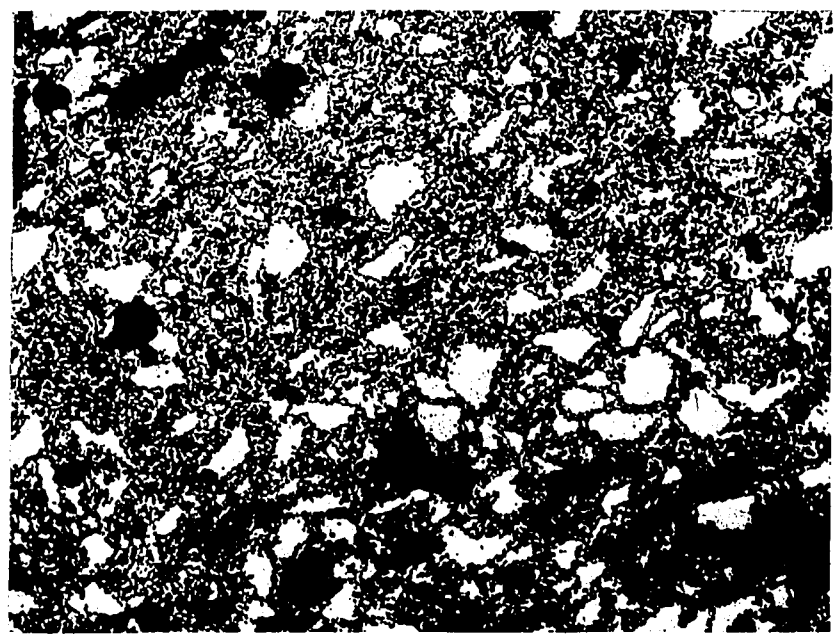


Figure 32: Microstructure of the MgO - Si powder compacts, with round silicon particles. Exposed at 2660°F for 15 minutes in air.

2. The rate of the reaction is about an order of magnitude greater in an air atmosphere than in argon. The presence of significant forsterite in an argon atmosphere, while surprising at first, can be explained because the partial pressure of oxygen in the argon is probably greater than 10^{-10} atm. The oxygen partial pressures required for the two possible reactions to proceed were calculated from the thermodynamic data[28] and are shown below for 2650°F.

$$Si + O_2 = SiO_2 \qquad P_{O_2} = 6.3 \times 10^{-18} \text{ atm} \qquad (23)$$

$$Si + O_2 + 2MgO = Mg_2SiO_4 \qquad P_{O_2} = 6.3 \times 10^{-20} \text{ atm} \qquad (24)$$

Therefore, either reaction is possible in the argon atmosphere, and the only effect of the argon is to reduce the rate of the reaction by limiting the supply of oxygen to the reactants.

In view of the observed influence of the oxygen partial pressure on the reaction rate and in accordance with Ostwald's Rule for successive reactions, the mechanism for the formation of forsterite is believed to be the prior oxidation of the silicon to form silica. The silica can subsequently react with the MgO to form the forsterite.

A good deal of effort was expended trying to find silica layers between the silicon and the forsterite. No silica was found either optically or with the electron microprobe, Fig. 33. However, the strongest diffraction peak from quartz was faintly observed on a Debye-Scherrer x-ray diffraction photograph. Since the silica layer which forms must be extremely thin, it is probable that the rate limiting step is the formation of the silica layer. The MgO would then react with the silica almost immediately to form forsterite.

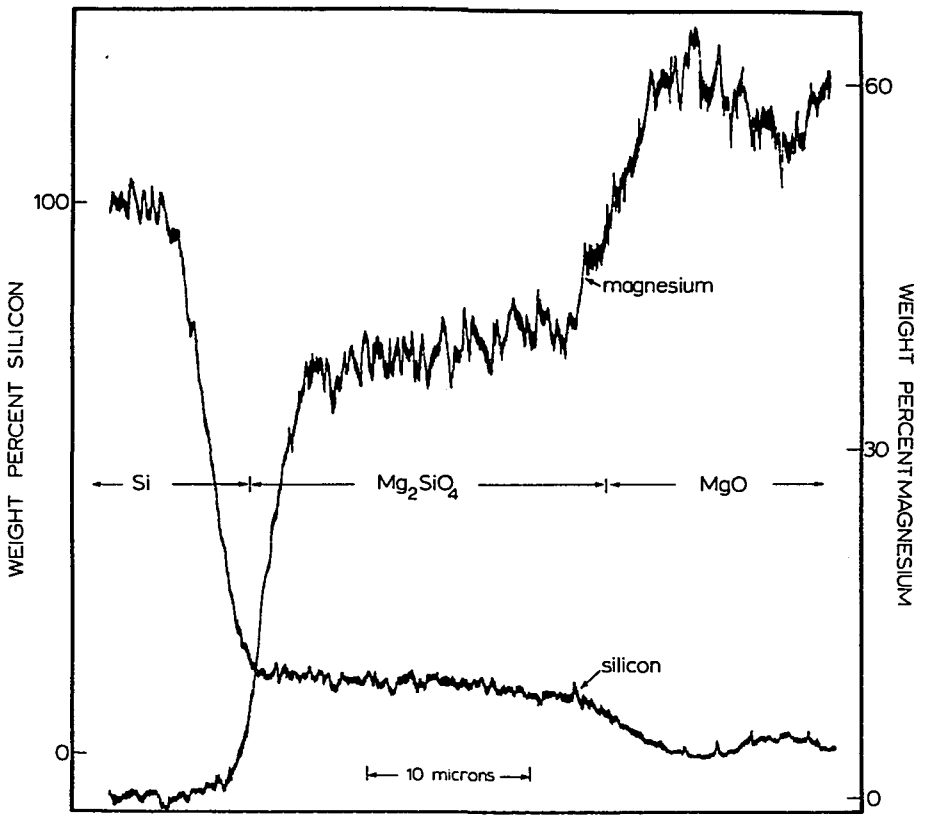


Figure 33: Electron microprobe trace through the interface between $Si/Mg_2SiO_4/MgO$ in an MgO-silicon compact fired at 2530°F for 15 minutes.

The alternative, the direct reaction between silicon, oxygen, and MgO, is favored thermodynamically but not kinetically. The thermodynamic considerations are discussed further in Appendix V.

3. Activation energies can be calculated from the slopes of the curves in Fig. 30 and are summarized in Table V.

TABLE V

ACTIVATION ENERGIES FOR THE REACTIONS BETWEEN DISSOLVED SILICON AND MgO

Atmosphere	Temperature Range	Activation Energy (cal/g·mole)
air	<2608°F	310,000
air	>2608°F	216,000
argon	<2608°F	72,000
argon	>2608°F	120,000

where 2608°F is the melting point of silicon

The difference in the activation energy between air and argon may lie in differences in the mechanisms as the partial pressure of oxygen is changed from .2 to about 10^{-8} atmosphere.

C. The Effect of Iron-Silicon Solutions

Similar behavior is observed when a ferrosilicon alloy is substituted for the pure silicon in the compacts. Both 50%FeSi and a commercial 75%FeSi alloy frequently used as a post-inoculant in nodular iron-making were tried. The amount of forsterite is only slightly lower than in the pure silicon metal, but this is not surprising since the activity of the silicon does not change drastically in this composition range.[44]

In addition, there is a discontinuity near the liquidus temperature of the ferrosilicon alloys, where the ferrosilicon melts and has a smaller surface energy, just as in the pure silicon.

In summary, it has been demonstrated that forsterite forms during the reaction between MgO and silicon. The amount of forsterite increases with increasing oxygen partial pressure and with increasing concentration of silicon. A discontinuity in the rate of the reaction with temperature is not an inherent property but is a result of the change in surface area during the melting of the silicon.

The mechanism of the reaction is probably the prior oxidation of the silicon to form silica, followed by the reaction between MgO and silica to form forsterite, and the rate limiting step is the oxidation of the silicon.

This reaction is expected to contribute to dross primarily during the initial treatment, when there are regions very high in silicon due to the nodularizer and post-inoculant additions. Subsequent reaction by this mechanism would be minor due to the low silicon content in the melt. Also, even with pure silicon the rate of the formation of forsterite by this reaction is several orders of magnitude lower than by the reaction between MgO and SiO_2, as will be discussed in the next section.

V. REACTIONS BETWEEN MgO AND SiO_2

All of the reactions studied to this point have as their end product either MgO or SiO_2. Therefore, the reaction between MgO and SiO_2 is the principal method of forming the magnesium-silicates.

In the following discussion, the mechanism by which MgO and SiO_2 react to form forsterite or enstatite will be described. The data will be presented in the following order:

A. Reactions in Argon Atmospheres

1. The Mechanism of Formation of Forsterite and Enstatite

2. The Effect of Composition and Temperature

3. The Effect of Vitreous Silica

4. Calculation of the Rate Constants

5. Activation Energies

B. Reactions in Air Atmospheres

C. Effect of Third Oxides

D. Summary

It will be shown that in time intervals consistent with nodular iron making the primary dross phase is forsterite, regardless of the composition of the oxide mixtures, and that the rate at which the forsterite forms is very rapid above 2550°F.

A. The Reaction between MgO and SiO_2 in Argon

The oxide powders (about 60 microns in diameter) were compacted and fired in the silicon carbide resistance furnace using an argon atmosphere. The compositions of the powder compacts varied from 20 to 80 weight percent SiO_2. The percentages of forsterite and enstatite were then determined by x-ray diffraction. Typical results are shown in Fig. 34a-d for four different compositions at 2450°F.

1. The Mechanism of Formation of Forsterite and Enstatite

For the stoichiometric forsterite composition (Fig. 34b) and also for excess MgO compositions (Fig. 34a), a relatively small amount of

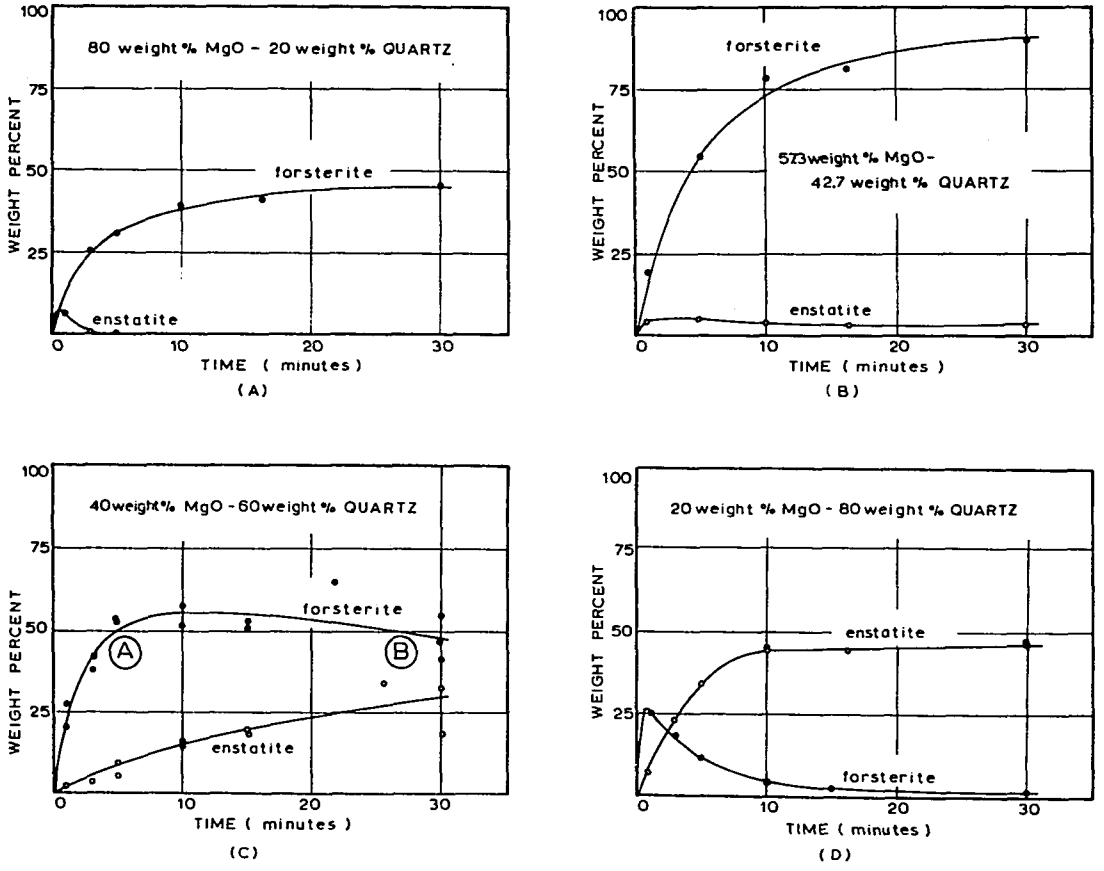


Figure 34: Typical development of forsterite and enstatite as a function of composition in MgO - SiO_2 powder compacts at 2450°F.

enstatite is observed while the forsterite increases continuously and rapidly. Aside from the presence of the enstatite, the reaction appears to proceed as predicted by the phase diagram and the original composition.

However, for the higher silica compacts, a different type of behavior is observed. Although enstatite is the stable phase, forsterite initially reaches very high values, then slowly decreases. Simultaneously, enstatite continues to increase slowly (Fig. 34c and 34d).

Both of these observations can be explained by the theory of Brindley and Hayami[21] on the basis of the relative rates of diffusion of the Mg and Si ions. Since Mg^{2+} is the faster diffusing species, the magnesium will initially begin to diffuse into the silica. Because there is very little solubility of Mg^{2+} in silica, the gradient will be very steep and Mg will rapidly build up to a level first approximating the stoichiometry of enstatite. Enstatite will therefore form first, regardless of the initial composition of the powders. With continuing diffusion of Mg^{2+}, the enstatite will advance further into the interior of the silica grain. Simultaneously, Mg^{2+} will begin to diffuse into the enstatite. Again, a very steep gradient will be established and the Mg^{2+} level will quickly attain the level of forsterite, which forms immediately behind the enstatite, Fig. 35. The reactions involved are

$$MgO + SiO_2 \rightarrow MgSiO_3 \quad \text{(enstatite)} \tag{25}$$

$$MgO + MgSiO_3 \rightarrow Mg_2SiO_4 \quad \text{(forsterite)} \tag{26}$$

These two reactions will proceed until either all of the MgO or SiO_2 is consumed. If the silica is consumed first, the Mg^{2+} continues to diffuse into the last bit of enstatite until only forsterite and excess MgO remain.

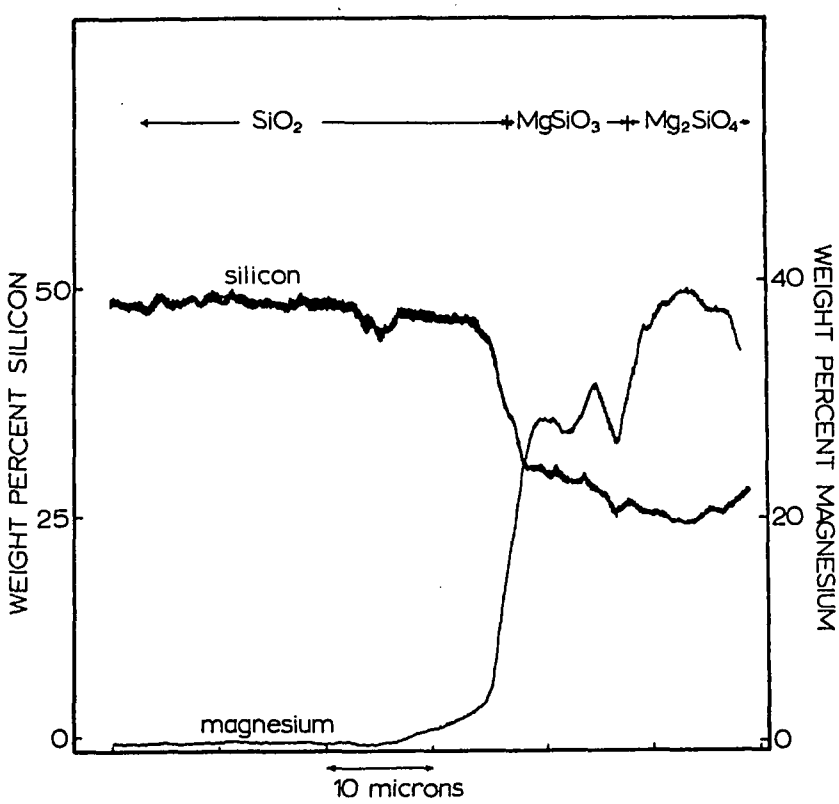


Figure 35: Electron microprobe trace through interface between $SiO_2/MgSiO_3/Mg_2SiO_4$ in MgO - SiO_2 powder compacts. Exposed at 2650°F for 10 minutes.

However, if excess silica is present, the above reactions cease when MgO is consumed and the structure is

$$\text{forsterite/enstatite/}SiO_2 \quad .$$

This is still not a stable configuration according to the phase diagram and Si^{4+} ions diffuse through the enstatite into the forsterite. As the silicon level builds up in the forsterite, enstatite forms by the reaction

$$Mg_2SiO_4 + SiO_2 \rightarrow 2MgSiO_3 \qquad (27)$$

which continues until all of the silica or forsterite is gone. If silica is depleted first, the final structure is forsterite plus enstatite; if forsterite is consumed first, the final structure is enstatite plus silica.

Therefore, the nature of the reaction is controlled by the diffusion of Mg and Si ions through the various phases. The rate limiting step in the formation of the forsterite, according to Brindley and Hayami,[21] is the diffusion of Mg^{2+} through the enstatite boundary layer; the limiting step for enstatite would then likely be the diffusion of Si^{4+} back through the enstatite.

2. The Effect of Temperature and Composition

A number of observations can be explained on the basis of this mechanism. Forsterite reaches a maximum in compositions containing high silica (greater than 50 percent SiO_2). At this maximum, all of the readily available MgO is consumed and the reaction in Eq. 27, involving the back diffusion of Si^{4+}, begins to dominate. This maximum in the forsterite content is observed to:

a. be higher at lower temperatures, Fig. 36. The back diffusion of Si^{4+} is very slow, hindering the formation of enstatite.

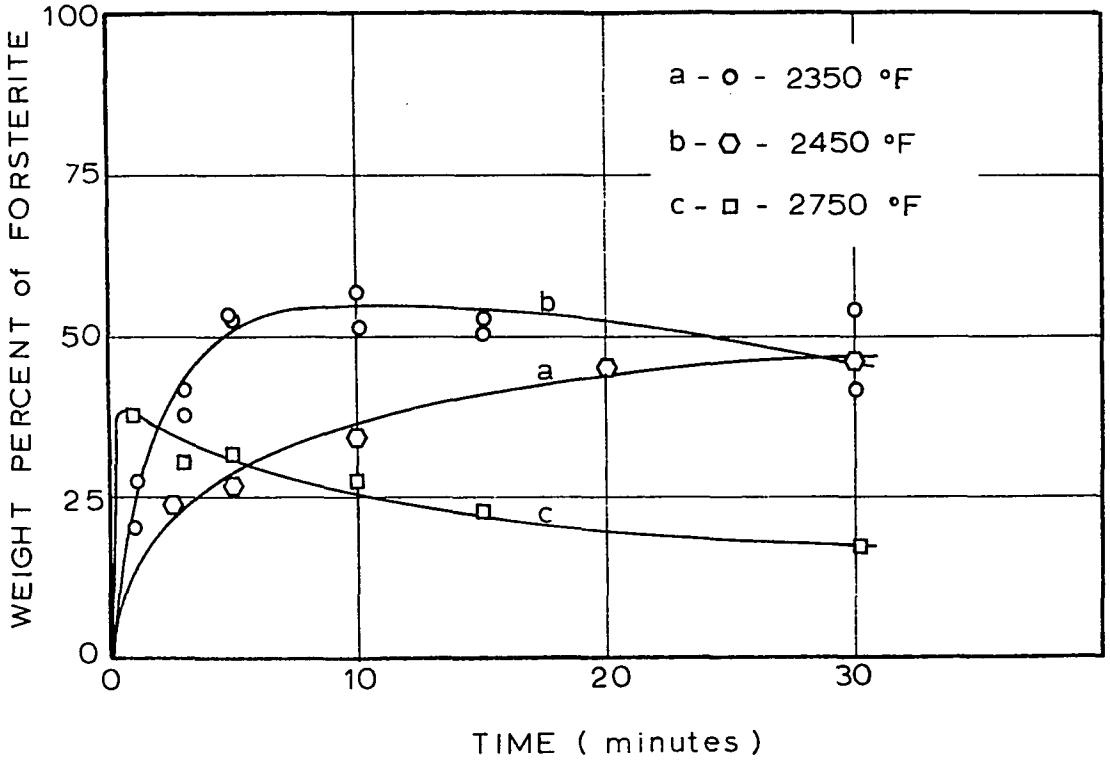


Figure 36: Effect of temperature on the development of forsterite in stoichiometric enstatite compositions (40 wt% MgO - 60 wt% SiO_2).

At higher temperatures, however, silicon ions diffuse more rapidly and enstatite can begin to form in local regions of the microstructure before the reaction to form forsterite is complete in other local regions. The net result is lowering the maximum in the forsterite curve;

b. occur at shorter times at higher temperatures, Fig. 36, because of the increased rate of diffusion of the Mg^{2+} through the enstatite boundary layer at higher temperatures;

c. occur at shorter times at lower MgO compositions, Fig. 34, because the MgO is rapidly consumed and forsterite can no longer form. For example, the time required to reach the maximum in the forsterite curve at 2650°F as a function of the composition of the powder compacts is shown in Table VI.

TABLE VI

EFFECT OF COMPOSITION ON THE TIME REQUIRED TO REACH THE MAXIMUM IN THE FORSTERITE CURVE AT 2650°F

Composition	Time
50 wt% MgO	10 minutes
40 wt% MgO	3 minutes
20 wt% MgO	1 minute

The rate at which the forsterite decreases from its maximum value is an indication of the rate at which enstatite forms from forsterite. This rate is found to

a. decrease more slowly at lower temperatures, Fig. 36, because of the lower rate of Si^{4+} diffusion at the lower temperatures; and

b. decrease more slowly at higher MgO compositions, Fig. 34, because there is less Si^{4+} remaining to back-diffuse and the Si^{4+} gradients are therefore smaller.

The results for all of the heats are summarized as time-temperature-transformation (isothermal transformation) plots, Figs. 37-41. The forsterite or enstatite percentages actually determined by x-ray diffraction are shown as small numbers on the diagrams. Superimposed are iso-concentration curves obtained by interpolating the data from plots such as Fig. 34.

The curves for enstatite are straightforward and indicate, for the temperatures studied, that increasing the temperature increases the amount of enstatite formed at any particular time.

The plots for forsterite are more complex and can be divided into three classes:

a. At high MgO contents (80 weight percent MgO, Fig. 37), the forsterite behaves in the same manner as the enstatite. Increasing the temperature increases the extent of the reaction for any particular time.

b. At intermediate MgO contents (57.3 weight percent MgO, Fig. 38) the isothermal transformation plot resembles the typical C-curves found for steels. This might suggest that the reaction to form forsterite is controlled by nucleation and growth, with low nucleation rates at high temperatures decreasing the extent of forsterite formation.

c. At low MgO contents (20 to 50 weight percent MgO, Figs. 39-41), enstatite is one of the stable end-products of the reaction and the third step in the reaction, the formation of enstatite from forsterite and silica, is necessary. Therefore, the forsterite reaches a maximum and then decreases with time. This is reflected by the complex TTT diagrams.

FIGURE 37

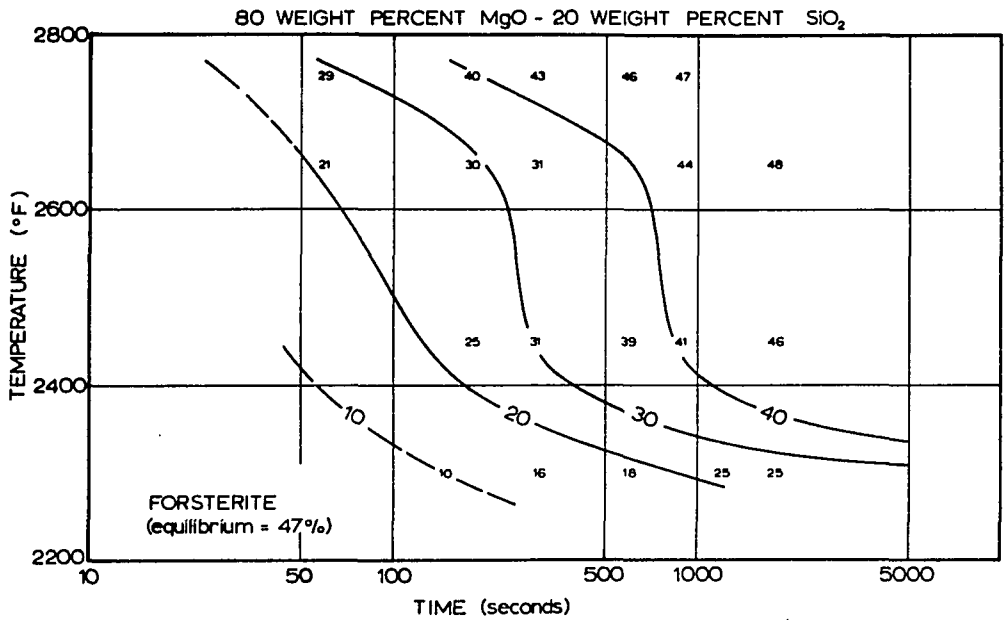


Figure 37: Isothermal transformation curves for the development of forsterite in 80 wt% MgO - 20 wt% SiO_2 powder compacts.

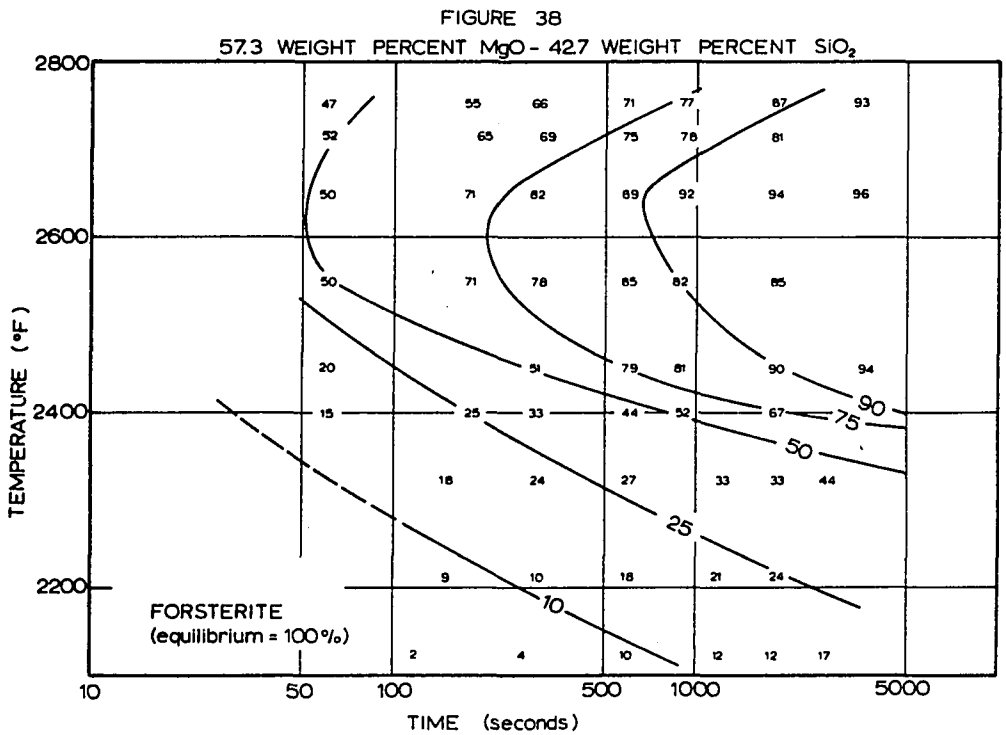


Figure 38: Isothermal transformation curves for the development of forsterite in 57.3 wt% MgO - 42.7 wt% SiO_2 powder compacts.

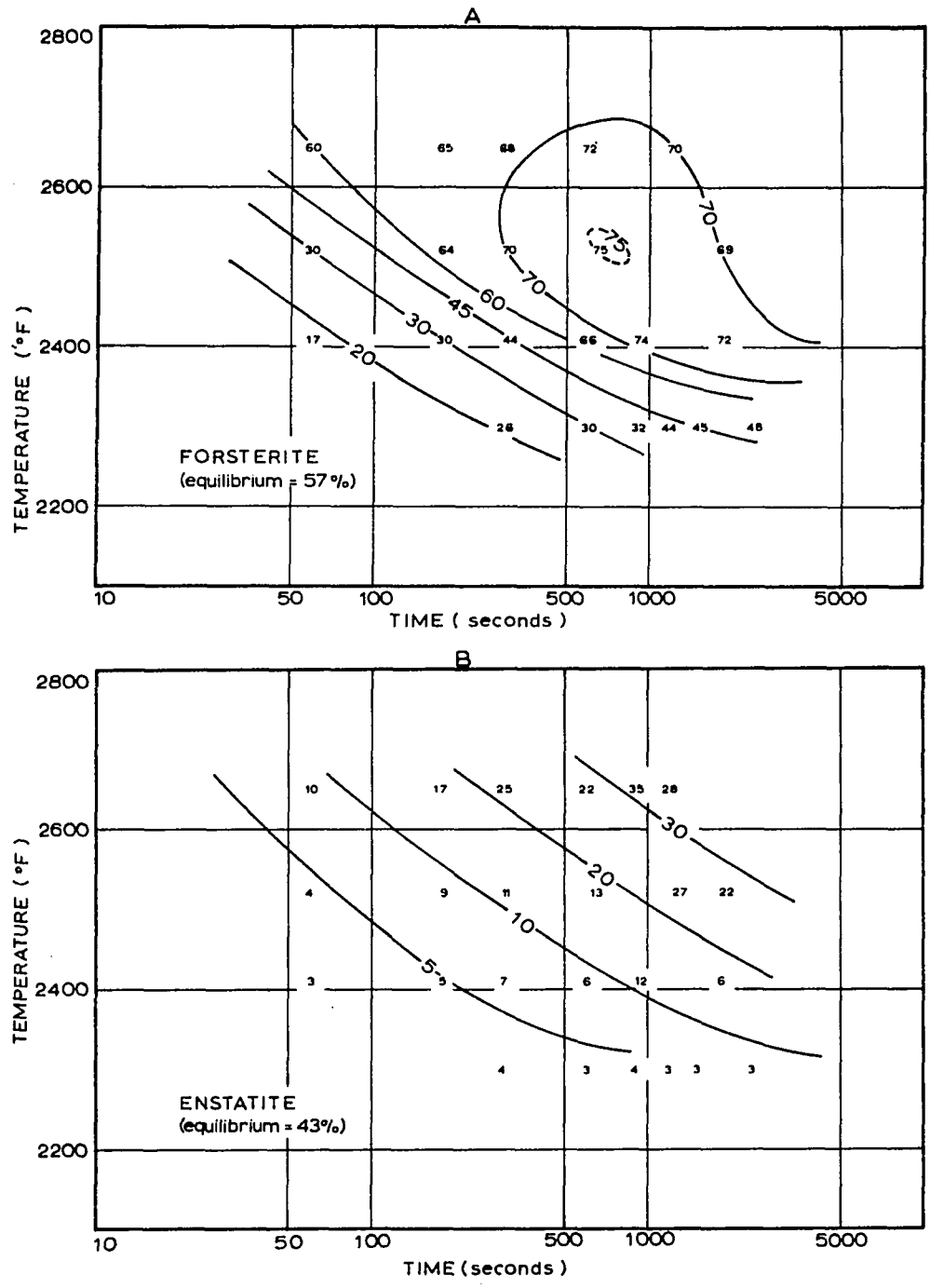


Figure 39: Isothermal transformation curves for the development of forsterite and enstatite in 50 wt% MgO - 50 wt% SiO_2 powder compacts.

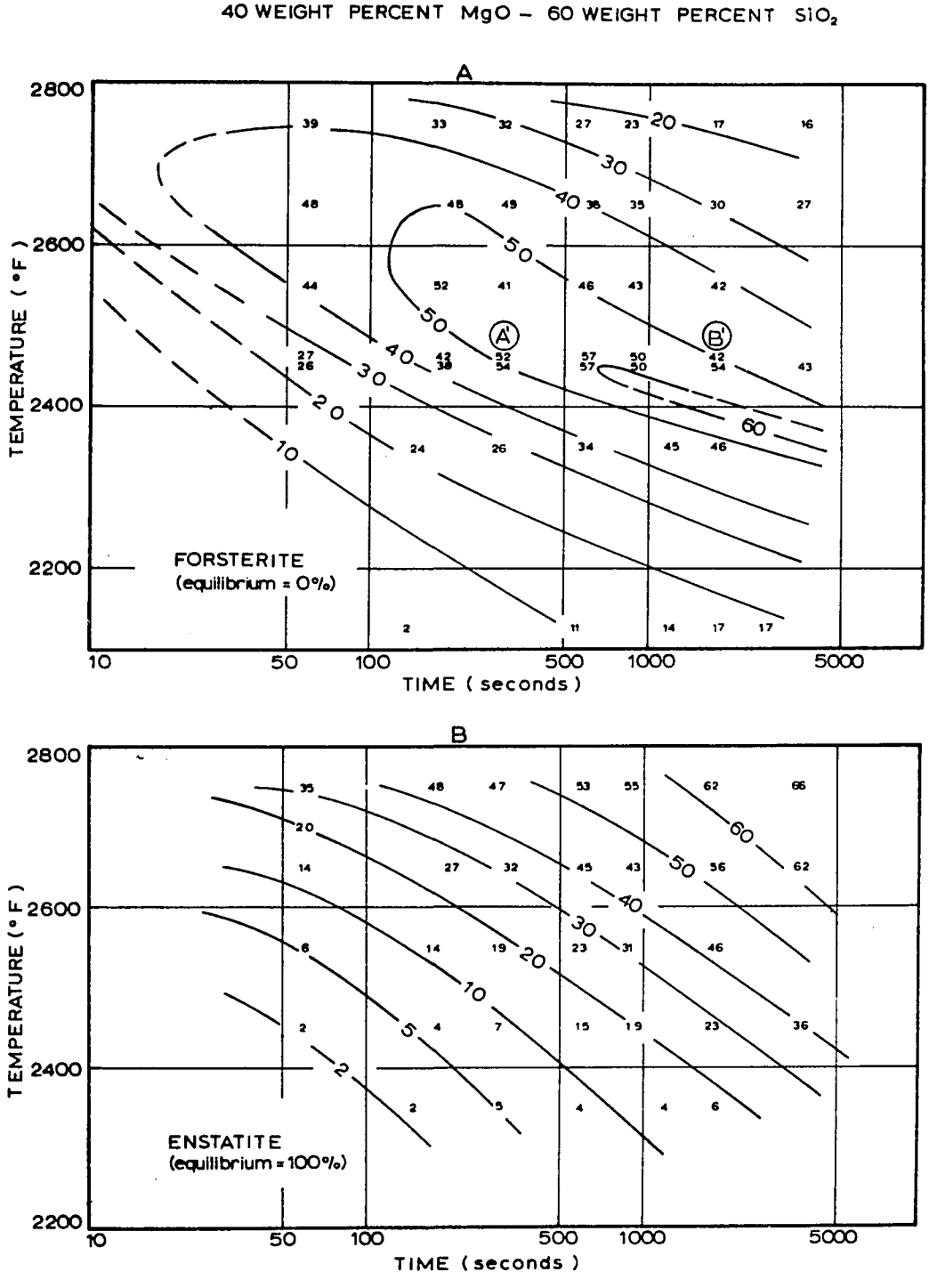


Figure 40: Isothermal transformation curves for the development of forsterite and enstatite in 40 wt% MgO - 60 wt% SiO_2 powder compacts.

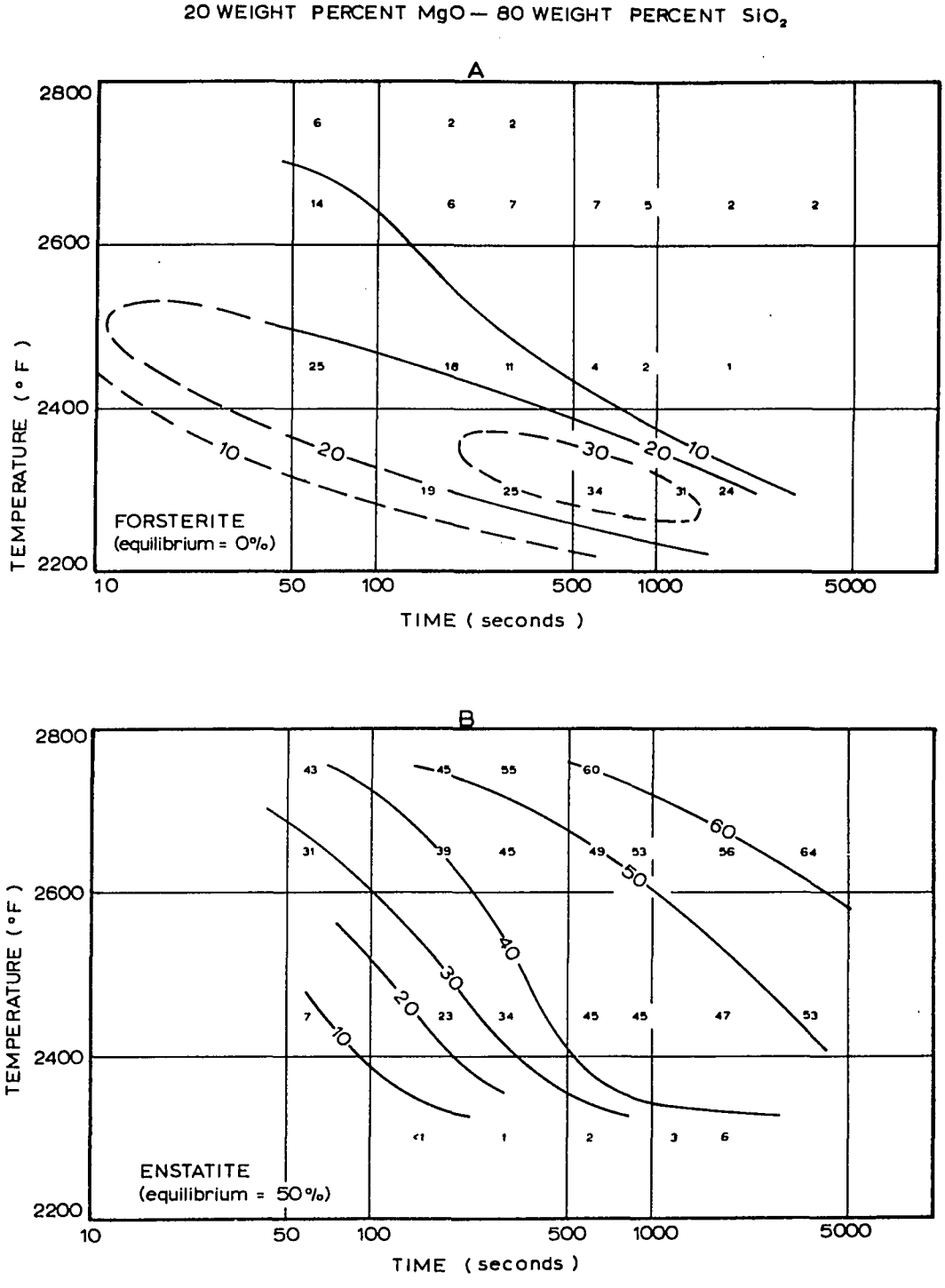


Figure 41: Isothermal transformation curves for the development of forsterite and enstatite in 20 wt% MgO - 80 wt% SiO_2 powder compacts.

The maximum forsterite that can form can be calculated on the basis of all of the MgO being consumed as forsterite. Also, the equilibrium forsterite that would be present if the reaction were carried to completion can be determined from the phase diagram. These are listed in Table VII for the high silica compositions.

TABLE VII

CALCULATED MAXIMUM AND EQUILIBRIUM FORSTERITE FOR HIGH SiO_2 POWDER COMPOSITIONS

Composition	Maximum Forsterite (%)	Equilibrium Forsterite (%)
50 wt% MgO– 50 wt% SiO_2	87	57.5
40 wt% MgO– 60 wt% SiO_2	70	0
20 wt% MgO– 80 wt% SiO_2	35	0

The construction of the TTT curves for the complex forsterite plots can be shown by an example. First, consider the curve for forsterite in Fig. 34c at 2450°F. At point A, 50% forsterite is obtained after 300 seconds (5 minutes) and the forsterite is still increasing. This point can be plotted in Fig. 40 as A'. At point B, the maximum has been passed and 50% forsterite is again observed at 1440 seconds (24 minutes). Forsterite is now decreasing, however. Therefore, point B' can be plotted in Fig. 40. After determining the time required to produce 50% forsterite at different temperatures, one can draw in a closed loop for the 50% iso-concentration curve. Other iso-concentration curves can be found in the same manner.

For MgO contents less than 40%, forsterite is not a stable end-product of the reaction, and all of the iso-concentration curves will be closed loops. The highest iso-concentration curve will be somewhat lower than that determined by the maximum value in Table VII and will depend on the composition of the powder compact. Therefore, Figs. 40 and 41, if carried to completion, would consist of a series of closed loops.

However, for MgO contents between 40 and 57.3% MgO, both forsterite and enstatite are found in the equilibrium structure. A maximum for forsterite will still be observed, but the forsterite will not drop below the equilibrium value in Table VII. Therefore, only the iso-concentration curves which are higher than the equilibrium value will be closed, Fig. 39.

3. The Effect of Vitreous Silica

The previous data were collected using quartz as the starting material for the silica. It was found during the course of the experiments that quartz did not transform to any large extent until above 2650°F, where cristobalite was found. Vitrification of the silica was observed at 2750°F.

To determine the effect of the nature of the starting materials on the reaction rate, a series of heats was made using vitreous silica rather than quartz as the SiO_2 source. The rate constants were found to be nearly the same as for quartz, Table VIII, indicating the reaction rate is independent of the initial type of silica used.

TABLE VIII

THE EFFECT OF THE TYPE OF SILICA ON THE RATE CONSTANT FOR THE FORMATION OF FORSTERITE AT 2650°F IN ARGON

Composition	Rate Constant
42.3 wt% quartz	1.63×10^{-8} sec^{-1}
41.0 wt% vitreous silica	1.47×10^{-8} sec^{-1}

The slight difference in the rate constants is within the limits of accuracy of the experiment.

Since a slower reaction rate is expected from the quartz, a boundary layer of cristobalite or vitreous silica must always be present. Thus, the reaction is always between MgO and either cristobalite or vitreous silica. Fig. 42 shows a quartz grain with a different phase at the margin.

4. The Rate Constants for the Reaction

The data presented in Figs. 37 to 41 for all of the experiments were replotted as $D(\alpha)$ versus time, Eq. 11, and the rate constants were calculated and are tabulated in Appendix III. The logarithm of the rate constants was then plotted versus reciprocal temperature, as in Fig. 43, for forsterite and enstatite. The rate constants for forsterite formation are an order of magnitude greater than for enstatite formation until the higher temperatures are attained. The reason for this is that three reactions are required for enstatite formation and only two for forsterite. Because the extra reaction for enstatite requires extensive diffusion of Si^{4+}, which is slower than Mg^{2+}, the rate is considerably slower.

However, at high temperatures the rate constants begin to come closer together primarily because that of forsterite reaches a peak and starts

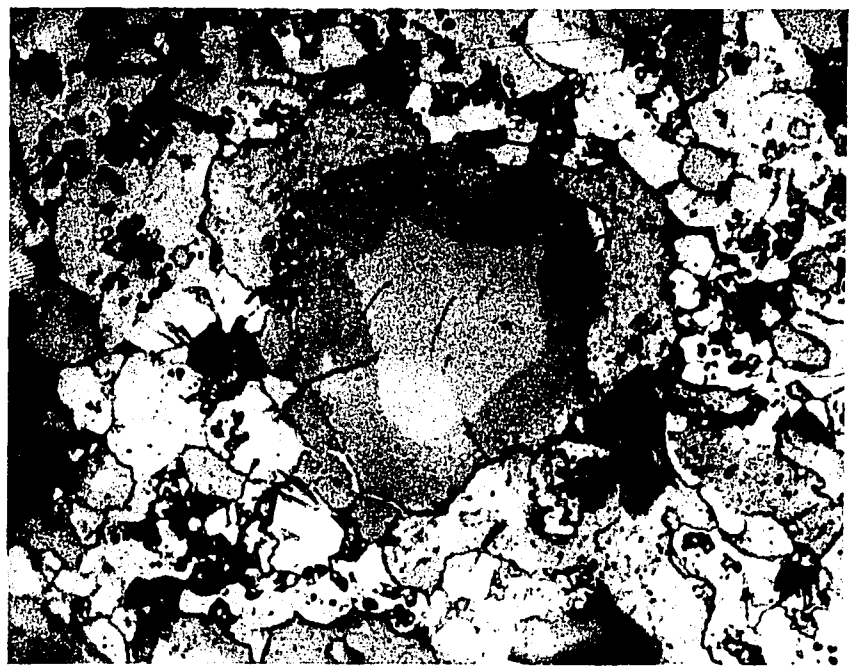


Figure 42: Micrograph of a silica grain showing the presence of a boundary phase. Matrix is forsterite and enstatite. 40 wt% MgO - 60 wt% SiO_2 exposed at 2750°F for 30 minutes.
750X.

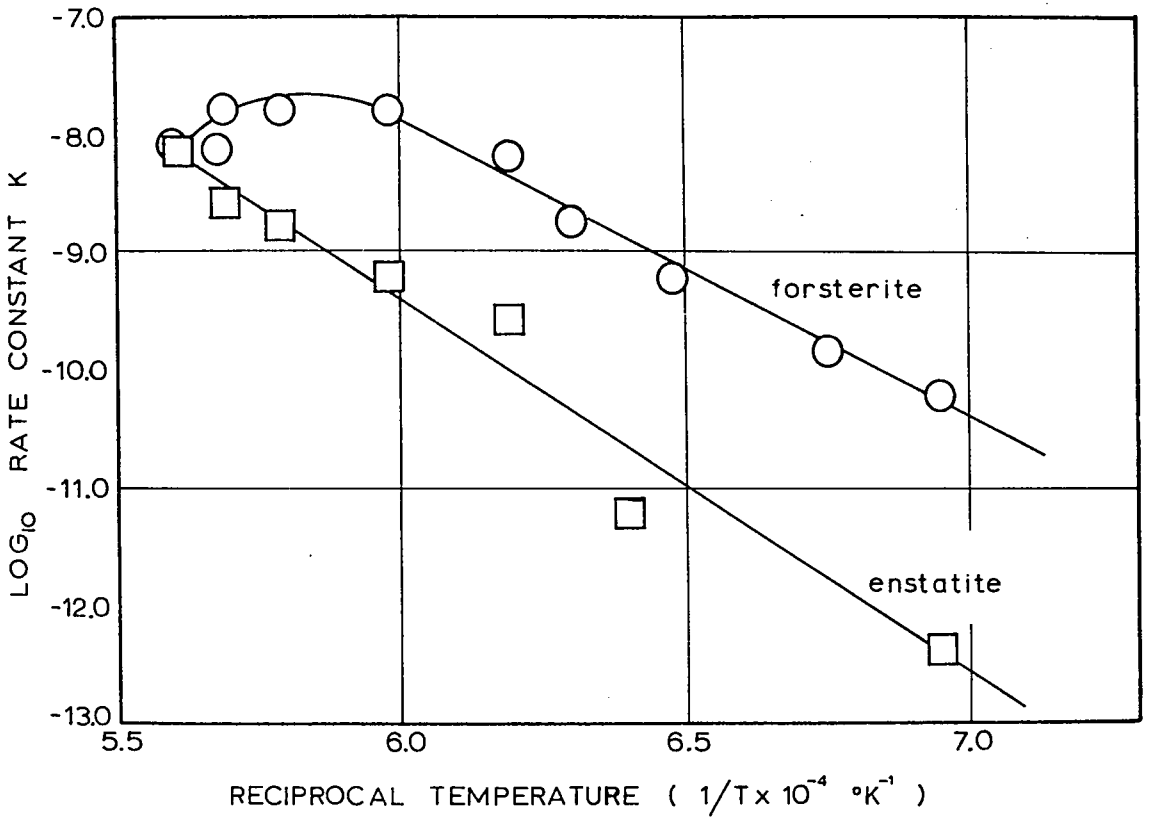


Figure 43: Rate constants versus reciprocal temperature for the formation of forsterite (in 57.3 wt% MgO - 42.7 wt% SiO_2) and enstatite (in 40 wt% MgO - 60 wt% SiO_2).

to decline. A possible explanation is that the reaction may be more difficult to nucleate at the higher temperatures, leading to the C-curve in Fig. 38. It is then possible that the driving force for the nucleation of the reaction is very small at temperatures greater than 2550 to 2650°F and that even the increased rate of diffusion cannot continue to increase the reaction rate. The enstatite TTT diagram might be expected to display the same behavior at higher temperatures.

5. The Activation Energy for the Reaction

The slopes of the log (rate constant) versus reciprocal temperature curves are used to calculate the activation energies for the reactions. The activation energies found by least squares analysis for each composition appear in Table IX and in Fig. 44.

TABLE IX

ACTIVATION ENERGIES FOR THE FORMATION OF FORSTERITE AND ENSTATITE

	Activation Energy (cal/g·mole) Forsterite	Enstatite
20 weight % MgO 80 weight % SiO_2	*	41,100
40 weight % MgO 60 weight % SiO_2	116,900	145,900
50 weight % MgO 50 weight % SiO_2	119,100	84,400
57.3 weight % MgO 42.7 weight % SiO_2	118,000	*
59 weight % MgO 41 weight % SiO_2 (as vitreous silica)	86,100	*
80 weight % MgO 20 weight % SiO_2	49,550	*

*The amounts of enstatite or forsterite were too small for the rate constants and activation energies to be calculated.

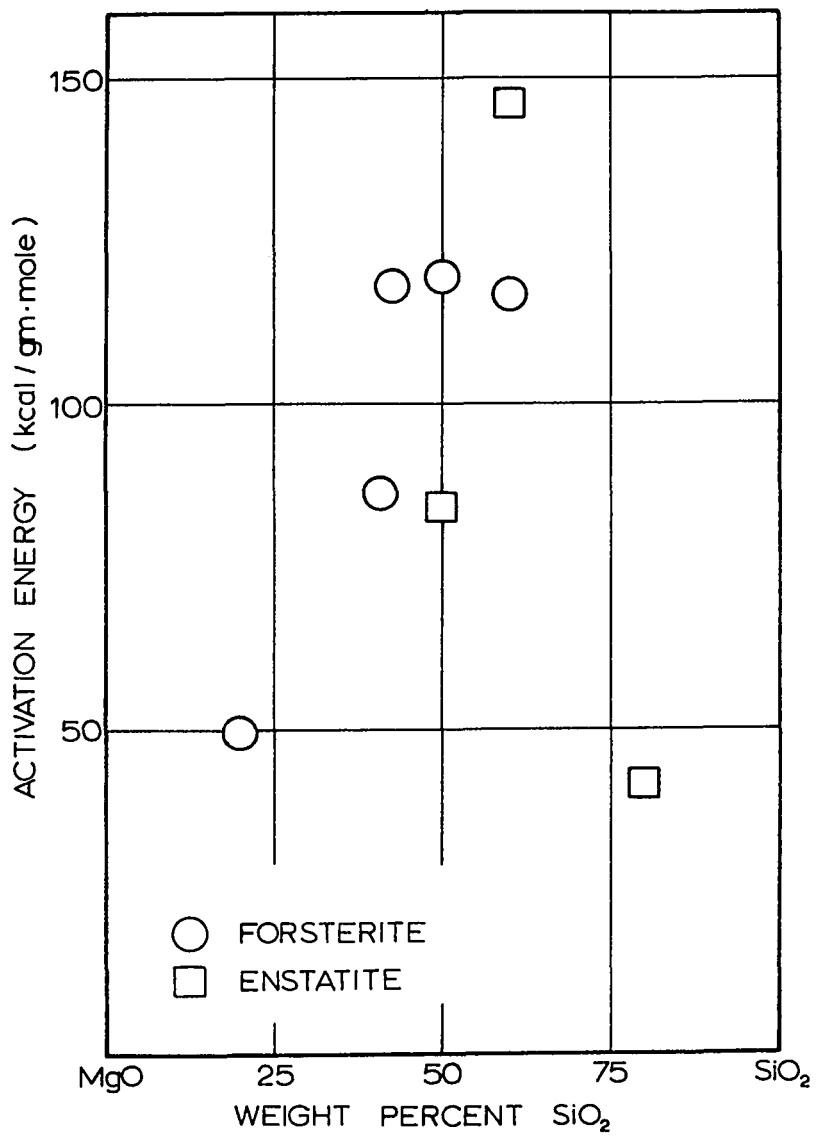


Figure 44: Activation energies for forsterite and enstatite as a function of percent SiO_2 in the powder compacts.

The activation energy for forsterite formation applies for the reaction

$$MgO + MgSiO_3 = Mg_2SiO_4 \quad (28)$$

while that for enstatite formation applies for the reaction

$$SiO_2 + Mg_2SiO_4 = 2MgSiO_3 \quad (29)$$

Brindley and Hayami found that at temperatures below 2350°F the activation energy, about 80 kcal/g·mole, was not a function of composition. However, their work was done at low temperatures and with silica contents less than sixty percent. At no time did they encounter significant amounts of enstatite or the reaction between silica and forsterite to form enstatite. In all cases, the diffusion of silicon ions was very sluggish and insignificant. Both the temperature and concentration could affect the diffusion coefficients of magnesium and silicon ions and thus affect the observed activation energy.

Also, the rate constants found in this investigation differ from those of Brindley and Hayami. The main reason for this discrepancy is the difference in the particle size of the raw materials, which can greatly affect the rate constant.[47]

B. Reaction in an Air Atmosphere

The same mechanism appears to operate in air as in argon; however, the rate constants were found to be lower by an order of magnitude or more in air. This is shown for several cases at 2650°F in Table X. Let us consider the case in which magnesium ions diffuse into the enstatite layer and the oxygen ions cannot keep up. However, gaseous oxygen is available. Then there is an excess of cations, and the reaction to form forsterite might look like the following:

$$2Mg^{2+} + O_2 + 4e^- + SiO_2 = Mg_2SiO_4 \quad (30)$$

Then by the law of Mass Action,

$$\frac{1}{(P_{O_2})(a_{Mg^{2+}})^2(a_{e^-})^4} = \text{constant} \qquad (31)$$

Since

$$a_{e^-} \sim C_{e^-} \qquad (32)$$

the concentration of the electrons is proportional to the oxygen partial pressure:

$$C_{e^-} \sim (P_{O_2})^{-1/4} \qquad (33)$$

Therefore, as the oxygen partial pressure increases, the concentration of the electrons decreases. In turn, this should decrease the rate at which the magnesium ions diffuse through the enstatite, since electrical neutrality is required.[48,49] The result will be that the air atmosphere will reduce the rate of the reaction as compared to the argon atmosphere.

TABLE X

EFFECT OF ATMOSPHERE ON THE RATE CONSTANT

Composition	Rate Constant K -- (sec^{-1}) Air	Argon
40 weight % MgO 60 weight % SiO_2 (K for enstatite)	0.398×10^{-9}	1.62×10^{-9}
40 weight % MgO 60 weight % SiO_2 (K for forsterite)	7.15×10^{-9}	504.0×10^{-9}
57.3 weight % MgO 42.7 weight % SiO_2 (K for forsterite)	6.74×10^{-9}	16.3×10^{-9}

C. The Effect of Other Oxides on the Reaction

Dross contains, in addition to MgO and silica, several other oxides in varying amounts. Therefore, an analysis of the formation of forsterite and enstatite from MgO and silica would not be complete without at least determining the qualitative effect that the addition of these other oxides have on the reaction. The objectives were to determine (1) whether the same mechanism for the formation of the silicates was followed, (2) the effect on the kinetics of the formation of forsterite and enstatite, and (3) the chief differences in the phases present. This was done for ternary oxide systems where the third oxide was present in amounts generally found in actual dross. The effects of Fe_2O_3, CaO and Al_2O_3 were studied.

The investigation and the results remain qualitative for the following reasons:

1. The presence of new phases for which no calibration curves were obtained. The ternary phase diagrams[50] show that a liquid phase can appear during firing of the samples which can remain as a glass after cooling. Particularly in the iron oxide ternary, a new crystalline phase, magnesioferrite ($MgO \cdot Fe_2O_3$), may appear.

2. The change in intensity of the diffracted radiation from forsterite and enstatite during x-ray diffraction. This results from the solid solution of Fe^{2+} and Ca^{2+} to form olivine (solid solution of cations in forsterite) and pyroxene (solid solution of cations in enstatite). Up to 100% FeO and 12% CaO can substitute for MgO in forsterite and about the same in enstatite.[50] This will produce errors in the calibration curves in Fig. 12, with the calculated composition being less

than the actual composition. This same difficulty would be experienced if a calibration curve for magnesioferrite was constructed.

3. The ternary system with iron oxide is really a quaternary.[51] Depending on the partial pressure of oxygen and the temperature, the iron oxide may exist as FeO, Fe_2O_3, or Fe_3O_4. Furthermore, in olivine refractories the iron oxide in the olivine may oxidize to form a separate magnesioferrite phase in equilibrium with nearly pure forsterite. Silica, which is also released, can combine with additional MgO to form pyroxene.[51] This further complicates the analysis of the results.

In spite of these difficulties, it was possible to determine, in conjunction with the published ternary phase diagrams, how the reactions between MgO and SiO_2 are affected by the addition of the third oxides.

In this series of experiments, the compacts were fired in an argon atmosphere where the partial pressure of oxygen was quite low ($\sim 10^{-8}$ atmospheres). The iron oxide, added as Fe_2O_3, should exist at the firing temperature as wüstite (FeO) and a flame presumably due to the extra oxygen could generally be observed during heating.

The results were obtained for a 2:1 molar ratio of MgO to SiO_2 (forsterite) and a 1:1 molar ratio of MgO to SiO_2 (enstatite). A number of observations and trends are summarized in Table XI. Typical results at 2650°F for the additions of Fe_2O_3 are shown in Figs. 45 and 46. These will be discussed below.

1. The basic mechanism for the formation of forsterite and enstatite appears to be identical with that observed in the binary system. Forsterite is the most important phase present at any time. Although an enstatite layer may form initially, forsterite is stable unless the MgO is entirely

TABLE XI

SUMMARY OF TRENDS IN THE TERNARY POWDER COMPACTS

Effect of the Following Variables on the Incidence of the Phases

Phases	Increasing SiO_2	Increasing Third Oxide Fe_2O_3	Increasing Third Oxide CaO	Increasing Third Oxide Al_2O_3	Increasing Time	Increasing Temperature
Forsterite	decreases	decreases	decreases	decreases	variable (Figs. 45 and 46)	increases
Enstatite	increases	decreases	decreases	n.d.*	variable (Figs. 45 and 46)	increases
$MgO \cdot Fe_2O_3$	decreases	increases	n.a.**	n.a.**	increases	decreases
Glasses	increases	increases	increases	increases	variable (Figs. 45 and 46)	increases

*n.d. - not determined

**n.a. - no magnesioferrite can form in ternaries without iron oxide

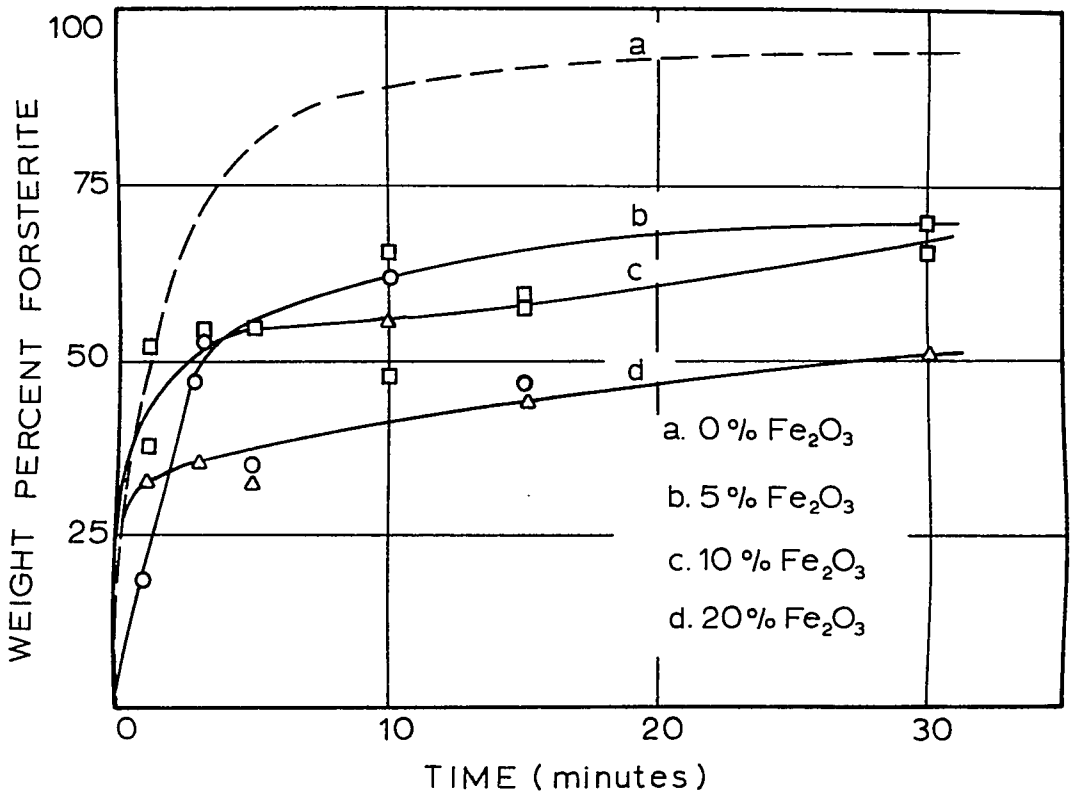


Figure 45: The effect of %Fe_2O_3 on the development of forsterite in ternary MgO - SiO_2 - Fe_2O_3 powder compacts with a 2:1 molar ratio of MgO to SiO_2. Exposed at 2650°F.

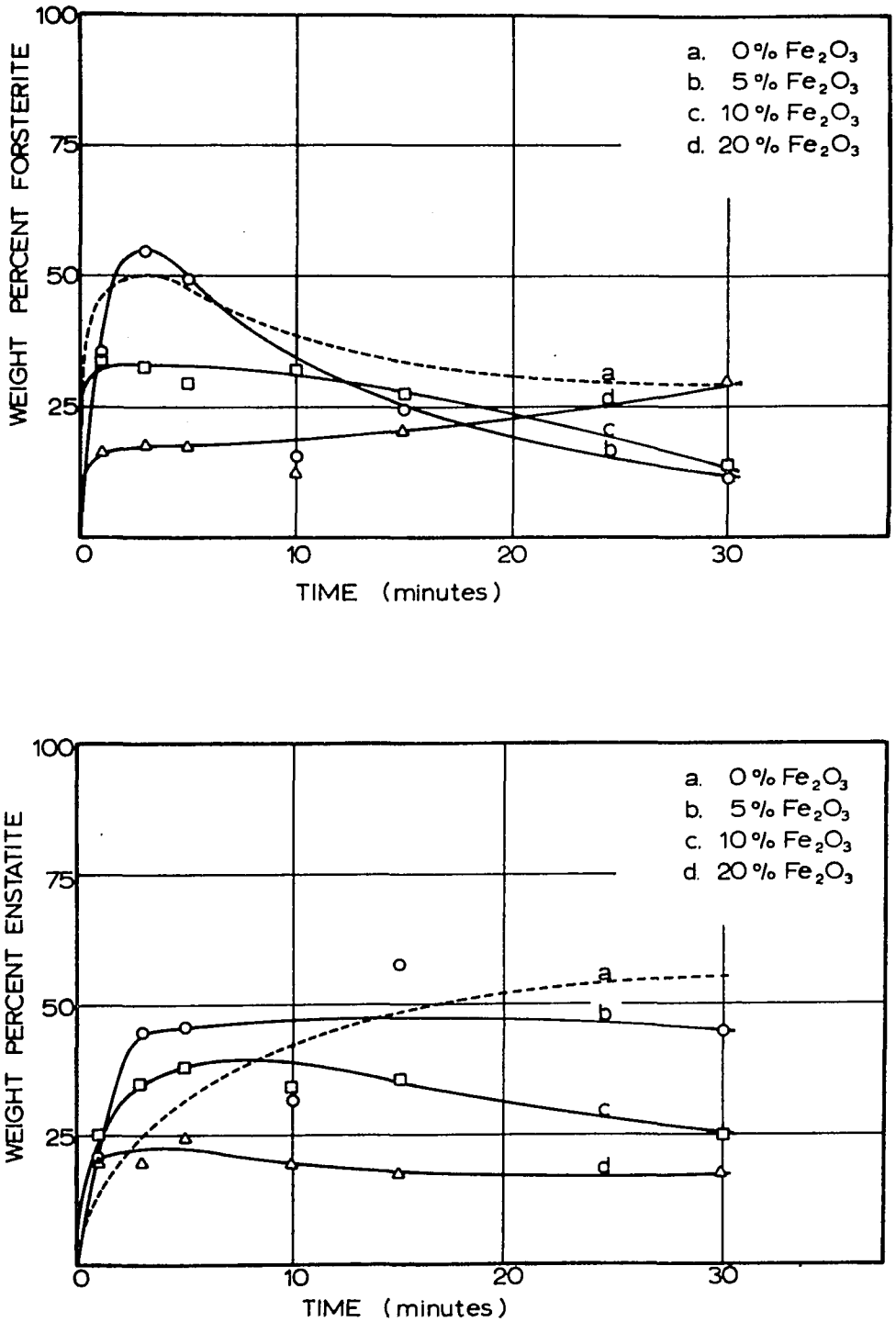


Figure 46: The effect of %Fe_2O_3 on the development of forsterite and enstatite in ternary MgO - SiO_2 - Fe_2O_3 powder compacts with a 1:1 molar ratio of MgO to SiO_2. Exposed at 2650°F.

consumed. Then the enstatite can again form by the reaction of silica with forsterite. Therefore, a maximum is observed in the forsterite curve for high silica compositions.

2. Both the rate of formation of forsterite and enstatite and the total amount of each that forms are decreased as the amount of the third oxide increases. The rate and amount increase with increasing temperature. For equivalent amounts of CaO and Fe_2O_3, the effect on the silicates is roughly the same; however, compacts containing Al_2O_3 are affected only slightly. The effects of the third oxides cannot be determined quantitatively because of the difficulties discussed previously.

3. The compositions of forsterite and enstatite change with the composition of the ternary system. These changes were determined by measuring the **d-values** for the (130) and (021) planes in forsterite and the (240), (221) planes in enstatite and comparing them with the published **d-values** for forsterite and enstatite of varying FeO and CaO contents.[33]

The FeO and CaO dissolved in forsterite and enstatite increase with increasing third oxide in the original composition, Fig. 47. However, only half of the total available third oxide enters the silicate, with the remainder forming new phases.

In one instance, the FeO content in forsterite for a 2:1 MgO to SiO_2 molar ratio containing ten weight percent Fe_2O_3 was determined as a function of time, Fig. 48. The FeO is initially quite high in the forsterite but slowly decreases with increased holding time. This corresponds to the previous observations that the iron present in olivines oxidizes and is rejected in the form of a magnesioferrite ($MgO \cdot Fe_2O_3$) phase.

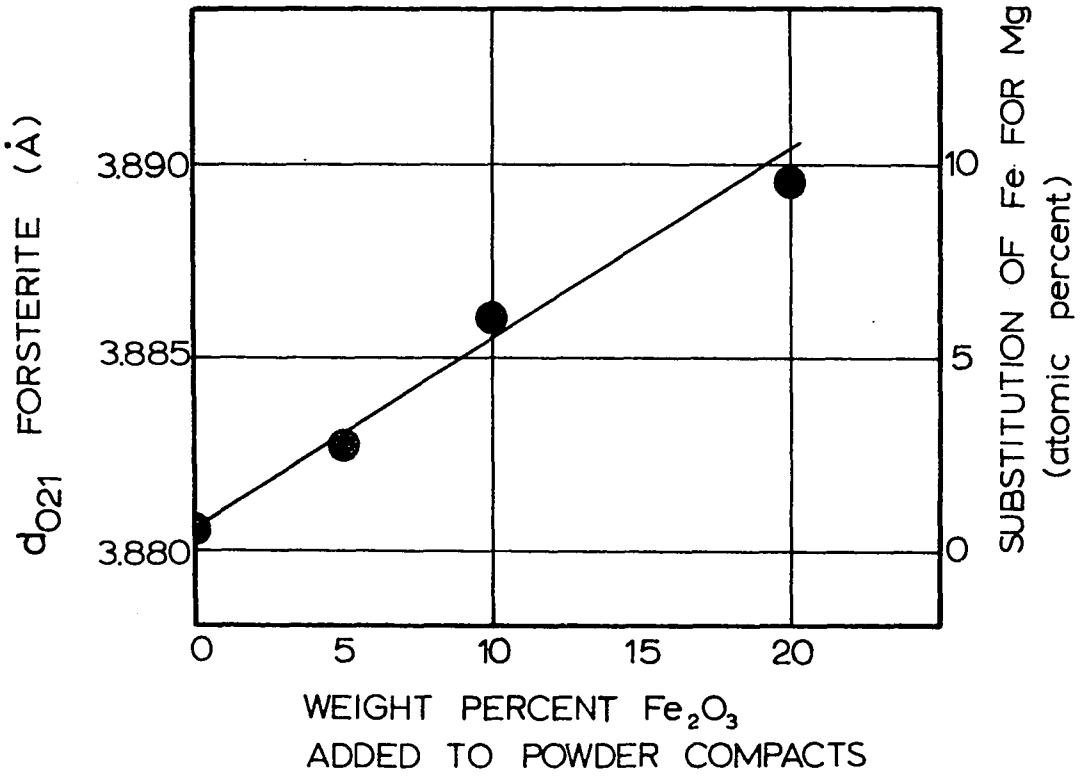


Figure 47: The effect of $\%Fe_2O_3$ on the interplanar spacing d_{021} of forsterite in ternary MgO - SiO_2 - Fe_2O_3 powder compacts with a 2:1 molar ratio of MgO to SiO_2. Exposed at 2650°F for 30 minutes.

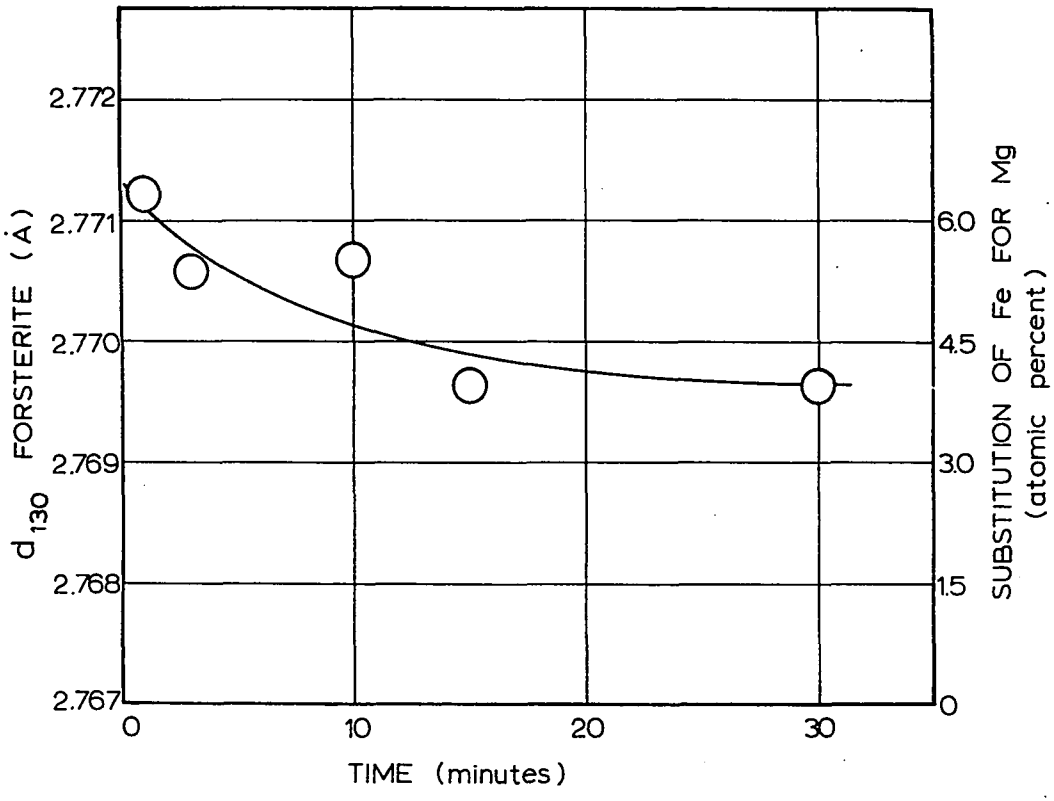


Figure 48: Effect of time on the interplanar spacing d_{031} of forsterite in a ternary $MgO - SiO_2 - Fe_2O_3$ powder compact with a 2:1 molar ratio of MgO to SiO_2. 10 wt% Fe_2O_3 added. Exposed at 2650°F.

4. In the compacts containing iron oxide, a new phase is observed microscopically, Fig. 49. This was identified, with the aid of the electron microprobe, as $MgO \cdot Fe_2O_3$. It is observed for all levels of iron oxide and for both the 1:1 and 2:1 molar ratios of MgO and SiO_2. The amount increases with holding time, confirming the observations on the forsterite composition discussed above. The amount also increases with increasing iron oxide, decreasing temperature, and decreasing silica, in accordance with the ternary phase diagram.

5. In adding up the percentages of each phase as calculated from the x-ray diffraction results, a large quantity is found to be unaccounted for. Part of this is due to the change in the intensity of the diffracted radiation from the forsterite and enstatite as a result of substitution by CaO or FeO. However, some is undoubtedly due to the presence of other crystalline phases, such as the magnesioferrite, and glasses. Glasses were particularly noticeable in the high silica compositions, where the samples "slumped" after long exposure times. The amount of the unaccounted material is also high in the CaO and Fe_2O_3 ternaries, since a large amount of liquid which can form glass is present at the firing temperatures. There is a smaller unidentified fraction in the Al_2O_3 ternary, since only a small liquid region is present at the firing temperature.[50] The amount of glass increases with increasing temperature, increasing third oxide, and increasing silica, again in accordance with the ternary phase diagrams.

In conclusion, the magnesium silicate compounds are also found in the ternary systems, although in smaller amounts and with slightly different chemistry. It appears that the mechanism by which they form is

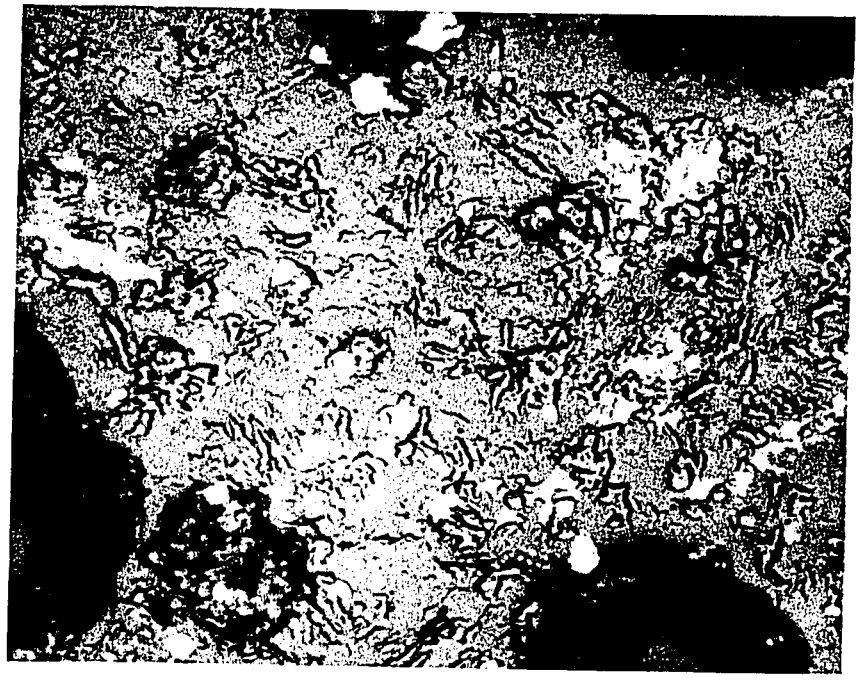


Figure 49: Micrograph showing the presence of $MgO \cdot Fe_2O_3$ (bright round phase) in a 57.3 wt% MgO - 42.7 wt% SiO_2 - 20 wt% Fe_2O_3 ternary exposed at 2650°F for 30 minutes.
750X.

similar to that in the binary system, with the diffusion of magnesium ions being the key step leading to an initial layer of enstatite, then followed by forsterite. Excess silica, if present, reacts with forsterite to form enstatite.

The addition of ions of the third oxide complicates matters but does not seem to affect the basic mechanism. However, additional reactions also proceed, as glasses and other phases are formed. The glasses probably initiate as the silica vitrifies and combines with iron oxide to form low melting point liquids. These liquids can eventually dissolve some of the magnesium oxide, but the solubility at the firing temperatures is limited. If the solubility is exceeded, an olivine will be forced to precipitate on cooling, leading to another mechanism for the formation of forsterite--the precipitation from supersaturated glasses. If iron is present in the olivine, the iron can oxidize to form the magnesiowustite, leaving a purer forsterite behind.

D. Summary

The reaction between MgO and SiO_2 proceeds by the mechanism described earlier--the rapid diffusion of Mg^{2+} into the silica grains to form forsterite, followed by the slower back-diffusion of Si^{4+} after the depletion of MgO to form enstatite. By virtue of the particular mechanism and its kinetics, the phase most prevalent during the initial stages of the reaction is forsterite, regardless of the initial composition. The forsterite forms very rapidly at about 2550°F and above.

The rates of these reactions are influenced by the atmosphere and the composition. The addition of third oxides yields similar results, although a number of additional complications may also occur.

In terms of dross formation, the reaction between the two oxides to form forsterite is probably the dominant effect. First, it explains the absence of significant enstatite in dross, since very little enstatite forms until all of the readily available MgO is consumed as forsterite. In view of the temperatures and times prevalent in nodular iron treatment, forsterite should be the dominant phase.

Secondly, the rate at which forsterite forms by the reaction between MgO and SiO_2 is from one to three orders of magnitude faster than the reaction between MgO and silicon. The other possible reaction (between magnesium and SiO_2) did not produce forsterite or enstatite directly. Other possibilities, such as the formation of forsterite from liquid phases or precipitation from glass phases, have not been studied in any detail.

Finally, it has been shown that both MgO and silica are produced on the surface of the melt by oxidation during treatment and can also be produced by various side reactions. Therefore, there are numerous sources of MgO and SiO_2 which react rapidly to form forsterite.

ENGINEERING ASPECTS

The sequence of events which may lead to the formation of forsterite and enstatite has been followed from the introduction of magnesium and silicon into the iron melt. Factors which affect the rate at which the magnesium and silicon oxidize have been discussed and various ways in which the oxides and the dissolved elements might interact have been followed in simplified systems. It appears that the results of these reactions are simply to form additional magnesium and silicon oxides and that the magnesium silicates cannot form until both MgO and SiO_2 are present and in contact with one another. The prior reactions simply determine the amount and rate at which MgO and SiO_2 are generated, and a number of environmental conditions determine the progress of these reactions.

Once both oxides are present, the silicates can be formed, and it has been shown that after reasonable holding times forsterite is the predominant phase present. However, again the amount that is formed is determined by the environmental conditions--the atmosphere, temperature and additional phases to which it is exposed.

The results then indicate the sequence by which forsterite and enstatite form and point out the effects of the surroundings on their formation. It remains to be investigated how these phenomena which were discovered under more or less ideal situations contribute to the dross which is found under production conditions. Here it will be difficult, if not impossible, to follow each step in the sequence of forsterite formation; however, the effect of the processing variables may be observed

on the over-all reaction to form forsterite. The variations caused by the processing variables may be assessed using the guidelines developed during the preceding discussion. These production-type experiments will be discussed under the following headings:

I. Experimental Procedure

II. Discussion of the Results for the Formation of Dross in Nodular Iron Melts

III. Discussion of Dross Formation and Dross Defects in Nodular Iron Castings

The discussion will include the results from the present work as well as results and observations found in the literature.

I. EXPERIMENTAL PROCEDURE

Nodular iron melts were produced in the laboratory by two techniques which will be described first. This will be followed by a discussion of the method by which the resulting dross was analyzed.

A. Experimental Equipment

Nodular iron was made by a transfer method and by a plunging method, and the experimental equipment used for each method was different.

1. The Transfer Method--One Hundred-Pound Heats

Several nodular iron melts were manufactured in the 100-pound capacity alumina-lined high-frequency induction furnace. The base iron was melted, superheated to 2900°F, and allowed to cool to 2750°F. The melt was tapped into an alumina-lined open ladle where a 9% magnesium ferrosilicon alloy was added during the tap. After the magnesium flare, the melt was poured back into the furnace with the addition of the 75%

ferrosilicon post-inoculant. The final composition of the melt was 3.85 - 4.06% carbon, 2.29 - 2.69% silicon, 0.40 - 0.50% manganese, and about 0.04% magnesium.

In the furnace, the melt was either allowed to furnace cool or was held at a constant temperature by a low power input. Metal samples were removed at various time intervals with vycor suction tubes; dross samples were removed with a cast iron scoop from the top of the melt. Only a representative portion of the total dross was removed during each sampling.

2. The Plunging Method--Five-Pound Heats

A large number of heats of nodular iron were produced in a small high-frequency induction furnace using a MgO crucible. The melt was superheated to 2900°F and cooled before nodularization as in (1).

The nodularizer was added to the melt by a plunging technique. A removable transite hood fit over the top of the induction furnace, Fig. 50. A six-inch length of 1/2-inch diameter pipe was welded to the center of a steel plate which formed the top of the hood. The pipe was situated so that it was centered over the MgO crucible.

The nodularizer was introduced by means of a graphite bell, which was later attached to a steel rod. The nodularizing alloy, wrapped in thin iron foil, was wedged into the cavity of the bell, the upper half of a two-piece splash plate was placed on the stem of the bell and the lower part of the bell screwed into the stem. The steel rod was then attached to the stem and inserted into the pipe, which guided the bell into the melt.

After the melt had been superheated, the lower splash plate was cemented to the top of the MgO crucible with "Core-fix." The entire

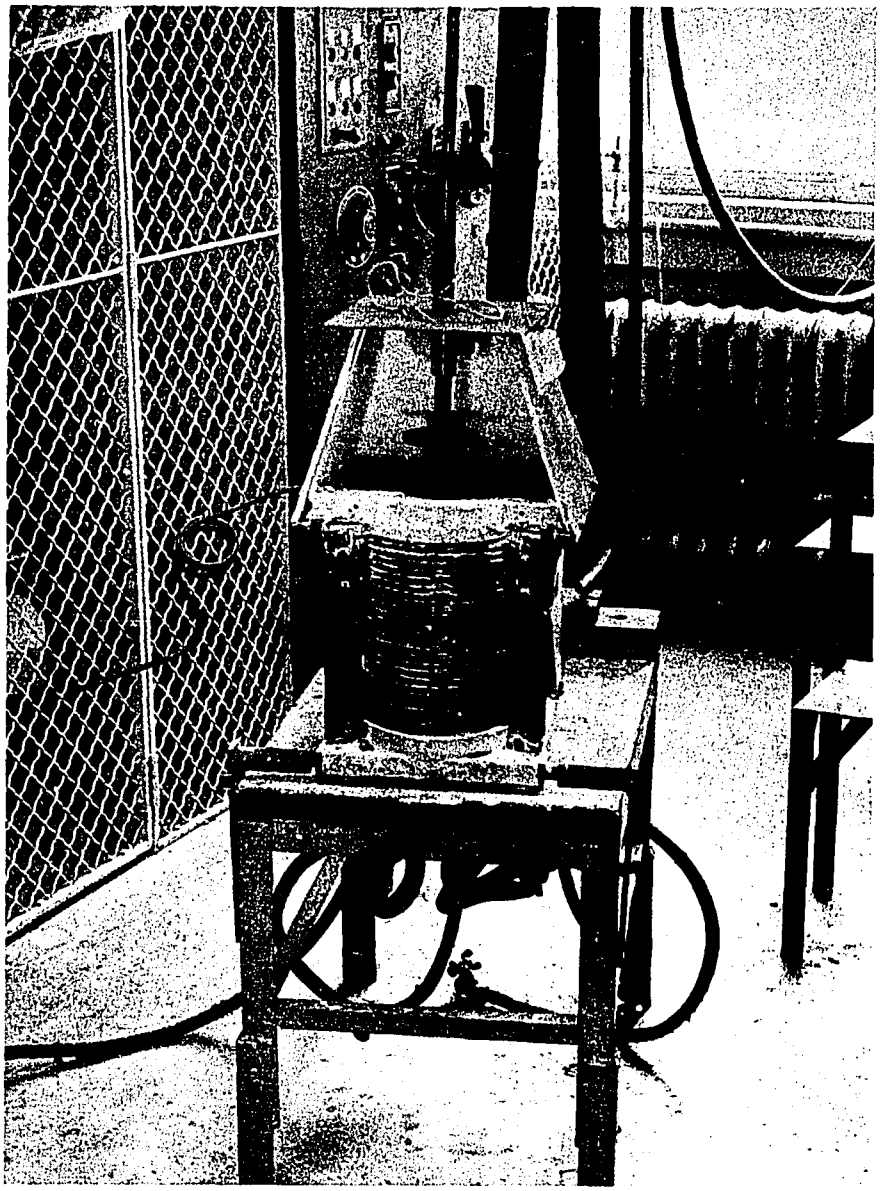


Figure 50: Experimental apparatus for the production of nodular iron in the five-pound induction furnace. (front panel of hood removed)

assembly of nodularizer, bell, steel rod, and steel plate was positioned above the melt and the bell held in place by means of a pin through the steel rod resting on the pipe. When the temperature of the melt cooled to the nodularization temperature, the pin was pulled and the weight of the steel rod drove the bell into the melt. During this step, the bell automatically carried the upper splash plate, to which a layer of Core-fix had been applied, onto the matching lower splash plate, cementing the two together, Fig. 51. Therefore, no metal was lost by splashing during nodularization.

After the magnesium flare abated, the entire assembly was removed. The post-inoculant could then be added, again by plunging a smaller graphite bell into the melt.

Dross samples were removed, generally after an extended holding period at 2500°F, by means of a small graphite shovel. All of the dross was removed each time. Metal samples were obtained using vycor suction tubes. The chemistry of the raw materials used in these experiments is contained in Appendix I.

B. Analysis of the Dross

The dross was initially examined for large pieces of iron collected inadvertently with the dross, and the iron was discarded. The dross was then crushed in a steel mortar and screened. Some metal droplets were held by a 30-mesh screen size and were also discarded as accidentally removed with the dross. Material held by a 270-mesh screen was considered to be metallic dross, small particles of iron trapped during nodularization and undissolved nodularizer and post-inoculant alloy. The material that passed through the 270-mesh was found to be primarily oxide material and was called fine dross. The total material passing through the 30 and 270

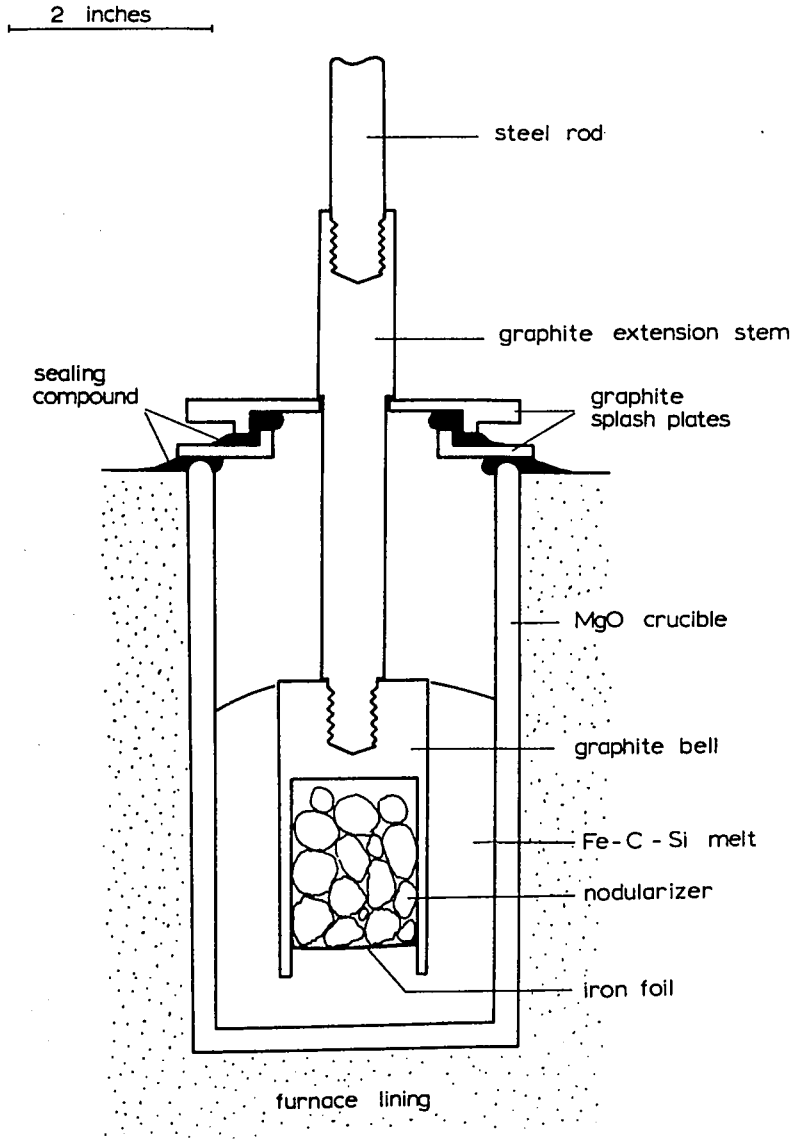


Figure 51: Schematic diagram of the graphite bell assembly for plunging in the five-pound induction furnace.

mesh screens was called total dross. These classification were quite arbitrary--some very fine metallic particles, for example, can be found in the fine dross. However, this classification does permit the dross obtained using different processing variables to be compared objectively and the effect of these variables to be assessed.

The amounts of both the fine and metallic dross were determined by weighing. Since the same amount of metal was not used during each heat, the amount of dross, weighed in grams, was converted to the equivalent number of grams that would be obtained had the melt been 100 pounds--hence, the units of grams of dross per 100 pounds of metal. The crystalline composition of the fine dross, particularly with reference to the MgO, SiO_2, and the magnesium-silicates, was determined by quantitative x-ray analysis, using the calibration curves developed earlier. No corrections were made for the possibility of additional cations being dissolved in the forsterite or enstatite.

A description of each heat, complete with the amount and composition of the dross, is given in Appendix IV.

II. DISCUSSION OF THE RESULTS FOR THE FORMATION OF LADLE DROSS IN NODULAR IRON

The formation of dross in nodular cast iron is complex because of the variety of components that may be present and, since equilibrium is difficult to achieve, these components continue to react. Even when only the reactions required to produce MgO, SiO_2, and the magnesium silicates are considered, the dross formation is difficult to follow because of the variety of reactions required and because of the profound influence of numerous processing variables on reactions. In this

section, a number of variables will be discussed in relation to their effect on the amount of dross which is formed and on the amount of MgO, SiO_2, forsterite, and enstatite that are present in the dross. These variables will be discussed in the following order:

A. Time of Holding at Temperature

B. Nodularizing Temperature and Holding Temperature

C. Atmosphere

D. Metal Chemistry, Including Sulfur, Magnesium, Cerium, and Silicon

The effects of each will be interpreted in view of the results obtained in the magnesium-silicon-oxygen system.

A. The Effect of Time

A study of the processing variables is complicated by the fact that the dross constantly changes with time in approaching equilibrium in the melt-slag system. Fig. 52 shows how the amount and composition of the dross varies as a function of time in the five-pound heats. In this case, no post-inoculant was used, and the dross was initially removed immediately after the magnesium flare. The melt was then held at 2500°F as new dross began to form on the melt surface. After 300 seconds, this dross was again removed, and the melt was maintained at temperature. This procedure was continued for 15 minutes at intervals. The quantity of dross as plotted in Fig. 52 is then the cumulative dross removed. The increase in the amount of dross with time is not just a reflection of the oxidation of the unprotected surface but is also due to flotation of fine particles and subsurface reactions. The same behavior is observed when a series of heats is run, with the dross being removed at different times in different heats. The results of two such series are shown in Fig. 53.

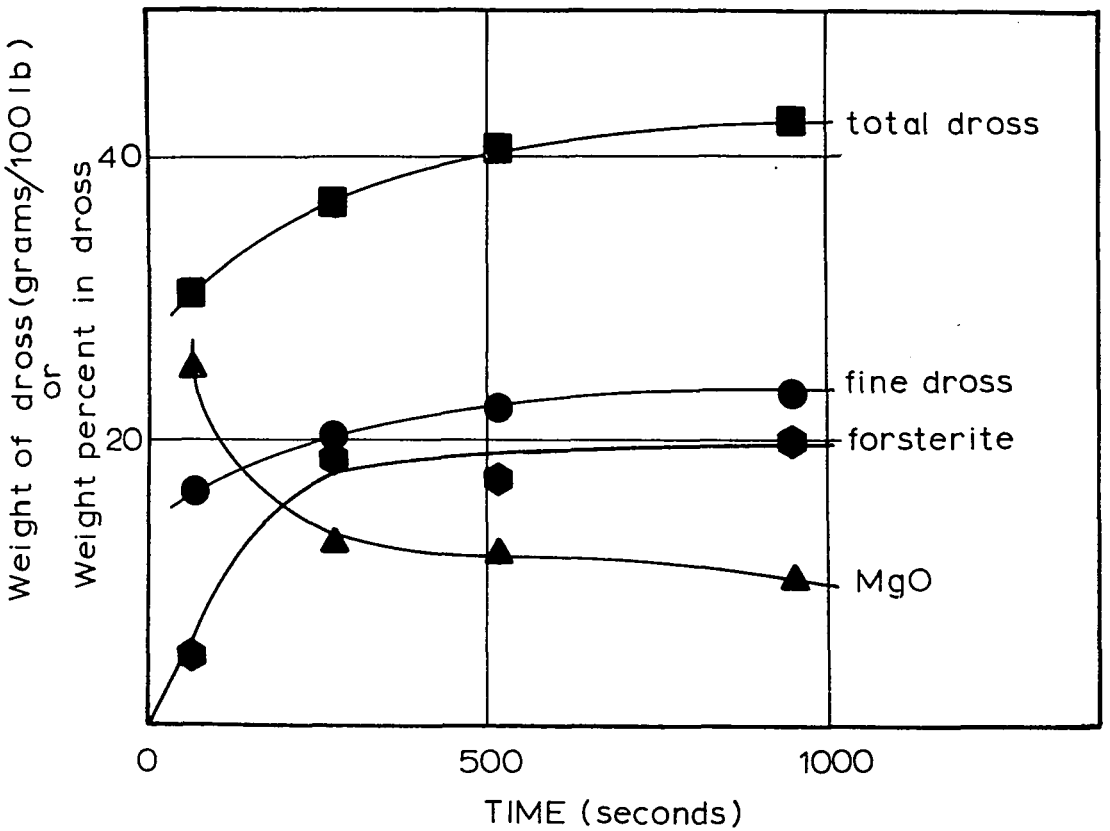


Figure 52: The effect of holding time on the quantity and chemistry of dross. Experiments were performed in the five-pound induction furnace and dross samples removed intermittently. Nodularized at 2750°F with 9% MgFeSi; no post-inoculant.

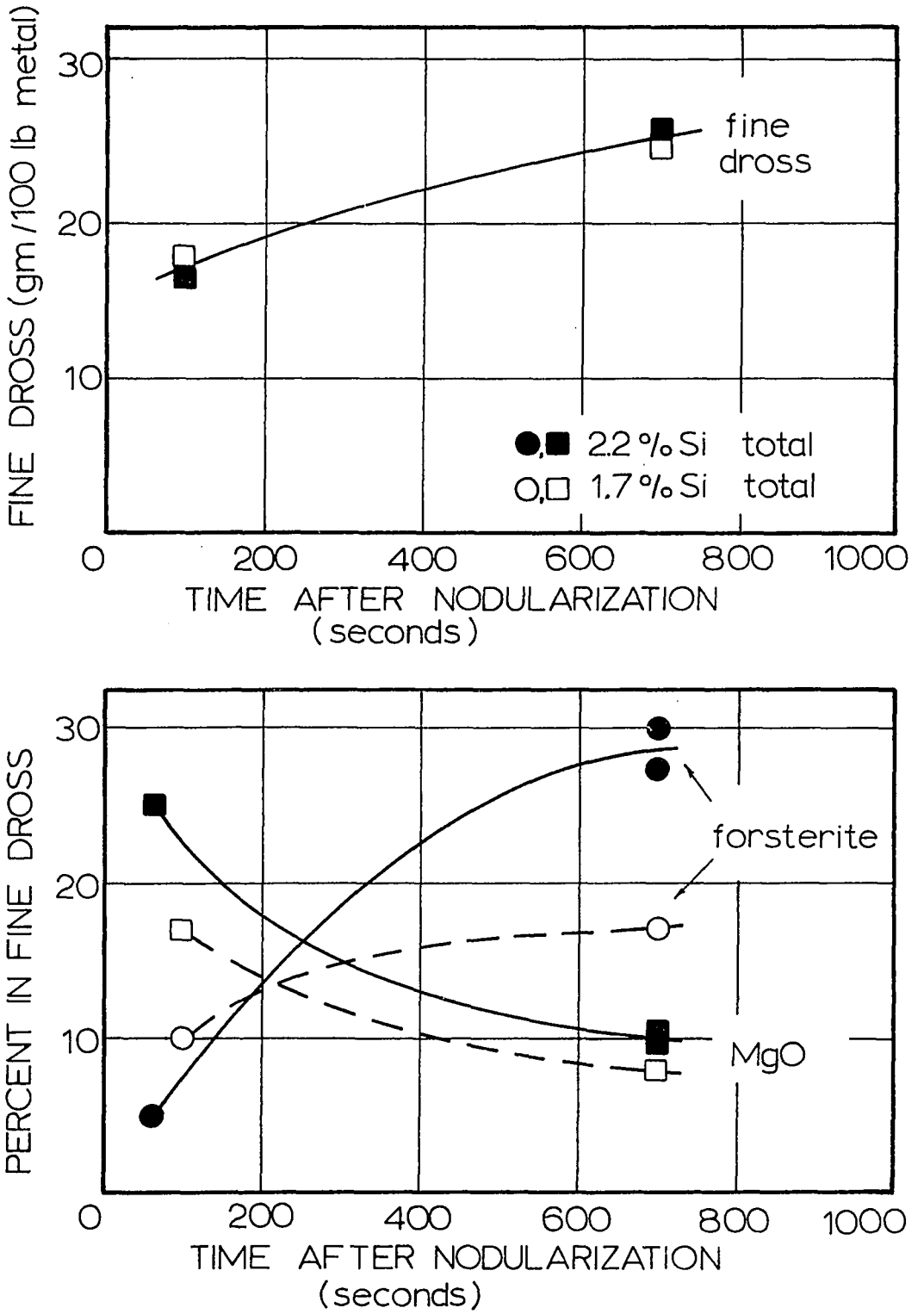


Figure 53: The effect of holding time on the quantity and chemistry of dross. Experiments were performed in the five-pound induction furnace. Dross was removed immediately after the magnesium flare in one heat and after 700 seconds in a second heat. Nodularized with 9%MgFeSi at 2750°F and held at 2500°F. No post-inoculant added.

The amounts of MgO and forsterite also change with time. The initial dross formed during the nodularization treatment is high in MgO but low in forsterite. However, if the melt is skimmed after a period of time and then the newly formed dross is collected, it is found to be considerably higher in forsterite than MgO. A holding temperature of 2500°F is in the center of the temperature range for the CO/SiO_2 inversion, see Fig. 16; as a result, silica will form on the melt surface (if the dissolved magnesium does not interfere).

Because MgO continues to form by oxidation, the result is that in the newly forming dross, MgO and silica can exist intimately, and consequently forsterite can form.

Immediately after nodularization, the forsterite is quite low while the MgO is high. If the dross is not removed until 700 seconds have elapsed, however, there is time for reaction between the MgO and silica already present in the dross to form forsterite, Fig. 53. Part of the increase in forsterite, of course, is due to the later formed dross, which is high in forsterite. The fraction of the forsterite from later formed dross and that from reactions in the original dross has been calculated. The later formed dross comprises 20 to 30 percent of the forsterite observed after holding 700 seconds. The remainder of the forsterite forms by reactions in the dross produced during the initial nodularizing treatment.

This same behavior was observed in the 100-pound heats where only a portion of the dross was removed each time. The composition of the initial dross can be followed in Fig. 54 as it changes due to the reactions proceeding within the dross. As can be seen, the MgO and crystalline silica (only part of the total silica) initially rise to

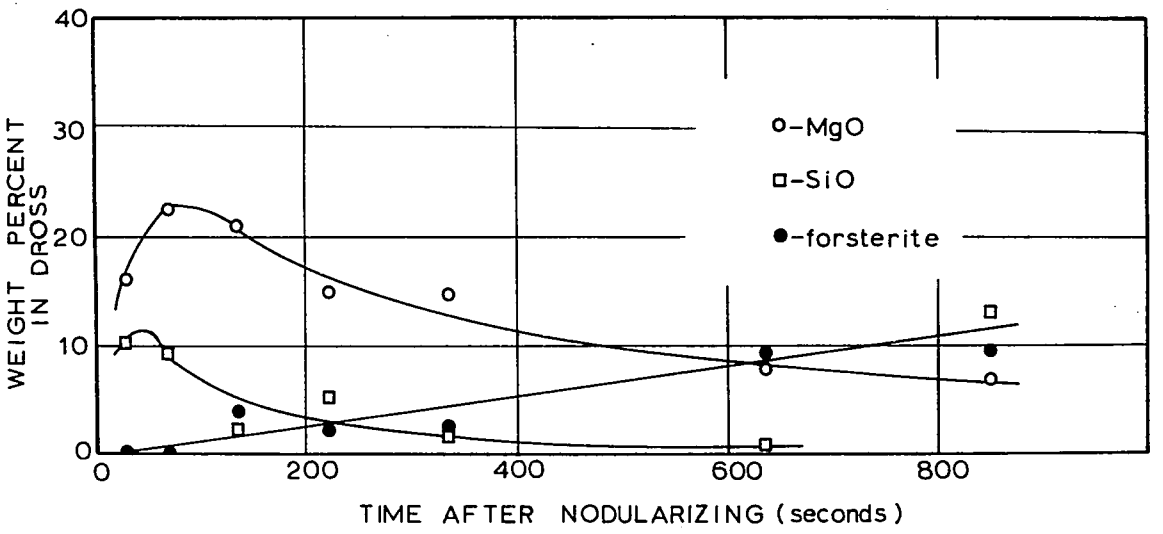


Figure 54: The effect of holding time on the chemistry of dross. Experiments were performed in the 100-pound induction furnace and representative dross samples removed intermittently. Melt nodularized with 9% MgFeSi and post-inoculated with 75% FeSi at 2750°F and held at 2500°F.

a peak and then decrease, while the forsterite continues to increase. The increase in forsterite again is partially attributable to the newly formed dross, and the balance is due to the reaction between the MgO and silica, which decrease concurrently.

The initial increase in MgO and silica is believed to be due to the rapid and continuing oxidation of the magnesium and silicon, partly from the melt and partly from the unreacted nodularizer and post-inoculant. This proposal is supported by the fact that the fine dross increases directly after inoculation, as the metallic dross passes to the non-metallic dross and the melt, Fig. 55.

Heats were run in which only the nodularizing alloy was added, and the melt was furnace cooled. When compared to a similar heat in which a post-inoculant was added before furnace cooling, the MgO peak (see Fig. 54) was higher but the silica peak and the forsterite were lower than the post-inoculant heat. This is an indication that the silicon added in the post-inoculant is important in the formation of the forsterite--that without the late addition of silicon, the supply of silica which is necessary for the formation of forsterite is considerably restricted.

The important point to note in this discussion is that the dross is continuously forming and changing. The change in the composition is due both to the different chemistry of the late forming dross and to reactions proceeding in the originally formed dross. The major crystalline phases are MgO and forsterite. Very little enstatite is ever observed in the dross, for reasons explained in Section V of the Results and Discussion. Therefore, it is apparent that the dross can never be completely eliminated, no matter how good the skimming technique may be. However, the

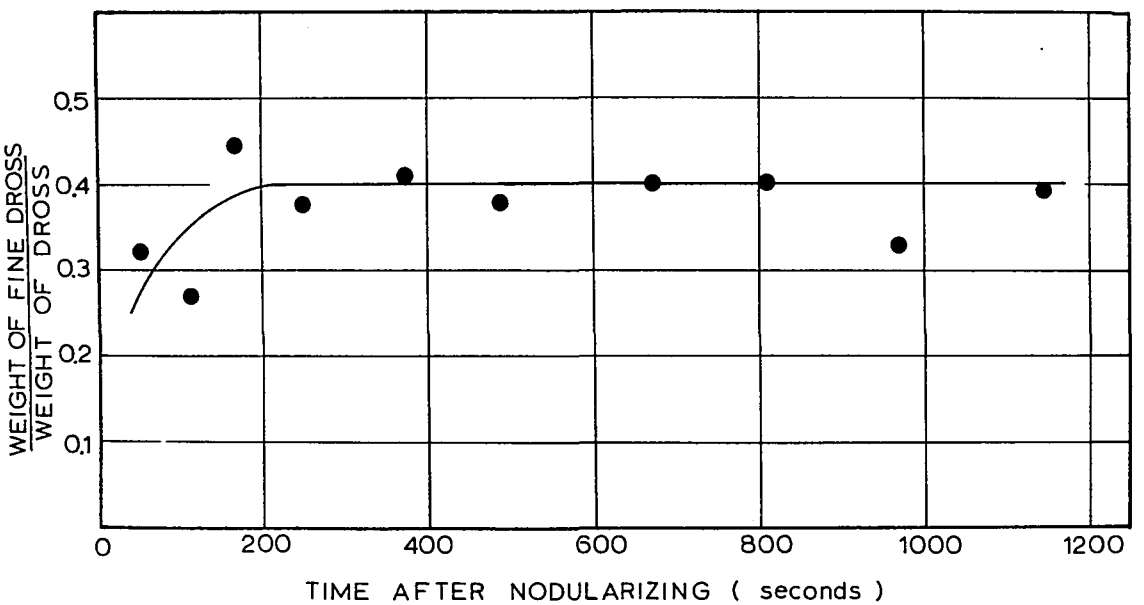


Figure 55: The effect of holding time on the ratio of fine dross to total dross for the experiment in Fig. 54.

quantity and composition of the dross can be adjusted by choosing appropriate pouring times, pouring temperatures, processing sequence, and quantities of inoculants.

B. The Effect of Holding and Nodularizing Temperatures

1. Holding Temperature

The nature of the dross produced by nodularizing a 100-pound melt with 9%MgFeSi and post-inoculating with 75%FeSi at 2750°F and holding at various temperatures for 700 seconds is shown in Table XII. The melt cooled to the holding temperature in less than 60 seconds.

TABLE XII

EFFECT OF HOLDING TEMPERATURE ON QUANTITY AND CHEMISTRY OF DROSS

Holding Temperature (°F)	Fine Dross (grams/100 lb. of Metal)	Forsterite (% in Fine Dross)	MgO (% in Fine Dross)
2400	10.3	10.5	2.5
2500	9.1	8.5	8.0
2600	8.3	8.7	4.3

*Post-inoculating at 2750°F, power used to hold melt at indicated temperature.

Dross increases with decreasing holding temperature. As the temperature decreases, the silica becomes more stable as a consequence of the CO/SiO_2 inversion temperature, Fig. 16. The increase in the silica can first increase the quantity of dross and second, by entering into the reaction with MgO, can increase the percentage of forsterite. The MgO reaches a maximum near 2500°F, however, because this is the temperature at which magnesium is lost most rapidly from the melt (see Fig. 20).

2. Nodularizing Temperature

In addition, different nodularizing temperatures were tried in the 100-pound heats under the same conditions, Table XIII.

TABLE XIII

EFFECT OF NODULARIZING TEMPERATURE ON QUANTITY AND CHEMISTRY OF DROSS IN 100-POUND MELTS

Nodularizing Temperature (°F)	Fine Dross (grams/100 lb. of Metal)	Forsterite (% in Fine Dross)	MgO (% in Fine Dross)
2600	14.5	5.0	17.5
2750	10.3	10.5	2.5

Melt held at 2500°F for 700 seconds, then dross collected.

The effect of nodularizing temperature was also investigated in a series of five-pound heats treated with 9%MgFeSi and held at 2500°F for 700 seconds, Table XIV.

TABLE XIV

EFFECT OF NODULARIZING TEMPERATURE ON QUANTITY AND CHEMISTRY OF DROSS IN FIVE-POUND MELTS

Nodularizing Temperature (°F)	Fine Dross (grams/100 lb. of Metal)	Forsterite (% in Fine Dross)	MgO (% in Fine Dross)
2550	24.0	15.1	15.3
2650	28.7	11.8	8.8
2750	24.8	15.8	8.1

Melt held at 2500°F for 700 seconds, then dross collected.

The large differences between the two sets of data for the nodularizing temperature are a result of the different treatment methods. In the 100-pound melts, the metal was treated by the transfer technique, in which the metal was poured into a ladle for nodularization and back into the furnace for post-inoculation. Some of the dross was lost during this transfer, explaining the lower quantity in the 100-pound case.

The second difference is that the 100-pound melts were post-inoculated while the five-pound melts were not.

When the nodularizing temperature changes, the quantity of dross reaches a maximum in the temperature range 2600 to 2650°F because of the effect of the inversion temperature. The quantity decreases again at lower temperatures because the lower magnesium loss rate produces a limited supply of MgO. The forsterite is at a minimum near the inversion temperature for the following reasons. At higher temperatures, MgO can react rapidly with silica to form forsterite; however, this is limited by the availability of silica. At lower temperatures, the reaction between MgO and silica is enhanced because of the large amount of silica which is present as a result of the inversion between CO and SiO_2. Finally, the MgO increases with decreasing nodularization temperature because the magnesium loss rate increases as the temperature is reduced towards 2500°F, Fig. 20.

Therefore, the effect of the temperature can be explained in terms of the CO/SiO_2 inversion temperature, the magnesium loss rate, and the various reactions in the Mg-Si-O system. These factors affect the availability of MgO and silica and subsequently the quantity and composition of the dross.

C. The Effect of Atmosphere

A special five-pound heat was run using an argon atmosphere which was contained within the transite hood. A comparison between air and argon for melts treated at 2750°F with 9%MgFeSi and held for 700 seconds at 2500°F is shown in Table XV.

TABLE XV

EFFECT OF ATMOSPHERE ON QUANTITY AND CHEMISTRY OF DROSS

Atmosphere	Fine Dross (grams/100 lb. of Metal)	Forsterite (% in Fine Dross)	MgO (% in Fine Dross)
air	20.0	28.5	10.0
argon	21.6	10.5	50.2

Nodularized at 2750°F with 9%MgFeSi, held at 2500°F for 700 seconds, then dross removed.

The quantity of dross is about the same in both atmospheres; however, the composition is drastically altered. The argon atmosphere lowers the oxygen pressure over the melt, which in turn will lower the CO/SiO_2 inversion temperature (all other factors remaining constant), Fig. 16. However, the argon atmosphere is not very pure and some oxygen will still be available to the melt. Therefore, there can be a competition for the oxygen between magnesium and silicon. In previous discussions of the Mg-Si-O system, it was pointed out that the magnesium would scavenge all available oxygen until all of the magnesium was chemically combined. Only then could silicon oxidize. This effect is accentuated when the inversion temperature for the silica is lowered, and almost all of the limited supply of oxygen will be combined with the magnesium. This explains the large amount of MgO formed in argon. A direct result

of the competition for oxygen and the resulting low level of silica is that forsterite cannot form in large quantities because silica is necessary. This is true even though a large amount of MgO is present.

Therefore, lowering the oxygen partial pressure does not necessarily prevent dross formation but merely changes the composition of the dross which is formed.

D. The Effect of Chemistry of Melt, Nodularizer, and Post-inoculant

Previous investigators have observed that the metal chemistry as well as the chemistry of the nodularizing and post-inoculant alloys has an effect on the incidence of dross defects.[1-5] Several of these variables were investigated quantitatively in this study.

1. Sulfur in the Metal

Sulfur has in general been found to be deleterious to nodular iron, both because it lowers the efficiency of magnesium additions (since desulfurization must occur) and because the incidence of the dross defect increases. The influence of a high sulfur melt is shown in Table XVI.

TABLE XVI

EFFECT OF SULFUR ON QUANTITY AND CHEMISTRY OF DROSS

Sulfur (%)	Fine Dross (grams/100 lb. of Metal)	Forsterite (% of Fine Dross)	MgO (% of Fine Dross)
0.012	20.0	28.5	10.0
0.05	36.4	18.0	7.0

Nodularized at 2750°F with 9%MgFeSi, held at 2500°F for 700 seconds, then dross removed.

The competition of sulfur and oxygen for the magnesium causes the dross to greatly increase while both MgO and forsterite decrease. Even though MgO is thermodynamically more stable than MgS, extensive desulfurization during nodularization does occur, thereby combining much of the magnesium as MgS rather than MgO and consequently making it more difficult for forsterite to form. The limiting factor in the formation of forsterite in this instance, as compared to the effect of argon on the quantity of forsterite, Table XV, is the amount of MgO available rather than the amount of silica.

2. Magnesium in the Metal

Increasing the residual magnesium in the melt increases the incidence of dross defects. The residual magnesium level can be adjusted two ways--either by the amount of nodularizer added or by the type of nodularizer added (thereby affecting the recovery and the loss rate of the magnesium). Figs. 56 and 57 show the effect on the quantity and composition of the dross by these two considerations.

The amount of dross formed and the MgO content of the dross, Fig. 56, are not greatly influenced by additions of magnesium over 0.10%, although at lower magnesium levels the dross decreases with decreasing magnesium. However, the forsterite continually increases with increasing magnesium, so that the total MgO content (as MgO + magnesium silicates) also continuously increases. The forsterite increases because of the greater availability of MgO to react with silica. This then implies that at low magnesium levels, the lack of MgO is responsible for low forsterite.

This analysis is complicated by the fact that when the amount of magnesium is increased, the silicon also increases, since the nodularizer

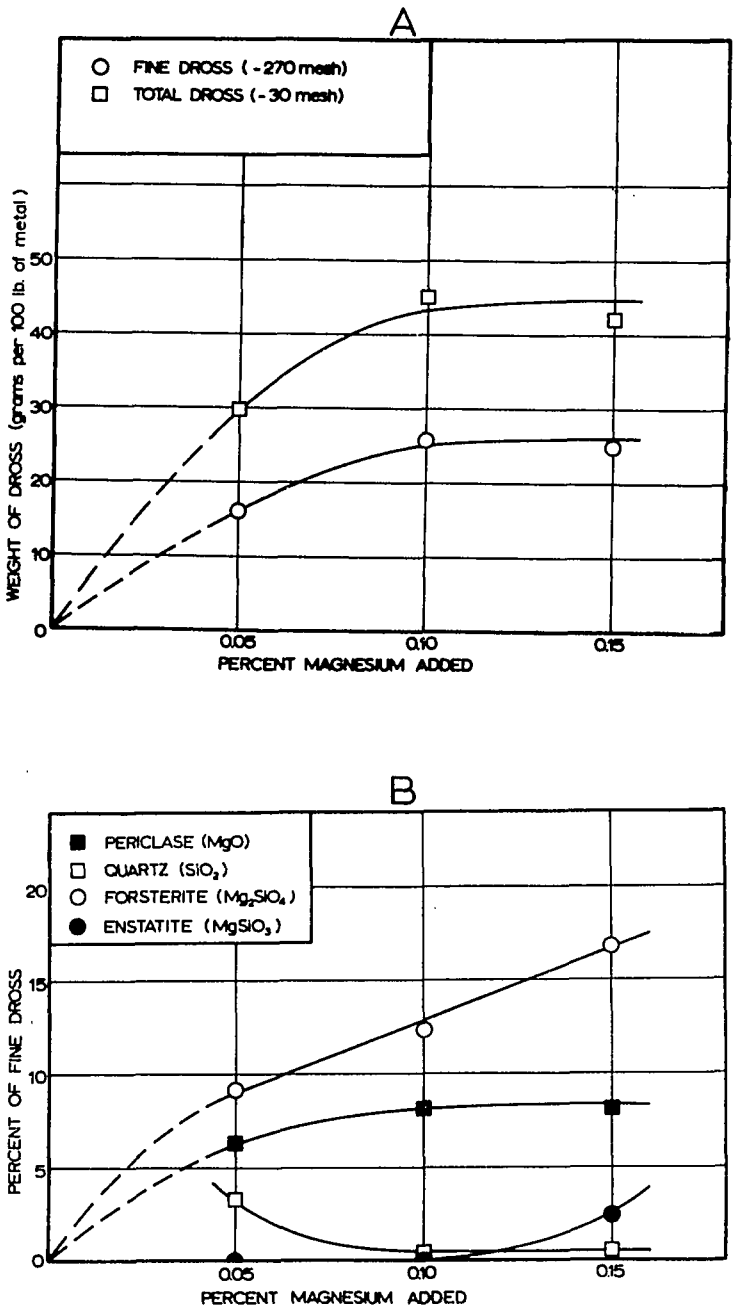


Figure 56: The effect of the magnesium added to the melt on the quantity (A) and chemistry (B) of dross. Experiments run in five-pound induction furnace. Nodularized with 9% MgFeSi at 2750°F; held at 2500°F for 700 seconds.

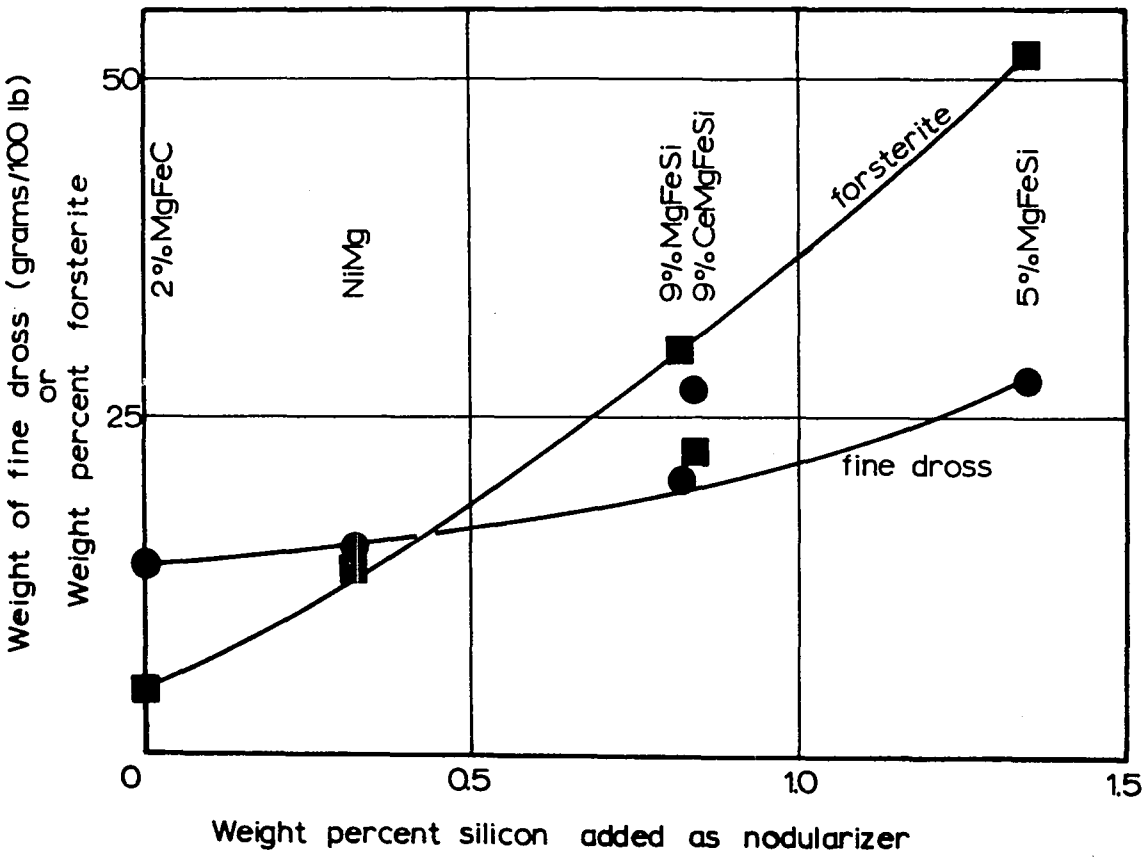


Figure 57: The effect of the silicon present in the nodularizer on the fine dross and forsterite. Experiments run in five-pound induction furnace. 0.15%Mg added in various nodularizers at 2750°F. No post-inoculant added. Melt held 700 seconds at 2500°F.

may contain as much as 50 percent silicon. Therefore, the role of silicon and magnesium in Fig. 56 cannot really be properly assessed.

By using nodularizers containing 0 to 50 percent of silicon and adding a constant percent magnesium (0.15%) to the melt, part of this difficulty may be overcome. These results are shown in Fig. 57 where both the fine dross and the forsterite increase with increasing silicon added in the nodularizer. The increasing silicon level makes it easier for more silica to form (since it raises the CO/SiO_2 inversion temperature and also provides local regions very high in silica which can easily oxidize) and combine with MgO to form forsterite. However, both forsterite and the fine dross are present even when the nodularizer contains no silicon and no post-inoculant is added; therefore, some silica is produced by oxidation of the silicon in the base melt.

3. Cerium in the Nodularizer

Even a small amount of cerium can affect the quantity and composition of the dross. The effects of adding a cerium-bearing 9%MgFeSi nodularizer are compared to the standard 9%MgFeSi alloy in Fig. 57 and Table XVII. The cerium is responsible for a higher amount of dross and a lower percentage of forsterite within the dross.

TABLE XVII

EFFECT OF CERIUM ON QUANTITY AND CHEMISTRY OF DROSS

Inoculant	Fine Dross (grams/100 lb. of Metal)	Forsterite (% in Fine Dross)	MgO (% in Fine Dross)
9%MgFeSi	20.0	28.5	10.0
9%CeMgFeSi	27.0	22.4	23.9

Nodularized at 2750°F, held at 2500°F for 700 seconds, then dross removed.

The greater dross is due to the fact that the cerium competes with magnesium and silicon for oxygen and sulfur and probably forms cerium oxides and sulfides. Cerium oxide (CeO_2) has a free energy of formation only slightly less negative than MgO and cerium sulfide (CeS) is even more stable than MgS. Also, by deoxidation of the melt, the cerium can block the oxidation of silicon. The result is that silica does not form to as great an extent as in the absence of cerium, and therefore the MgO cannot be readily combined as forsterite. The net effect is to decrease the forsterite and increase the uncombined MgO.

4. Silicon in the Metal, Nodularizer, and Post-inoculant

Previous investigators have found that increasing silicon increases the incidence of dross defects in nodular iron castings, although no differentiation as to the source of the silicon was made. The sources of the silicon are the base metal, the nodularizer, and the post-inoculant. The influence of silicon added in the nodularizer has already been discussed (see Fig. 57) and increasing silicon was found to increase both the amount of dross and the forsterite in the dross.

Table XVIII shows the effect of the inital silicon in the melt prior to treatment. A 9%MgFeSi nodularizer with no post-inoculant was introduced at 2750°F and the melt held at 2500°F for 700 seconds. The silicon initially in the melt varied from zero to 1.38%. The total silicon after nodularization also increases, however, since a constant amount of silicon was added with the nodularizer. Therefore, it is not clear whether the changes are due to the melt silicon or the total silicon.

TABLE XVIII

EFFECT OF MELT SILICON ON QUANTITY AND CHEMISTRY OF DROSS

Melt Silicon (%)	Total Silicon (%)	Fine Dross (grams/100 lb. of Metal)	Forsterite (% in Fine Dross)	MgO (% in Fine Dross)
0.00	0.83	32.7	16.9	9.4
0.88	1.70	24.8	15.8	8.1
1.38	2.20	20.0	28.5	10.0

Nodularized at 2750°F with 9%MgFeSi, held at 2500°F for 700 seconds, then dross removed. Silicon added as nodularizer held constant.

Increasing the silicon in the melt therefore decreases the quantity of dross and increases the percentage of forsterite in the dross.

In another series of heats, the amount of post-inoculant was varied; in this series, the total silicon was held constant at 2.2%. Therefore, the melt silicon varied inversely to the post-inoculant silicon. Table XIX shows that increasing the post-inoculant and therefore decreasing the melt silicon increases the dross and decreases the forsterite.

TABLE XIX

EFFECT OF POST-INOCULANT ON QUANTITY AND CHEMISTRY OF DROSS

Post-inoculant Silicon (%)	Melt Silicon (%)	Fine Dross (grams/100 lb. of Metal)	Forsterite (% in Fine Dross)	MgO (% in fine Dross)
0.00	1.38	20.0	28.5	10.0
0.50	0.76	36.5	27.8	19.8
1.00	0.36	38.4	20.4	21.1

Nodularized at 2750°F with 9%MgFeSi, held at 2750°F for 700 seconds, then dross removed. Silicon added as nodularizer and total silicon held constant.

Obviously, part of this effect can be explained by the influence of the melt silicon. However, if the data from Tables XVIII and XIX are compared and the effect of the melt silicon taken into account, the post-inoculant is found to increase the quantity of dross, the forsterite, and the MgO.

It is apparent that the effect of the silicon on the formation and composition of dross is quite complex and depends on the particular treatment step at which the silicon is added as well as the amount of silicon which is added. The amount of the dross is increased by increasing silicon in the nodularizer and post-inoculant and decreased by increasing silicon in the melt. Forsterite is increased by increasing silicon added in all three steps, simply because this provides more silica for reaction with MgO.

These data are summarized in Figs. 58 and 59 by plotting the forsterite and fine dross versus the total silicon added in the nodularizer and post-inoculant. A clear trend of increasing dross and forsterite with increasing silicon is observed. However, it must be emphasized that slight variations in other processing variables are contained within the data, accounting for the wide scatter.

All of the different variables which affect the quantity and composition of the dross are summarized in Table XX.

III. DISCUSSION OF DROSS FORMATION AND DROSS DEFECTS IN NODULAR IRON CASTINGS

It now remains to correlate the basic information from the Mg-Si-O system and the data just discussed regarding dross formation in the melt

TABLE XX

SUMMARY OF THE EFFECT OF PROCESSING VARIABLES ON THE QUANTITY AND CHEMISTRY OF DROSS

Variable	Effect of Increasing the Variable on: Quantity of Dross	%Forsterite	%MgO
time	increases	increases	decreases
holding temperature	decreases	decreases	maximum occurs
nodularization temperature	maximum occurs	minimum occurs	decreases
P_{O_2} in atmosphere	no effect	increases	decreases
Sulfur in the melt	increases	decreases	decreases
Magnesium added to the melt	increases	increases	no effect
Cerium added to the melt	increases	decreases	increases
Silicon in the melt	decreases	increases	increases
Silicon added in the nodularizer	increases	increases	no effect
Silicon added in the post-inoculant	increases	increases	increases

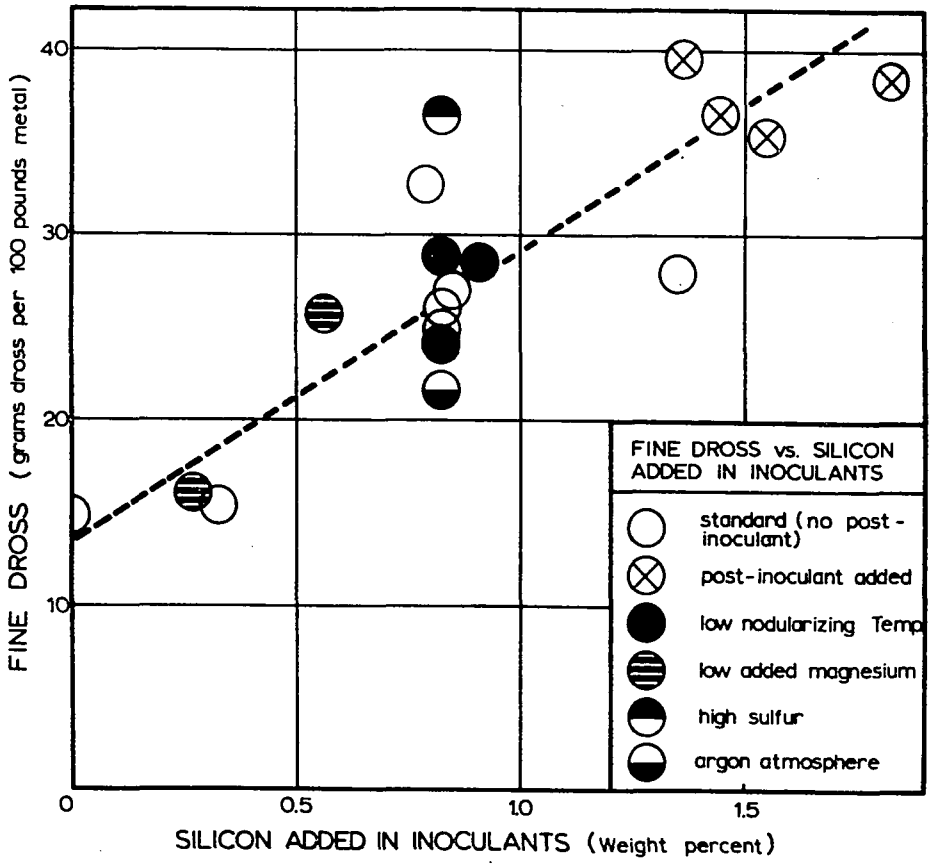


Figure 58: The effect of the silicon present in the nodularizer and post-inoculant on the amount of fine dross for experiments run under various conditions in the five-pound induction furnace. Standard conditions are for no post-inoculant, held at 2500°F for 700 seconds. Metal composition: 3.6%C, 0.8 - 2.2%Si, 0.4%Mn, 0.15%Mg added as various nodularizers.

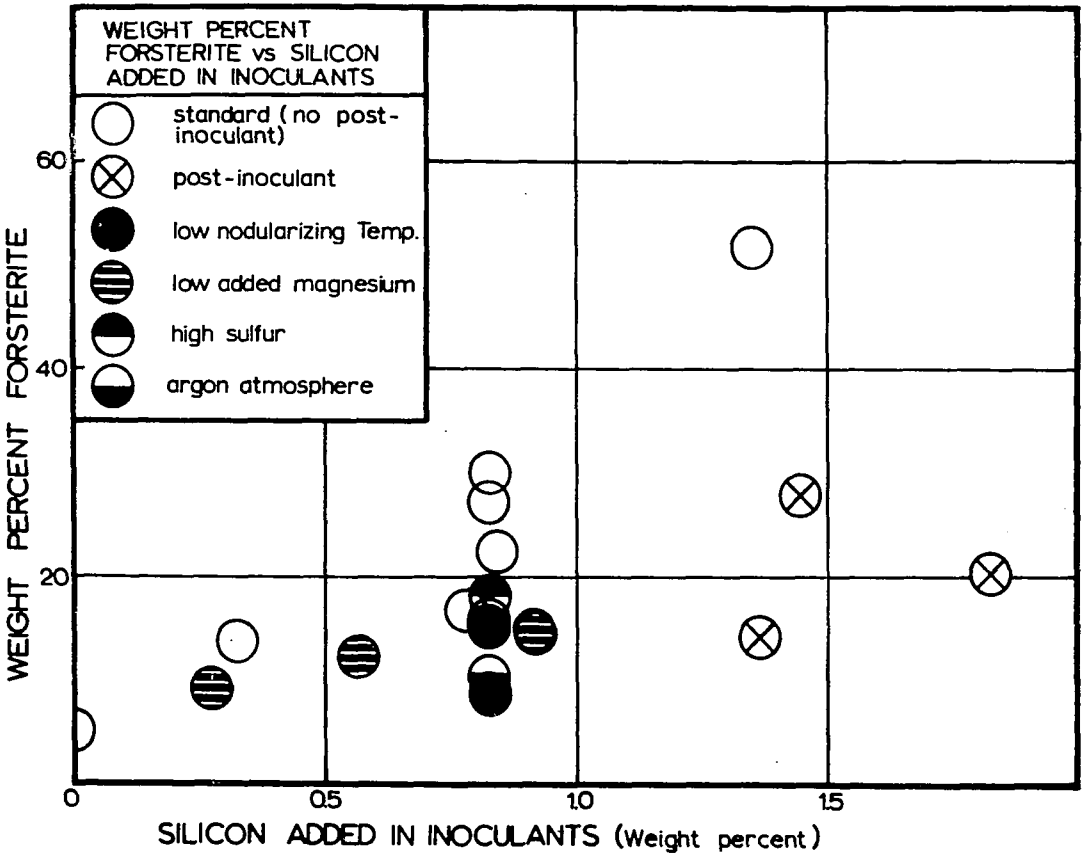


Figure 59: The effect of the silicon present in the nodularizer and post-inoculant on the amount of forsterite for experiments run under various conditions in the five-pound induction furnace.

with the actual defects observed in castings. First, however, a model for explaining the occurrence of the dross defects in the casting should be developed.

A. A Model for the Formation of Dross Defects in Nodular Iron

Two general types of dross layers on the surface of the melt have been observed. First, fluid dross films may be present which are very cohesive. Although they may not be removed either by manual skimming of the ladle or by the skimming action in the ladle or mold, with good gating practice they will remain in one piece after entering the mold cavity and will float on the top surface of the melt during the filling of the mold. Eventually, they will appear as a thin film on the upper surface of the casting. In this condition, they can be easily removed during cleaning or machining.

The second type of dross that may be found on the ladle consists of solid or crystalline phases bound weakly together by a more fluid phase. This layer is lumpy due to the coalescence of the solid particles in the dross and is much less cohesive than the fluid slag. Some of this material will evade the various skimming procedures, enter the mold cavity, and be easily broken up. The large lumps trapped on the surface during the mold filling produce large pits on the cope surface of the casting. Even worse, however, pieces of film and large dross lumps are trapped within the melt itself. Before they can float to the top, the mold is completely filled and a skin of metal frozen at the upper surface. The dross is then trapped just below the surface. This type of defect is very detrimental because it cannot be easily removed and is not easily found by inspection.

The dross trapped beneath the surface according to this model would then appear as gross dross particles and stringers, which are sections of the slag films. These are observed in nodular iron castings.[5] In addition, these particles and stringers are crystalline and high in MgO and forsterite in view of the type of dross film from which they originate.[52]

Therefore, the type of ladle dross which is most detrimental in the casting is that which contains a large fraction of solid crystalline oxides and silicates. According to this model, since MgO and forsterite have been found to be the principal crystalline components in ladle dross, methods which minimize MgO and forsterite also should minimize dross defects.

B. The Effect of Processing Variables on Dross Defects in the Casting

The formation of forsterite and MgO and the processing variables which affect them are now sufficiently well understood so that the previous empirical recommendations for dross control can be explained and new possibilities advanced. In this section, the effect of metal chemistry, nodularizer, post-inoculant, holding and pouring time, nodularizing and pouring temperature, mold design and turbulence, and fluxes will be discussed.

1. The Effect of Metal Chemistry

The metal chemistry has been repeatedly cited as affecting the amount and composition of dross and dross defects in castings. This can now be explained on the basis of a model for dross formation and of the parameters controlling the dross characteristics.

a. Magnesium

Magnesium increases the dross up to a certain point. Therefore, those in the literature who grade the effect of magnesium from being only slightly harmful to very harmful may be working at different magnesium levels. Furthermore, by speaking only of the residual magnesium levels, they neglect the amount of magnesium lost during actual nodularization and later dross formation, which is very important in shaping the composition of the resulting dross.

Increasing the magnesium increases the amount of forsterite which can form, Fig. 56, and consequently makes the dross film more crystalline and easier to break up during pouring of the castings. This effect is to a large extent a result of the reactions during the magnesium flare. However, as was pointed out earlier, Fig. 52, the dross which forms as a function of time is also quite high in forsterite and MgO. Therefore, high residual magnesium levels after nodularization can continue to increase the crystallinity of the dross. Finally, the magnesium dissolved in the melt can continue to oxidize and desulfurize under suitable conditions during pouring, filling of the mold, and solidification. This can result in the fine dispersions of dross, high in MgO and MgS, which are generally found in the castings.[52]

b. Sulfur

High sulfur melts have been observed to produce many dross defects, even though the sulfur decreases the MgO and forsterite composition of the dross. Part of this effect is due simply to a large increase in the amount of dross that is formed in the high sulfur melts. There may be surface tension effects as well since it is known that increasing sulfur content decreases the surface tension of slags.[53]

c. Silicon

The effect of silicon has been shown to be quite complex and dependent on the manner in which it is introduced into the nodular iron. Most investigators have noted that increasing silicon content is detrimental to the cleanliness of the castings. Both the amount of dross and the amount of forsterite are increased by the addition of silicon in the nodularizer and post-inoculant. Even when the silicon is added only to the base melt in increasing quantities, the forsterite level increases although the amount of dross decreases. Therefore, the result of the silicon is to provide increased silica which in turn can react with MgO to form forsterite. This produces a dross film which is increasingly crystalline and friable.

An interesting case in point is that in an iron containing zero silicon[4] no dross was found in the casting.

d. Aluminum and Calcium

Aluminum and calcium increase the incidence of dross defects. Both are easily oxidized and appear in the dross, primarily in the glassy phase as can be seen from the electron microprobe trace in Fig. 60. Only a small amount of calcium and no aluminum is present in the forsterite. These alumina and lime glasses have high melting ranges and add to the "lumpiness" of the crystalline aggregates.

e. Cerium

Cerium decreases the incidence of dross defects in castings, primarily by minimizing the formation of silica and consequently by decreasing the amount of forsterite. It also lowers the magnesium loss

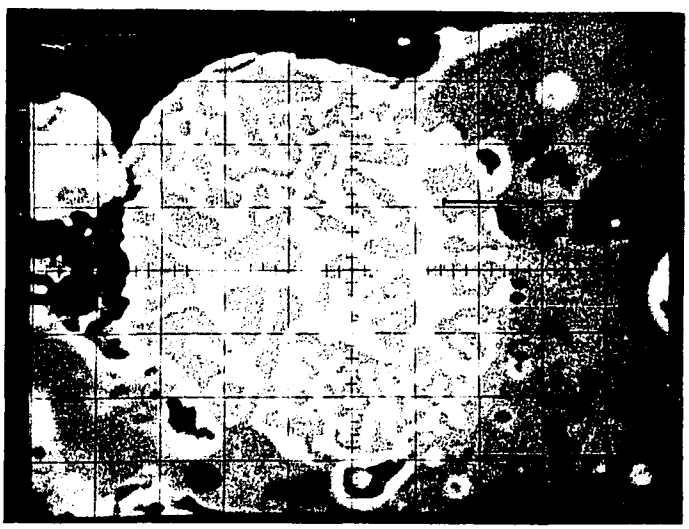


Figure 60a: Electron microprobe sample current micrograph showing a piece of 75% FeSi post-inoculant alloy (containing Si and $FeSi_2$)in ladle dross. Small dark particle at right is forsterite. Line indicates the region scanned in Fig. 60b. 300X.

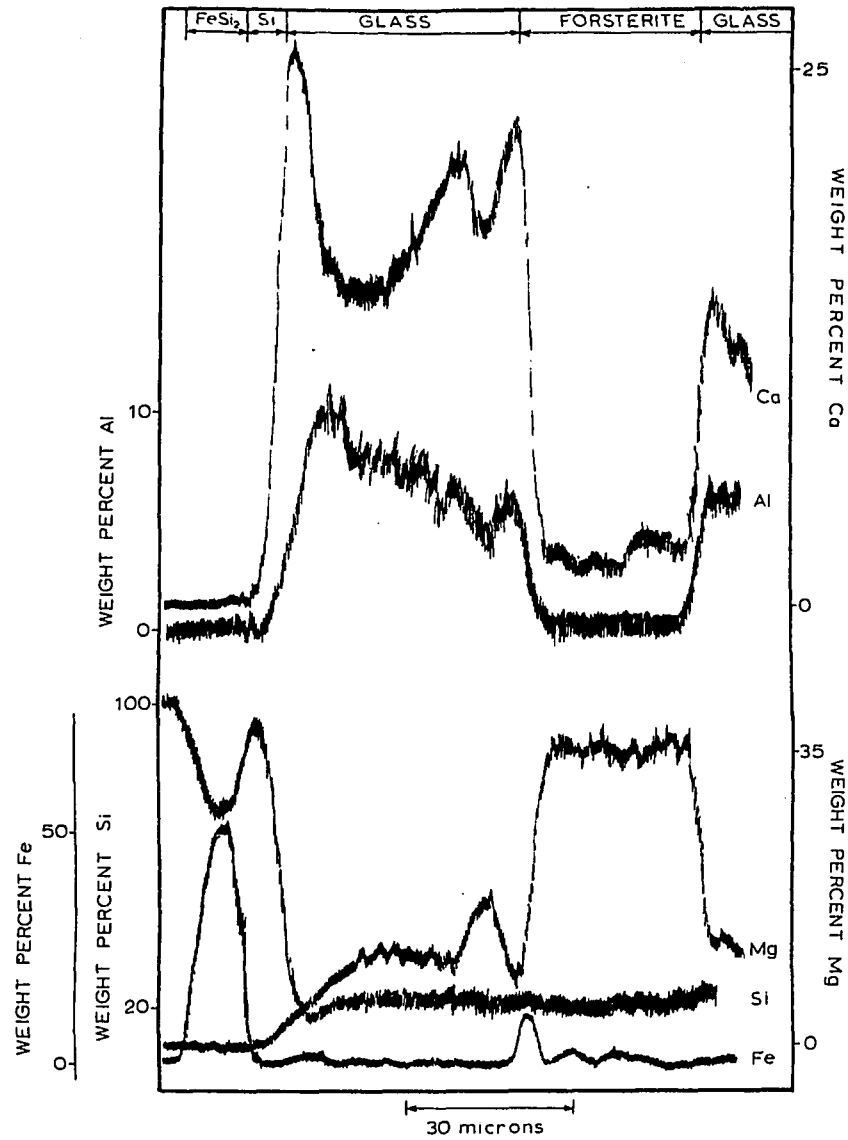


Figure 60b: Electron microprobe trace from the remains of 75%FeSi post-inoculant alloy (containing Si and $FeSi_2$) through a glass phase and into forsterite. Calcium, aluminum, silicon, iron, and magnesium traces are shown. Weight percents are approximate.

rate during holding and pouring and thus minimizes the formation of MgO and MgS which might otherwise appear as a fine dross.

2. The Effect of Nodularizer and Post-inoculant Alloys

The effect of various nodularizers and post-inoculants on dross defects that have been observed in the literature can also be explained by this model. Trojan et. al.[5] found that NiMg nodularizer produced fewer dross defects than 9%MgFeSi or 9%CeMgFeSi alloys. This has also been observed in this investigation and was related to the silicon input when equal amounts of magnesium were added by the different nodularizers. Increasing silicon increased both the total amount of ladle dross and the crystallinity of the dross.

Fuller found that kish graphite and SMZ alloy (63% silicon, 6% manganese, and 6% zirconium) used as post-inoculants produced a minimum number of dross defects, while CaSi and 75%FeSi led to more, and aluminum gave the worst effect. The SMZ was better than 75%FeSi because of a lower silicon level in the alloy, resulting in lower local silicon concentrations as the post-inoculant dissolved in the iron.

3. The Effect of Holding and Pouring Times

The long holding times and long pouring times previously found to increase dross defects are detrimental because they allow time for reactions to occur in the dross between MgO and silica, Figs. 52 to 54. This results in increased crystallinity of the slag film.

Long pouring times are also detrimental because they allow time for increased reaction between the atmosphere and the magnesium, resulting in the fine dross defect.

4. The Effect of Nodularization and Holding Temperatures

No published information has been found on the influence of the nodularizing temperature on the formation of dross defects. In this investigation it was observed that the total dross was at a maximum and the forsterite at a minimum near 2600 to 2650°F. This temperature range is somewhat lower than that recommended for the nodularizing temperature (2700 to 2750°F) necessary for the best nodular iron, although some foundries do use nodularization temperatures as low as 2650°F. Some balance must be struck between minimizing dross and maintaining the desirable properties of nodular iron.

When the pouring temperature is low (less than 2600°F), there is an opportunity for the silica to form by means of the inversion phenomenon. Both the amount of ladle dross and the forsterite content of the dross increase, and the dross film becomes more crystalline. High pouring temperatures which avoid the inversion temperature are then beneficial.

5. The Effect of Mold Design and Turbulence

Molds should be designed to permit a smooth flow of metal into the mold cavity. When the metal is subjected to turbulent flow, the dross films are broken up with the result that stringers and large dross defects can be trapped in the liquid metal. Also, during turbulence there is the opportunity for more contact between air in the mold cavity and the metal, with magnesium oxidizing to form fine dross particles. Pouring time should be minimum to reduce the mold-metal reaction time.

6. Fluxes

The use of a flux has been tried with a degree of success in some foundries. The fluxes used are generally either a chloride type or a

fluoride type (cryolite), with the fluoride type apparently more efficient. The ostensible purpose of the flux is simply to keep the ladles clean by fluxing the build-up of dross on the ladle linings. However, there may be beneficial side effects as well. The fluorine in the flux can compete with oxygen and sulfur for the magnesium ions and if successful can produce magnesium fluoride. In addition to the aluminum and sodium fluorides introduced by the flux, a liquid slag film can be produced which is very low in forsterite and MgO. Analysis of dross from a melt treated with a cryolite flux has shown that both forsterite and MgO are very low.

CONCLUSIONS

The investigation of the reactions occurring in the simple Mg-Si-O system and the effect of environmental conditions on the nature of these reactions has led to an understanding of the intermediate steps and the final reaction by which the magnesium silicates are formed.

It has been demonstrated that the simple oxides must be formed initially. Silica forms both by the thermodynamic inversion between carbon monoxide and silica and by the oxidation of silicon and ferrosilicon alloys added to the cast iron melt. The observed inversion temperature is non-equilibrium, being affected by the oxygen partial pressure over the melt, the refractory, the heating and cooling rates, and the inductive stirring of the melt. Inversion then occurs in cast irons between 2350 and 2600°F, even in the presence of small quantities of magnesium in the melt.

The formation of MgO occurs during nodularization by the oxidation of Mg_2Si

$$Mg_2Si + O_2 = 2MgO + Si$$

and also during holding by oxidation of the melt. The total magnesium lost during holding by vaporization and oxidation is minimized by avoiding silica crucibles, temperatures near 2500°F, contact with oxidizing conditions, and by using cerium-bearing nodularizers. Of the total magnesium lost during holding, about 15% is due to oxidation, the balance to vaporization.

In very high silicon-free magnesium melts, appreciable reduction of silica by magnesium to form MgO and silicon occurs. However, in nodular iron, where silicon is present and the magnesium level is very low, this reaction is negligible.

Forsterite can form from MgO and silicon in an air atmosphere but only after the silicon oxidizes; this reaction is several orders of magnitude slower than the reaction between MgO and SiO_2.

Forsterite (Mg_2SiO_4) is the principal product from the reaction between MgO and SiO_2. It forms very rapidly, regardless of the initial stoichiometry of the oxides, in the temperature range and times associated with nodular iron making, particularly at temperatures greater than 2550°F. The rate of formation is affected by the atmosphere and the addition of other oxides, which also produce new phases, including magnesioferrite and glass.

The simple oxides, MgO and SiO_2, and forsterite are found to be important constituents in nodular iron dross. An experimental procedure to evaluate the effect of typical nodular iron processing variables on both the amount and chemistry of dross has been developed. Factors which increase the total quantity of ladle dross are

1. increasing magnesium added to the melt
2. increasing silicon added to the melt as the nodularizer and post-inoculant
3. decreasing silicon added to the initial melt prior to treatment
4. increasing cerium and sulfur in the melt
5. increasing holding time and decreasing holding temperature

The amount of forsterite, which reflects the crystallinity of the dross, increases with

1. increasing magnesium and silicon added to the melt
2. decreasing cerium and sulfur added to the melt

3. increasing holding time and decreasing holding temperature

4. decreasing partial pressure of oxygen over the melt

This behavior is explained on the basis of the effect of the processing variables on the simple reactions in the Mg-Si-O system. Because both MgO and SiO_2 are necessary for the formation of forsterite, processing variables which minimize one of these oxides thereby minimize the total forsterite. On the other hand, variables which cause large amounts of one or both of the simple oxides or produces dross constituents in addition to MgO or SiO_2 will increase the total amount of dross.

A model for the formation of dross defects in the casting is proposed based on the nature of the dross film on the melt surface. A filmy dross is less objectionable than a lumpy, crystalline dross because the lumpy dross can produce subsurface inclusions more readily.

This model then can be used to explain the well-known effects of processing variables on the incidence of dross defects in castings.

This research opens several areas for further study. The effect of different CO atmospheres on the inversion temperature and on the nature of the silica film in grey and nodular iron would be useful. Secondly, a quantitative analysis of the glass phases present in the ladle dross, including the effects of aluminum and calcium, and a study of the interfacial energy between the dross film and the melt would provide information for controlling the slag to minimize defects in castings. Finally, in order to give the data more immediate utility, field studies in nodular iron foundries would be invaluable.

APPENDIX I

CHEMICAL ANALYSIS OF RAW MATERIALS

A. Magnesium-Silicon-Oxygen System Experiments

Material	Chemistry
Analytical Reagent Grade Magnesium Oxide (MgO) (Mallinckrodt Chemical Works)	MgO > 99.3%
Floated Silica Powder (SiO_2) about 240 mesh (Fisher Scientific)	SiO_2 > 99.5%
Reagent Grade Aluminum Oxide (Al_2O_3) (Merck and Co.)	Al_2O_3 > 99.3%
Reagent Grade Ferric Oxide (Fe_2O_3) (J. T. Baker Chemical Co.)	Fe_2O_3 > 99.3%
Reagent Grade Calcium Oxide (CaO) (J. T. Baker Chemical Co.)	CaO > 99.8%
Electronic Grade Silicon (Texas Instruments, Inc.)	Si > 99.9999%
Primary Stick Magnesium (Dow Metal Products Co.)	Mg > 99.84%

B. Engineering Aspects Experiments--Nodularizers and Post-inoculants

Material	%Si	%Mg	%Al	%Ni	%Ce	%Ca	%C
9%MgFeSi	46.5	8.49	0.75	-	-	1.48	-
CeMgFeSi	48.2	8.60	0.93	-	0.51	1.20	-
5%MgFeSi	46.95	5.0	-	-	0.17	1.05	-
NiMg	31.2	14.65	0.64	50.1	-	-	-
Synthetic MgFeC	-	2.1	-	-	-	-	4.9
75FeSi	75.94	-	1.30	-	-	1.05	-

C. Engineering Aspects Experiments--Pig Iron

Material	%C	%Si	%Mn	%P	%S	Others
Iron A	4.25	-	0.08	0.022	0.015	0.020Ti
Iron B	4.55	0.60	0.20	0.017	0.016	-

APPENDIX II

CALCULATION OF AVERAGE PENETRATION

The tube is characterized by

r_i = inside radius of tube

r_o = outside radius of tube

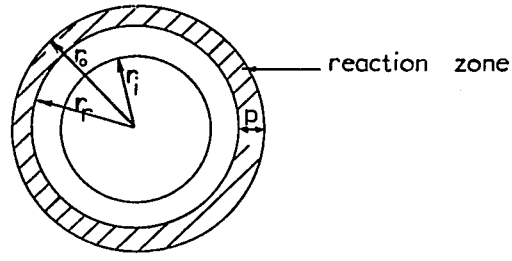
r_r = radius of the reaction zone - silica tube interface

p = penetration of the reacted zone

$A_i = \pi(r_o^2 - r_i^2)$ = initial area of tube

$A_r = \pi(r_o^2 - r_r^2)$ = reacted area

where the radii are shown schematically below.



The fraction of the tube reacted is given by

$$\frac{A_r}{A_i} = \frac{r_o^2 - r_r^2}{r_o^2 - r_i^2} = \frac{r_o^2 - (r_o - p)^2}{r_o^2 - r_i^2}$$

where

$$r_r = r_o - p$$

Solving for p,

$$p = \frac{2r_o \pm \sqrt{4r_o^2 - 4(r_o^2 - r_i^2)\frac{A_r}{A_i}}}{2}$$

or

$$p = r_o - \sqrt{r_o^2 - (r_o^2 - r_i^2)\frac{A_r}{A_i}}$$

For r_o = 4 mm and r_i = 2.5 mm,

$$p = 4 - \sqrt{16 - 9.75\,\frac{A_r}{A_i}}$$

APPENDIX III

RATE CONSTANTS FOR THE $MgO-SiO_2$ POWDER REACTIONS

Composition	Temperature (°F)	Rate Constant (sec^{-1}) Forsterite	Enstatite
20 wt% MgO-	2300	*	5.47×10^{-11}
80 wt% SiO_2	2450	*	1.41×10^{-8}
	2650	*	2.36×10^{-8}
	2750	*	4.90×10^{-8}
40 wt% MgO-	2125	2.11×10^{-10}	4.06×10^{-13}
60 wt% SiO_2	2350	2.20×10^{-9}	6.01×10^{-12}
	2450	1.30×10^{-8}	2.58×10^{-10}
	2550	3.60×10^{-7}	5.98×10^{-10}
	2650	5.04×10^{-7}	1.62×10^{-9}
	2700	1.83×10^{-8}	2.42×10^{-9}
	2750	*	7.36×10^{-9}
50 wt% MgO-	2315	3.31×10^{-9}	*
50 wt% SiO_2	2410	1.39×10^{-8}	5.90×10^{-10}
	2520	4.46×10^{-8}	1.80×10^{-9}
	2650	2.46×10^{-7}	1.33×10^{-9}
57.3 wt% MgO-	2125	6.20×10^{-11}	*
42.7 wt% SiO_2	2210	1.46×10^{-10}	*
	2320	6.04×10^{-10}	*
	2400	1.83×10^{-9}	*
	2450	6.55×10^{-9}	*
	2550	1.63×10^{-8}	*
	2650	1.63×10^{-8}	*
	2700	1.34×10^{-8}	*
	2715	7.92×10^{-9}	*
	2750	7.82×10^{-9}	*
60 wt% MgO-	2260	3.96×10^{-10}	*
40 wt% SiO_2	2420	2.81×10^{-9}	*
as vitreous	2500	5.64×10^{-9}	*
silica	2650	1.47×10^{-8}	*
80 wt% MgO-	2300	2.09×10^{-9}	*
20 wt% SiO_2	2450	9.40×10^{-9}	*
	2650	1.14×10^{-8}	*
	2750	2.84×10^{-8}	*

*Rate constants were not determined

APPENDIX IV

The experimental heats run in the five-pound induction furnace are tabulated in this section to serve as a cross-reference between the various figures and tables in the "Engineering Aspects" section. The amount of the silicon added as nodularizing and post-inoculant alloys (%Si added to ladle) and the total silicon after treatment, as well as the quantity and chemistry of the fine dross are listed for each heat. Unusual steps in the treatment are listed under "Description." Finally, the location in the text of the data from each of the heats is given in "Occurrence."

APPENDIX IV - SUMMARY OF LADLE DROSS HEATS

Melts with the standard treatment with no post-inoculant used:

0.15%Mg added; T_{nod} = 2750; T_h = 2500; air atmosphere; t_h = 12 min

Heat #	%Si Added to Ladle	%Si Total	Fine Dross (gm/100 lb)	% Forst	% MgO	% Quartz	% Unaccounted	Description	Occurrence
147	0	2.20	14.8	5.0	10.2	1.5	83.3	2%MgFeC no post-inoculant	Figs. 19, 57, 58, 59
143	.322	2.20	15.4	13.9	5.7	1.2	79.2	NiMg no post-inoculant	Figs. 19, 57, 58, 59
153	.822	2.20	26.0	27.1	9.5	0	63.4	9%MgFeSi no post-inoculant	Tables XV, XVI, XVII, XVIII, XIX Figs. 53, 57, 58, 59
142	.822	2.20	14.1	30.0	10.5	0.9	58.6	9%MgFeSi no post-inoculant	Tables XV, XVI, XVII, XVIII, XIX Figs. 19, 57, 59
146	1.35	2.20	27.8	51.8	13.0	0.1	35.1	5%MgFeSi no post-inoculant	Figs. 19, 57, 58, 59
144	.841	2.20	27.0	5.0	10.2	1.5	84.3	9%CeMgFeSi no post-inoculant	Table XVII Figs. 19, 57, 58, 59
111	.822	1.70	24.8	15.8	8.1	0.6	75.5	9%MgFeSi no post-inoculant (low total Si)	Tables XIV, XVII Figs. 53, 56, 58, 59
138	.828	.828	32.7	16.9	9.4	2.4	71.3	9%MgFeSi no post-inoculant (low total Si)	Table XVII Figs. 58, 59

Melts to which a post-inoculant was added:

0.15%Mg added as 9%MgFeSi; T_{nod} = 2750; T_h = 2500; air atmosphere; held 12 min

Heat #	%Si Added to Ladle	%Si Total	Fine Dross (gm/100 lb)	% Forst	% MgO	% Quartz	% Unaccounted	Description	Occurrence
141	1.445	2.20	36.5	27.8	26.0	3.0	43.2	0.5%Si as 75FeSi	Table XIX Figs. 58, 59
135	1.548	2.20	35.3	n.d.	n.d.	n.d.	n.d.	1.0%Si as 75FeSi	Fig. 58
139	1.361	1.361	39.5	14.2	15.0	2.5	68.3	0.5%Si as 75FeSi	Figs. 58, 59
145	1.822	2.200	38.4	20.4	21.1	1.8	56.7	1.0%Si as 75FeSi	Table XIX Figs. 58, 59

Melts to which low magnesium was added:

T_{nod} = 2750; T_h = 2500; air atmosphere; no post-inoculant; t_h = 12 min

107	.274	1.700	16.2	9.2	6.2	3.3	81.3	.05%Mg as 9%MgFeSi	Figs. 56, 58, 59
106	.562	1.742	25.7	12.3	8.2	0.5	79.0	.10%Mg as 9%MgFeSi	Figs. 56, 58, 59
151	.930	2.19	8.9	14.8	4.5	0.7	80.0	.10%Mg as 5%MgFeSi	Fig. 59

Melts for which a low nodularizing temperature was used:

0.15%Mg as 9%MgFeSi; no post-inoculant; T_h = 2500; air atmosphere; t_h = 12 min

Heat #	%Si Added to Ladle	%Si Total	Fine Dross (gm/100 lb)	% Forst	% MgO	% Quartz	% Unaccounted	Description	Occurrence
109	.914	1.70	28.5	15.0	5.0	0	80.0	T_n = 2650	Table XIV; Figs. 58, 59
110	.822	1.70	24.0	15.1	15.3	1.1	68.5	T_n = 2550	Table XIV; Figs. 58, 59
140	.827	1.71	28.8	8.7	12.5	1.0	77.8	T_n = 2650	Table XIV; Figs. 58, 59

Special melts: 0.15%Mg as 9%MgFeSi; no post-inoculant; T_n = 2750; T_h = 2500; t_h = 12 min

149	.822	2.20	36.4	18.0	7.0	0.4	74.6	.05%S Air atmos.	Table XVI; Figs. 58, 59
152	.81	2.19	21.6	10.5	50.2	0.4	38.9	Argon atmosphere	Table XV; Figs. 58, 59
150	.822	2.20	*	*	*	*	*	dross collected intermittently	Table III; Figs. 52, 53
137	.844	1.70	*	*	*	*	*	dross collected intermittently	Fig. 53

T_{nod} = nodularizing temperature (magnesium alloy added)

T_h = holding temperature

t_h = holding time

APPENDIX V

THERMODYNAMIC EQULIBRIUM: THE PARTIAL PRESSURE DIAGRAM

The stability of the phases in the Mg-Si-O system depends on the oxygen partial pressure, as shown in Fig. Va. According to equilibrium, as the partial pressure increases, magnesium will initially oxidize, then react with silicon to form forsterite. With excess silicon, the forsterite can then react with silicon to form enstatite. Finally, any remaining silicon can oxidize to silica.

Consequently, in the experiments between silicon and MgO, the partial pressure at the interface may be very low (so that silica is not stable) and silicon and MgO may react directly to produce forsterite. This could occur even though the over-all oxygen pressure is quite high. This would then explain the absence of a silica layer in Figs. 28 and 33.

However, in view of the strong effect of the atmosphere on the forsterite formation, it is believed that the kinetics involved in the direct reaction are very slow and that the principal method of forsterite formation is the prior oxidation of silicon to silica.

Fig. Va also suggests that, in the experiments in the pressure vessel between magnesium and silica, the oxygen partial pressure is very low (less than 10^{-19} atm) so that forsterite cannot form.

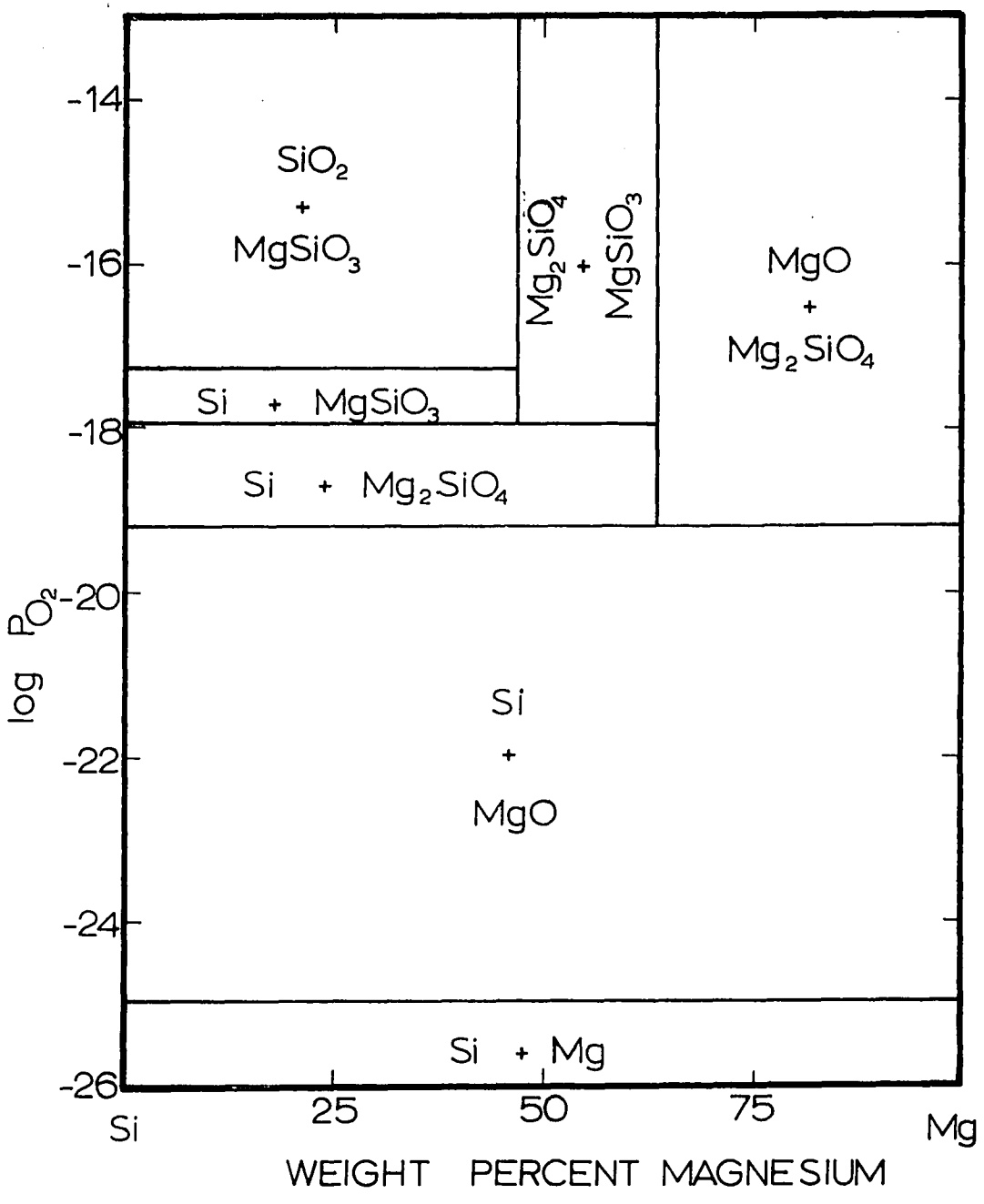


Figure Va: The partial pressure diagram for the Mg-Si-O system. The stable phases are determined by the oxygen partial pressure and the ratio of magnesium to silicon. This diagram represents the equilibrium, not the kinetics of the reactions in the system.

BIBLIOGRAPHY

1. R. Heine and C. Loper: Modern Castings, v. 50, 1966, p. 88.

2. A. Fuller: BCIRA J., v. 7, 1958, p. 268.

3. R. Barton and A. Fuller: BCIRA J., v. 9, 1961, p. 406.

4. R. Schelleng: The Internation Nickel Company, Inc., Suffern, New York, private communication, 1968.

5. P. Trojan, P. Guichelaar, W. Bargeron, and R. Flinn: Trans. AFS, v. 76, 1968, p. 323.

6. R. Kiessling and N. Lange: Non-Metallic Inclusions in Steel, Part II, Percy Lund, Humphries and Co., London, 1966.

7. P. Arsent'ev and Y. Orlova: Liteinoe Proizvodstvo, v. 4, 1957, p. 23.

8. R. Clark and T. McCluhan: Trans. AFS, v. 73, 1965, p. 442.

9. P. Trojan and R. Flinn: SAE Trans., v. 73, 1965, p. 265.

10. P. Trojan, W. Bargeron, and R. Flinn: Trans. AFS, v. 75, 1967, p. 611.

11. B. Mil'man and N. Popova: Gases in Cast Metals, English Transl. - Consultants Bureau, New York, 1965.

12. Y. Levchenko: Russian Castings Production, v. 1, 1968, p. 34.

13. A. de Sy: Trans. AFS, v. 75, 1967, p. 161.

14. R. Baker: J. Iron Steel Inst., v. 205, 1967, p. 637.

15. B. Lagowski and W. Pollard: Trans. AFS, v. 68, 1960, p. 7.

16. T. Bergstrom and R. Bassett: Trans. AFS, v. 67, 1959, p. 217.

17. E. Emley: J. Inst. Metals, v. 75, 1949, p. 481.

18. G. Economos and W. Kingery: J. Am. Cer. Soc., v. 36, 1953, p. 403.

19. W. Jander and J. Wuhrer: Z. anorg. Chem., v. 226, 1936, p. 225.

20. L. Degueldre: Bull. Soc. chim. Belg., v. 62, 1953, p. 347.

21. G. Brindley and R. Hayami: Phil. Mag., v. 12, 1965, p. 505.

22. A. Ginstling and B. Brounshtein: Zh. prikl., Khim., Mosk., v. 23, 1950, p. 1327.

23. R. Hayami and T. Ogura: Osaka Kogyo Gijutsu Shikenjo Kiho, v. 18, 1967, p. 360.

24. P. Trojan: 1961, Department of Chemical and Metallurgical Engineering, University of Michigan, Ann Arbor, Michigan, Ph.D. Thesis.

25. J. Elliott and M. Gleiser: Thermochemistry for Steelmaking, Vol. I, Addison-Wesley Publishing Co., Inc., Mass., 1960.

26. O. Kubaschewski and E. Evans: Metallurgical Thermochemistry, Pergamon Press, London, 1958.

27. K. Kelley: U.S. Bur. Mines Bull. No. 476, 1950.

28. J. Coughlin: U.S. Bur. Mines Bull. No. 542, 1954.

29. L. Darken and R. Gurry: Physical Chemistry of Metals, p. 311, McGraw-Hill Book Co., Inc., New York, 1953.

30. D. Sponseller: 1962, Department of Chemical and Metallurgical Engineering, University of Michigan, Ann Arbor, Michigan, Ph.D. Thesis.

31. P. Guichelaar: 1969, Department of Chemical and Metallurgical Engineering, University of Michigan, Ann Arbor, Michigan, Ph.D. Thesis.

32. B. Cullity: Elements of X-ray Diffraction, p. 396, Addison-Wesley Publishing Co., Inc., Mass., 1959.

33. X-ray Powder Data File, American Society for Testing and Materials, 1968.

34. K. Orths: Giesserei, v. 47, 1960, p. 595.

35. W. Wennmann and T. Kootz: Stahl und Eisen, v. 71, 1951, p. 992.

36. H. Merz and B. Marineck: Stahl und Eisen, v. 75, 1955, p. 196.

37. G. Nandori: Freiheiger Forschungshefte, B25, 1958, p. 70.

38. O. Madono: Giesserei, v. 44, 1957, p. 714.

39. A. Morgan: Foundry Trade Journal, v. 99, 1955, p. 4713.

40. W. Tonks: Trans. AFS, v. 64, 1956, p. 551.

41. C. Sanders, H. Heine, and R. Marande: Trans. AFS, v. 69, 1961, p. 340.

42. A. Dahlmann and K. Loeberg: Trans. AFS, v. 70, 1962, p. 612.

43. J. Chipman, J. Fulton, N. Gokcen, and G. Caskey: Acta. Met., v. 2, 1954, p. 439.

44. E. Turkdogan, L. Davis, L. Leake, and N. Gokcen: J. Iron Steel Inst., v. 181, 1955, p. 123.

45. E. Turkdogan, P. Grieveson, and J. Beisler: A.I.M.E. Trans., v. 227, 1963, p. 1258.

46. C. Taylor and J. Chipman: A.I.M.E. Trans., v. 154, 1943, p. 228,

47. W. Jander: Z. anorg. u. allgem. Chem., v. 163, 1927.

48. J. Scully: The Fundamentals of Corrosion, pp. 1-48, Pergamon Press, London, 1966.

49. W. Kingery: Introduction to Ceramics, pp. 234-236, John Wiley and Sons, Inc., New York, 1960.

50. E. Levin, C. Robbins, and H. McMurdie: Phase Diagrams for Ceramists, The American Ceramic Society, Ohio, 1964.

51. A.Muan and E. Osborn: Phase Equilibria Among Oxides in Steelmaking, Addison-Wesley Publishing Co., Inc., Mass., 1965.

52. D. Askeland and P. Trojan: Trans. AFS, v. 77, 1969, p. 344.

53. R. Boni and G. Derge: A.I.M.E. Trans., v. 206, 1956, p. 56.

54. R. Geffken and E. Miller: A.I.M.E. Trans., v. 242, 1968, p. 2323.